Regional climate dynamics

Antonello Provenzale
Istituto di Scienze dell'Atmosfera e del Clima
Consiglio Nazionale delle Ricerche

(with J. von Hardenberg, E.Palazzi)

Budapest, January 2013

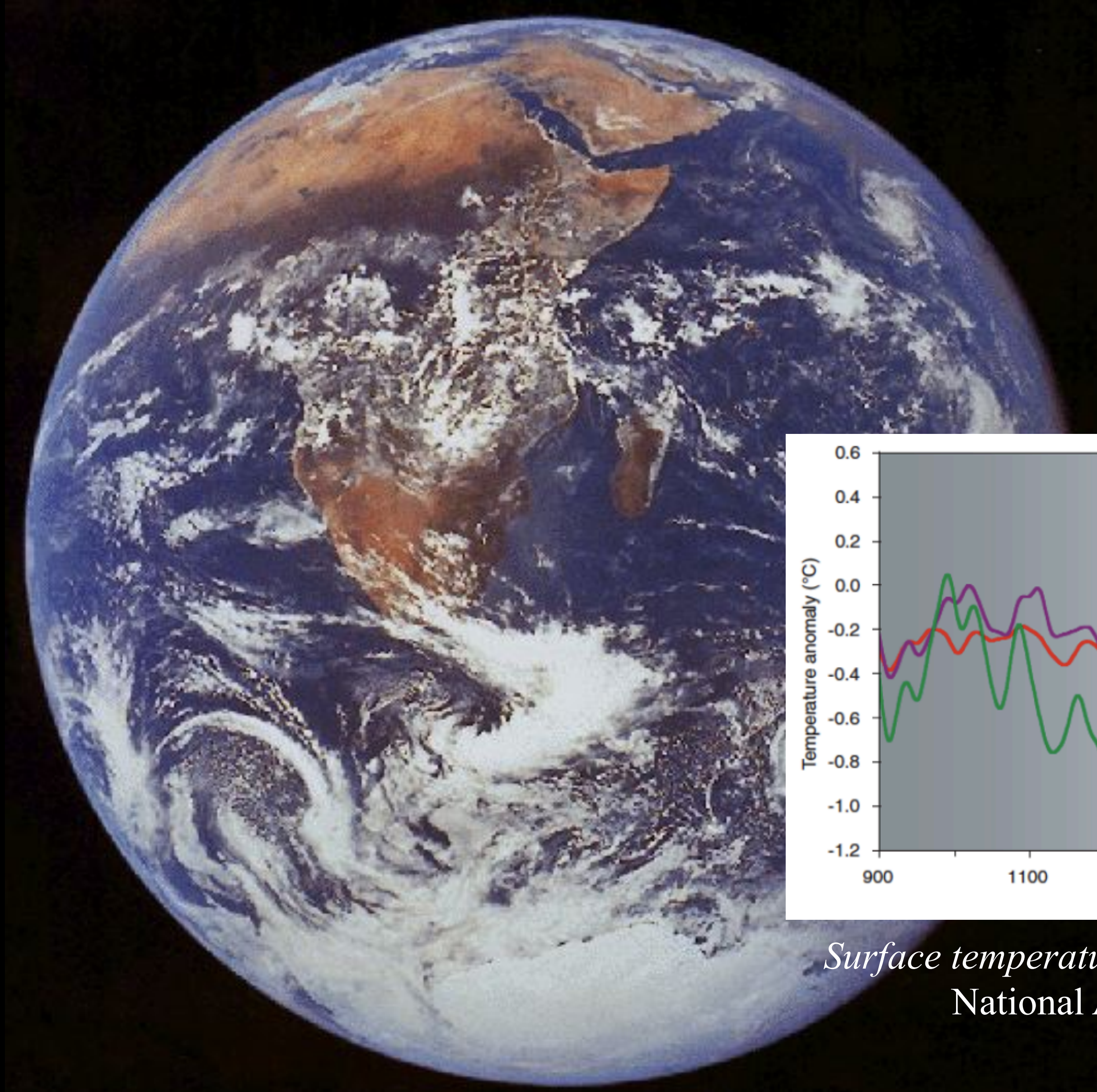

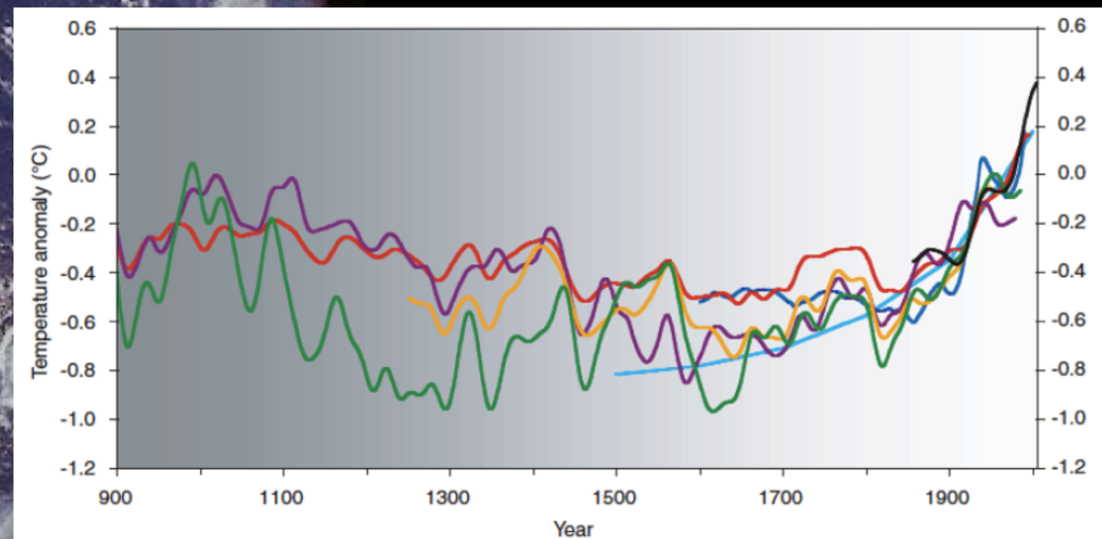

Surface temperature reconstruction for the last 2,000 years.
National Academy of Sciences, USA, 2006

Climate change is not homogeneous on the Earth surface

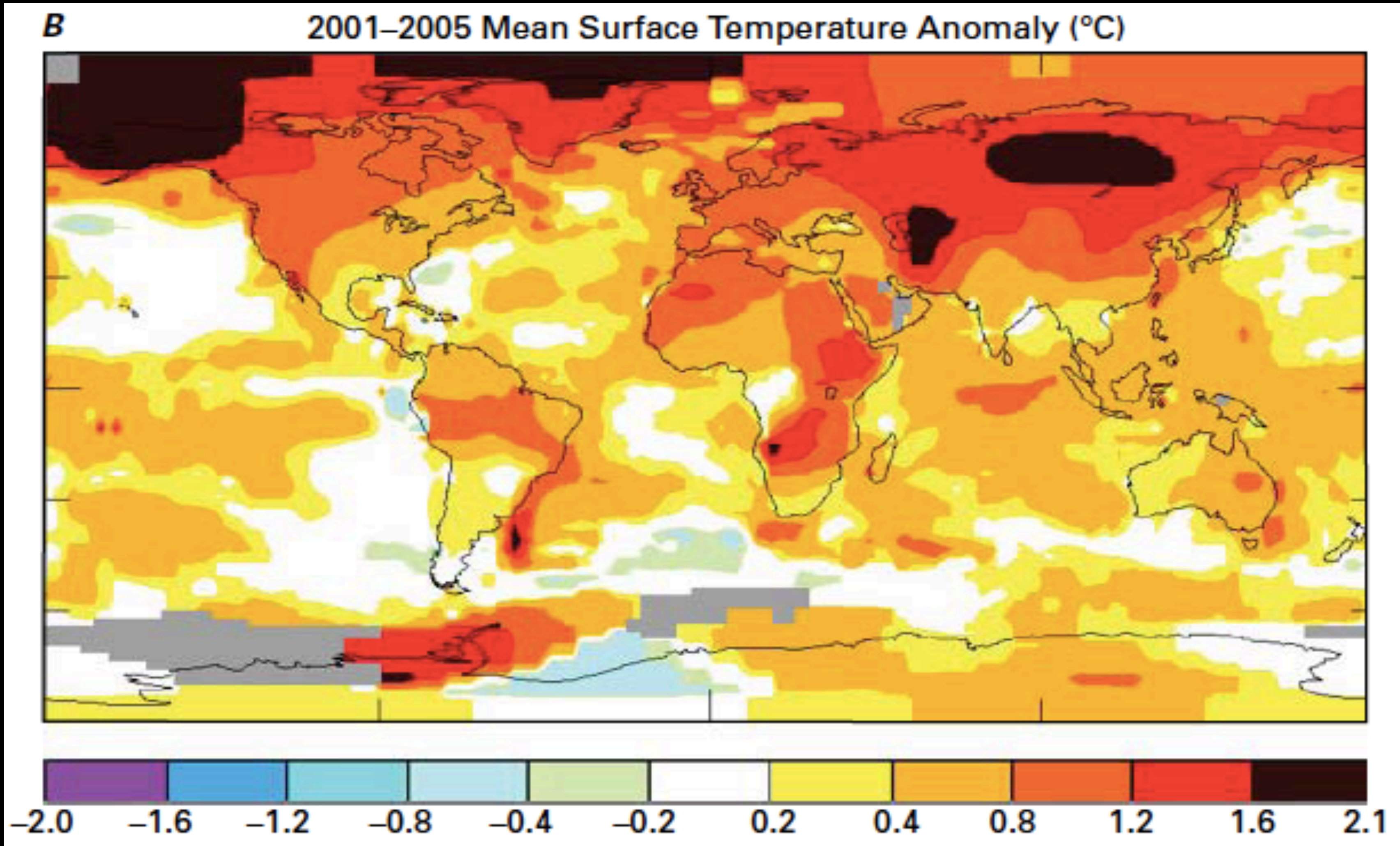

Past Climate Variability and Change in the Arctic and at High Latitudes
US Climate Change Science Program; from: Hansen et al. 2006

Climate change is not homogeneous on the Earth surface

Changes in precipitation:
1952-2002 trend

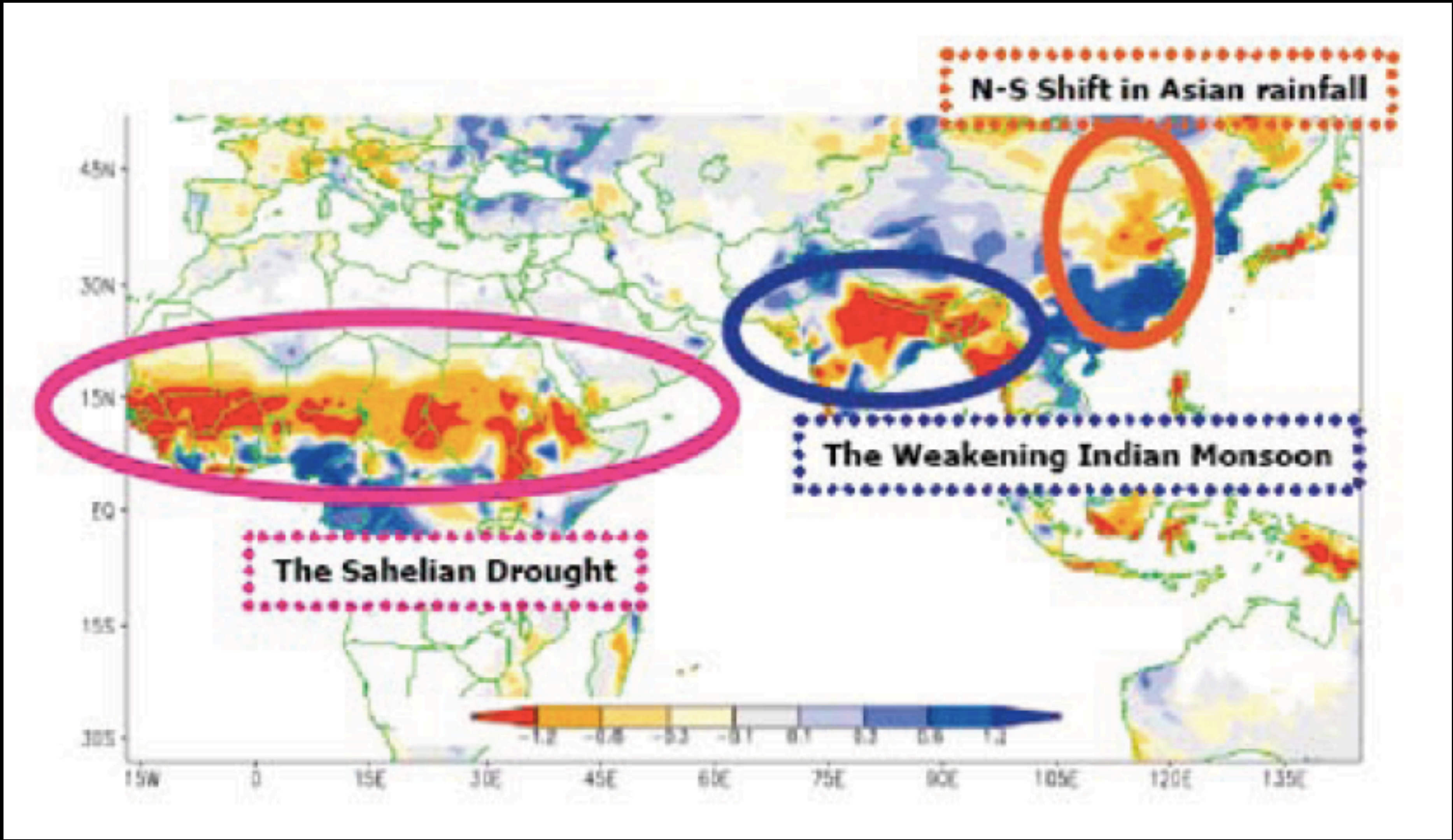

from Chung and Ramanathan 2006

Climate change and the hydrological cycle

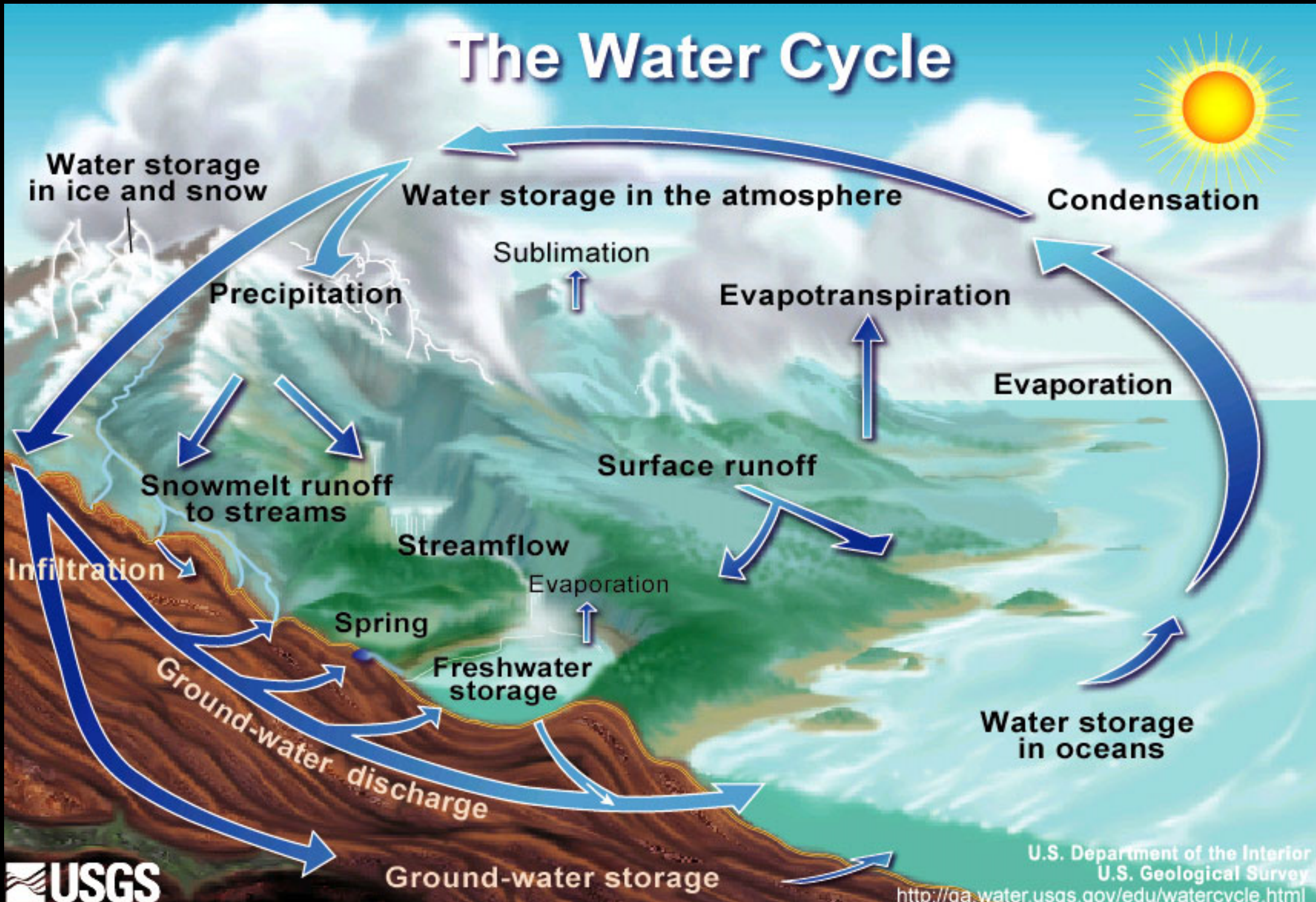

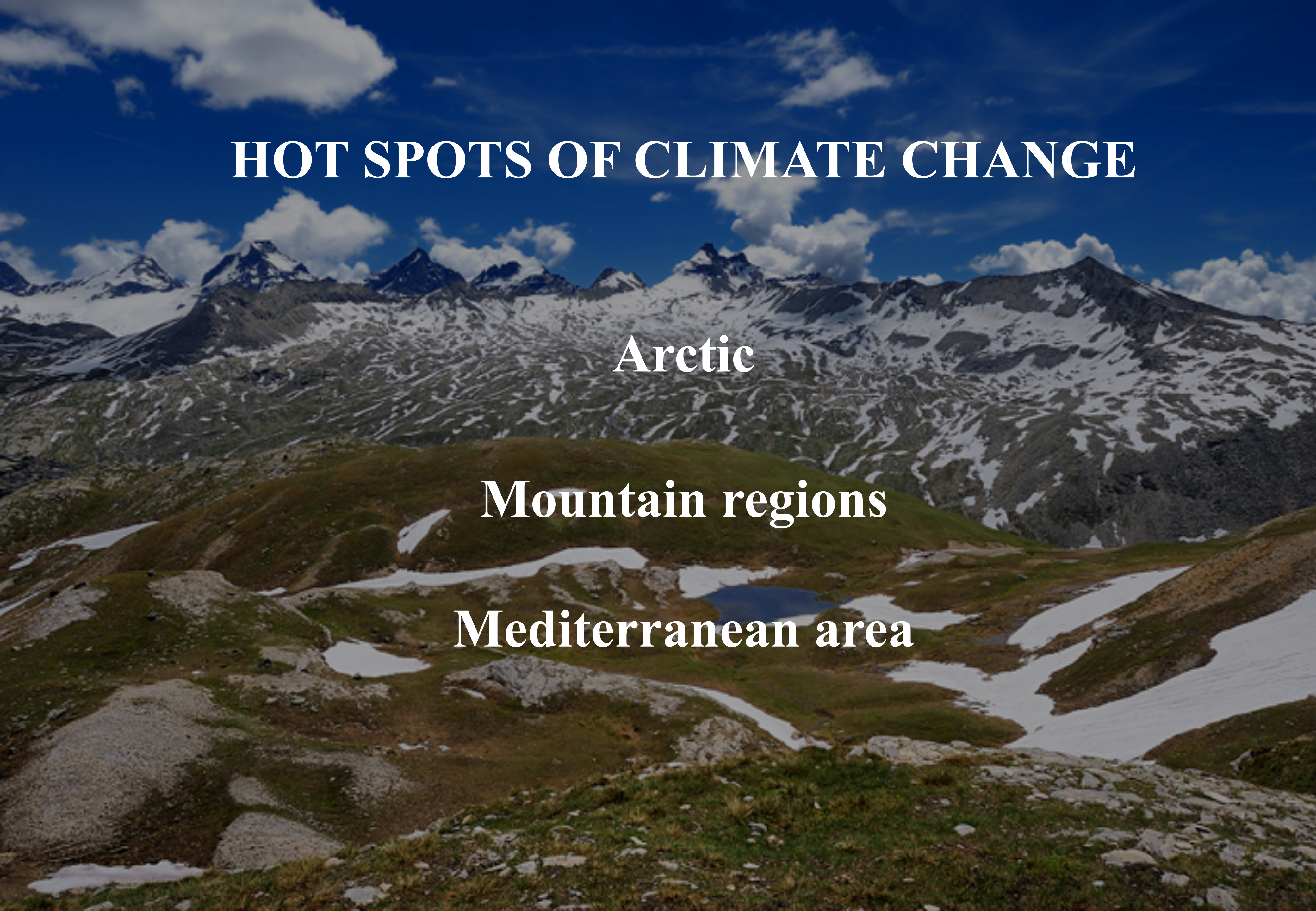

HOT SPOTS OF CLIMATE CHANGE

Arctic

Mountain regions

Mediterranean area

Temperature increase in the Arctic is 2-3 times larger than global average

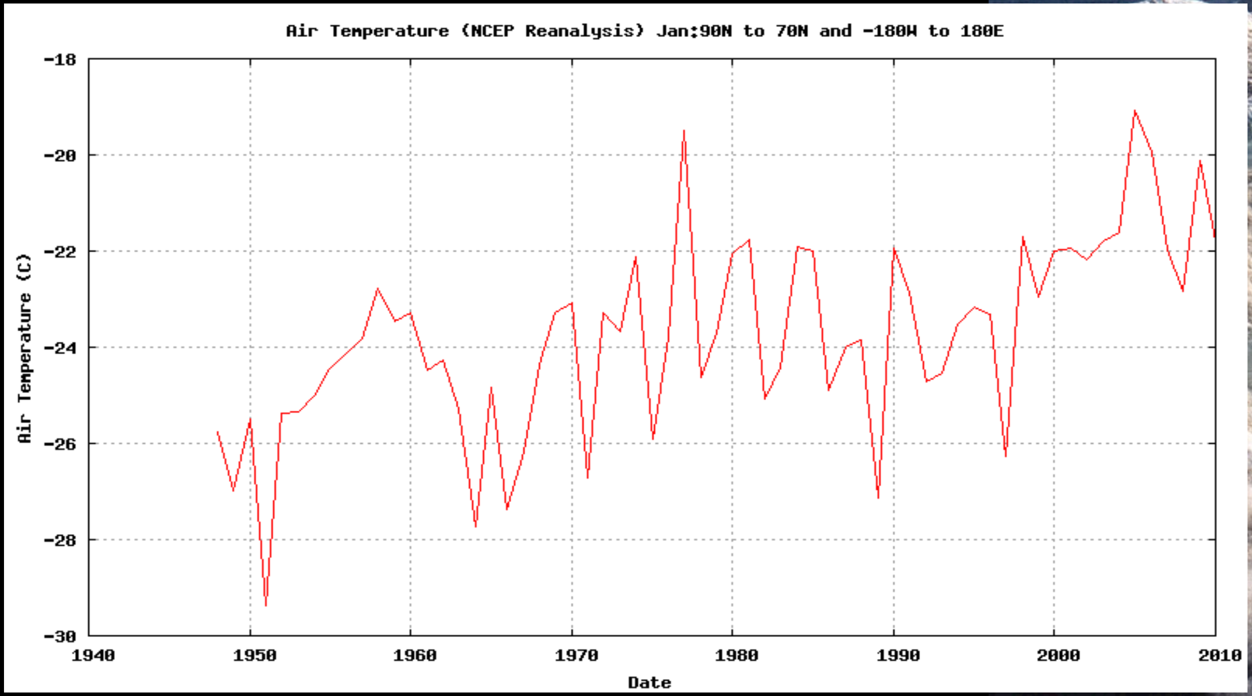

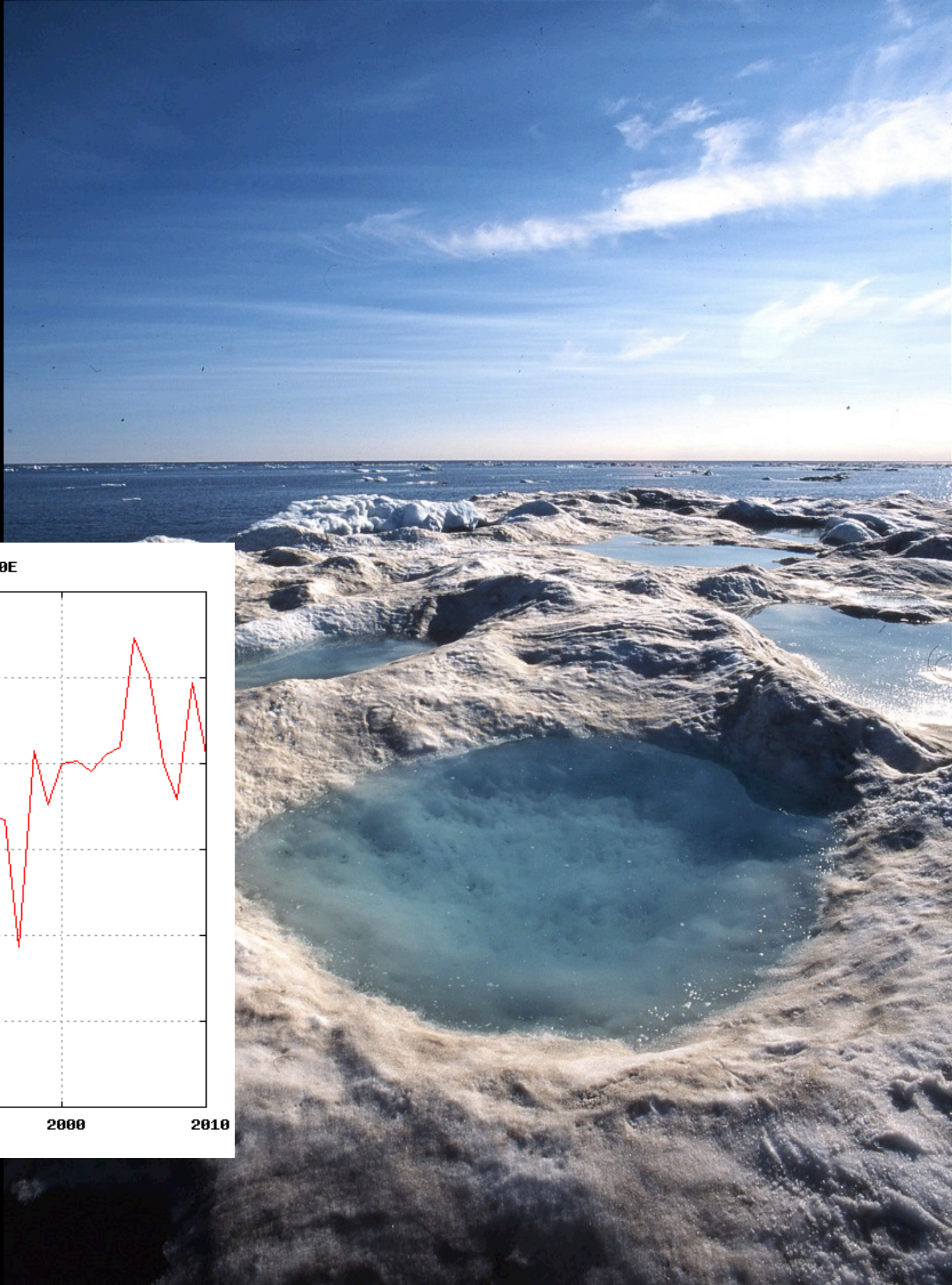

http://www.esrl.noaa.gov/

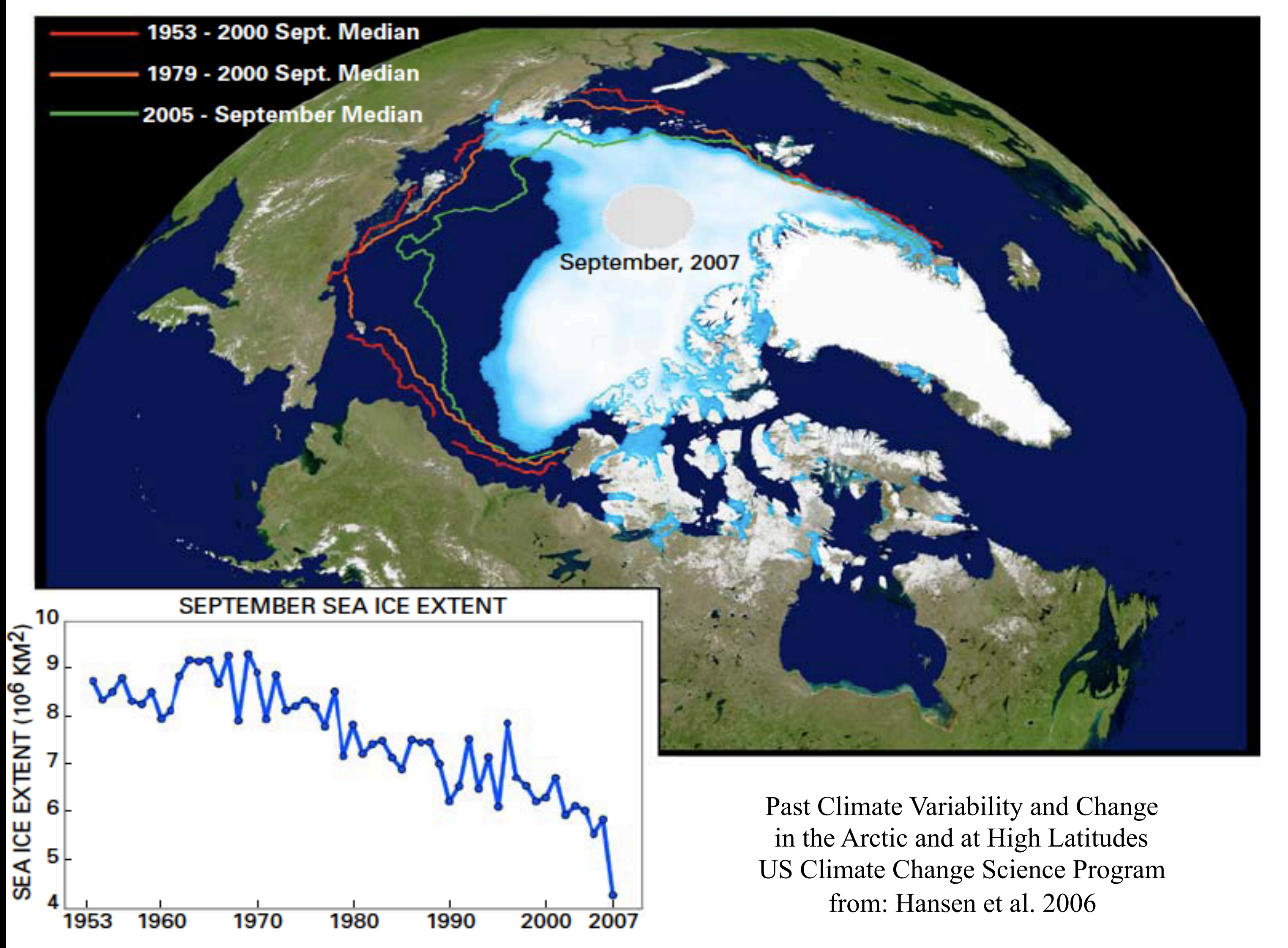

Past Climate Variability and Change
in the Arctic and at High Latitudes
US Climate Change Science Program
from: Hansen et al. 2006

Sea ice in the Arctic has dramatically decreased, both in total cover and thickness. In September 2007, the surface covered by sea ice has reached the historical minimum of 4.1 milion km^2, about half that of the '50. From 1975 to 2000, the average thickess of Arctic sea ice decreased by about 33%, from 3.7 to 2.5 meters.

Convection and overturning circulation

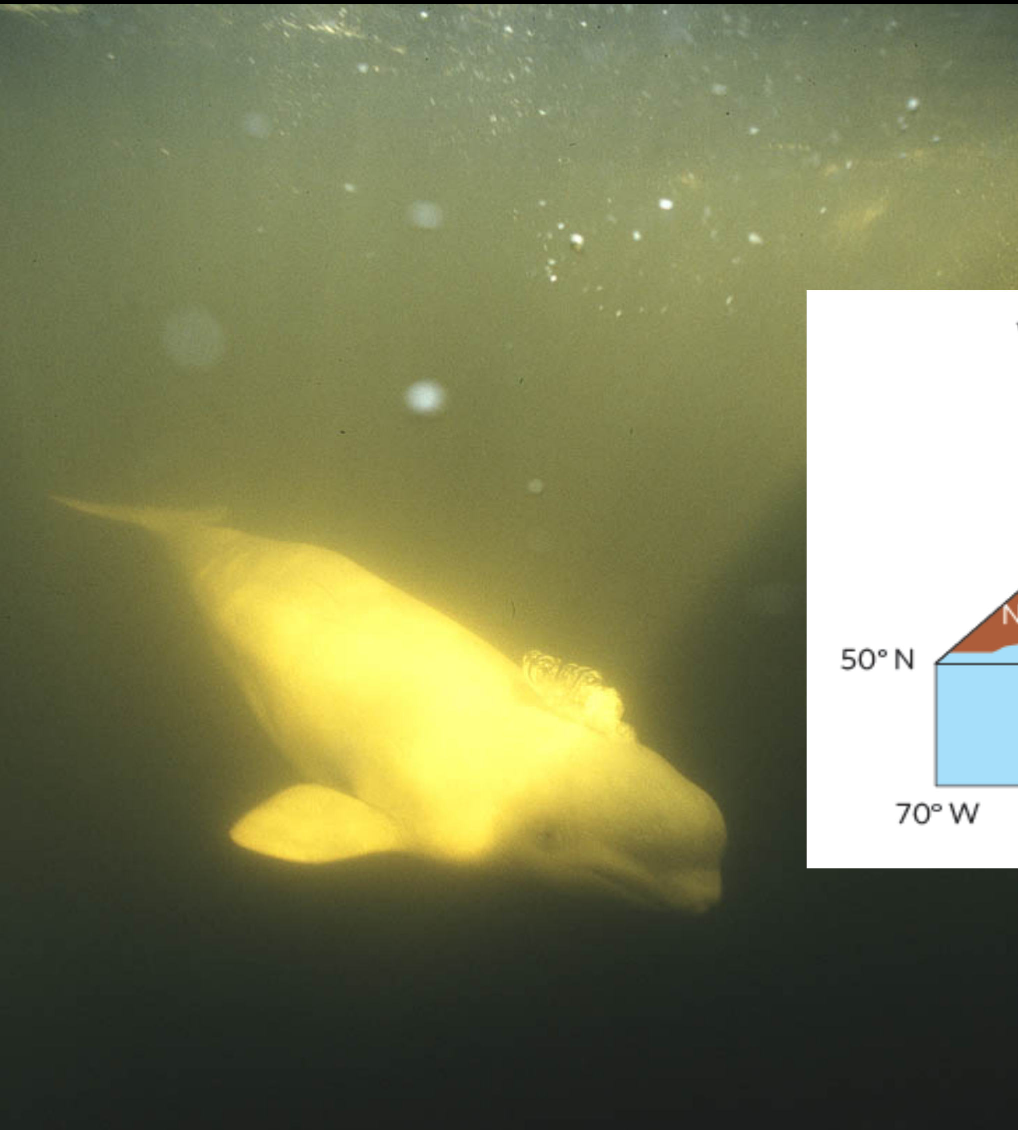

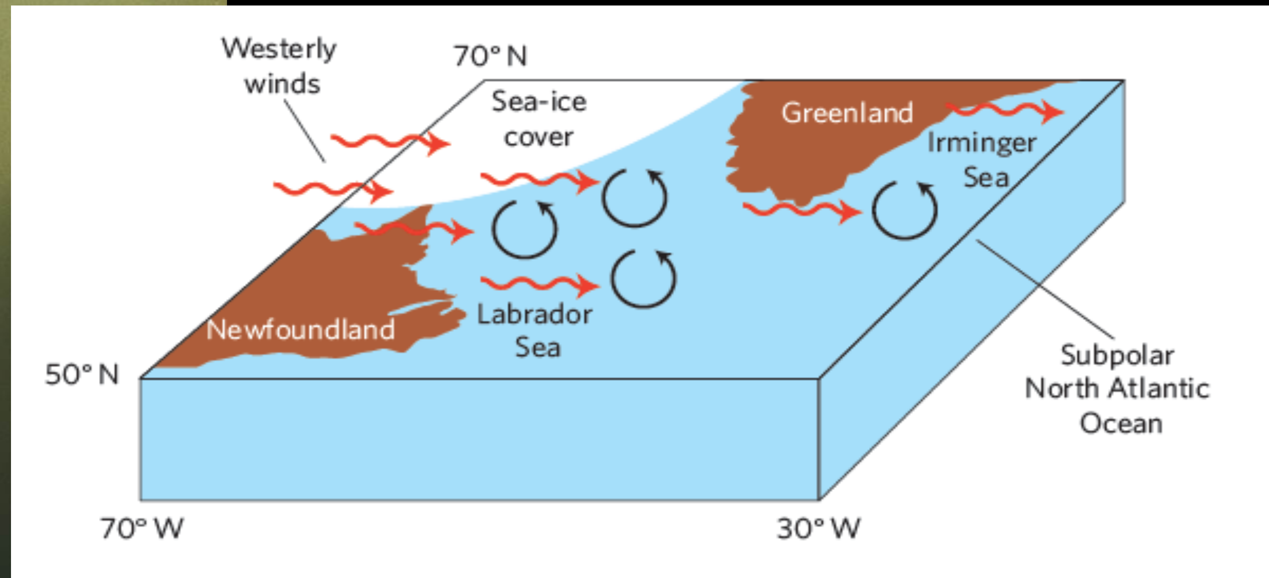

Lozier, *Nature Geoscience* 2008
Vage et al, *Nature Geoscience* 2008

General decrease of convection and of deep water formation, together with unexpected and surprising events (eg winter 2007/2008)

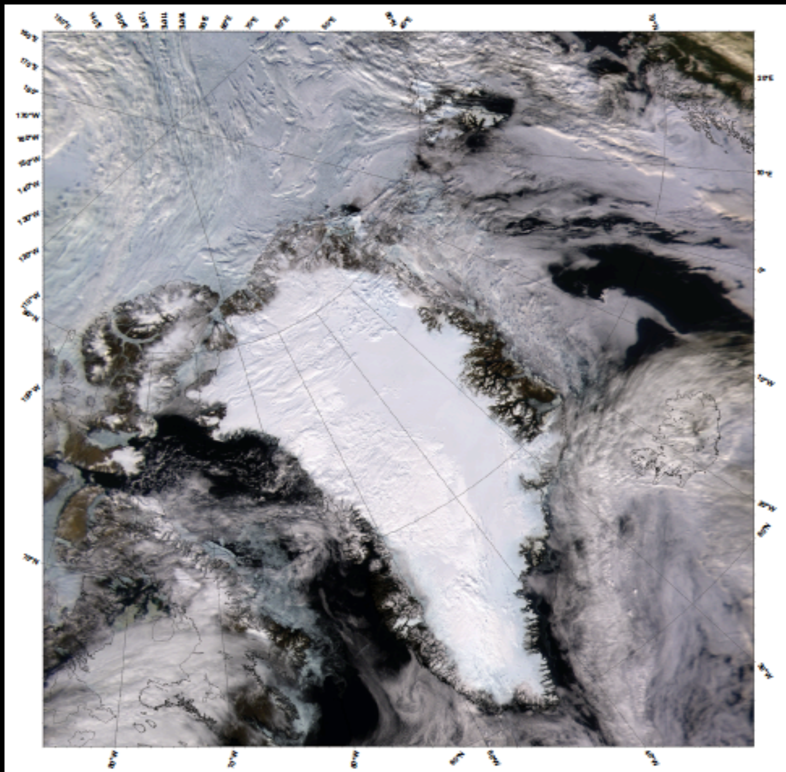

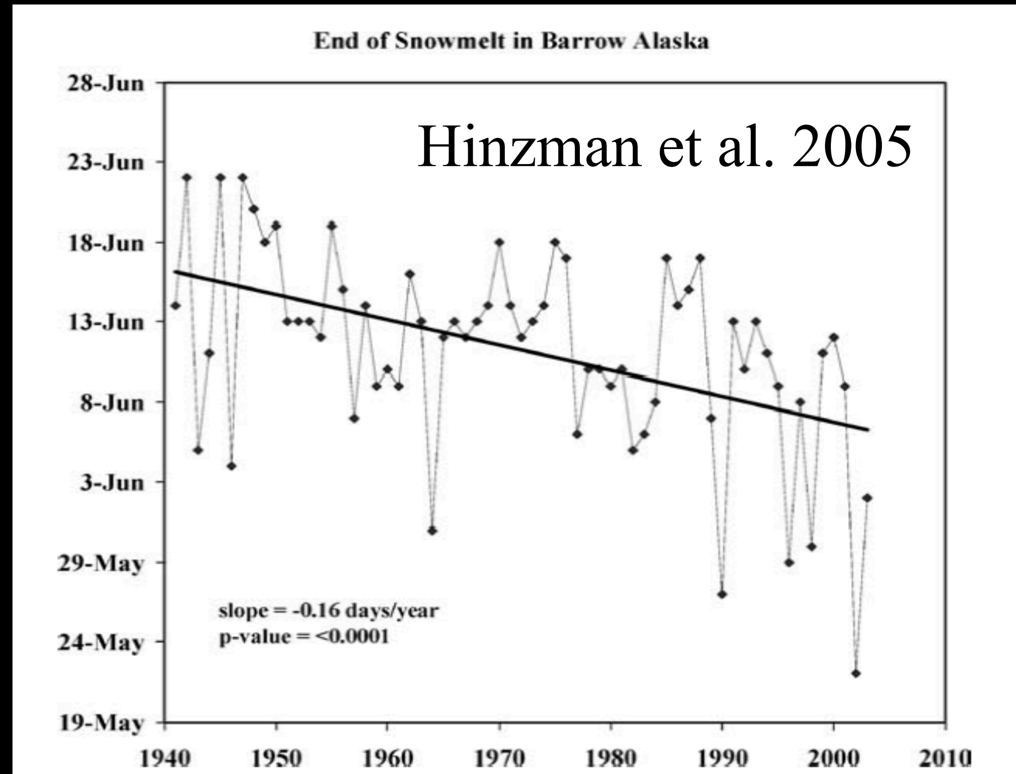

Continental ice cover in the polar regions of the northern emisphere decreases by about 160 billion tonnes per year. Satellite observations indicate that from 1996 to 2005 the Greenland ice mass balance deficit has doubled, mainly owing to the increase in the sliding velocity of ice towards the sea in the latitudinal belt below 70° N.

D.C.Slobbe, P. Ditmar, R.C. Lindenbergh, 2009. Estimating the rates of mass change, ice volume change and snow volume change in Greenland from ICESat and GRACE data. *Geophysical Journal International, 176:95106, doi:10.1111/j.1365-246X.2008.03978.x*

SEE ALSO FIAMMA STRANEO WORK, WHOI (Nature Geosciences)

Aerosol: transport of fire emissions to the Arctic

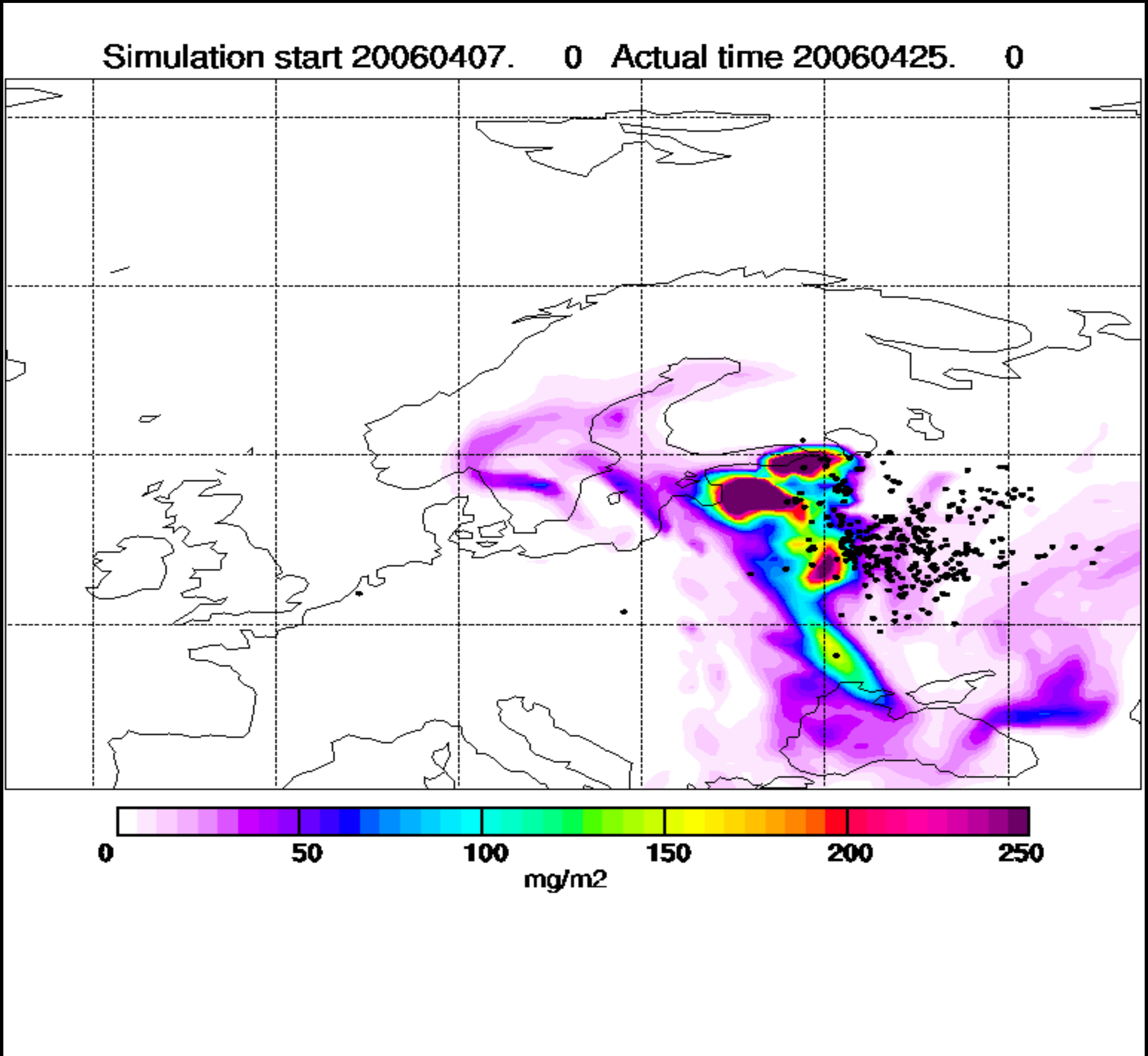

Model Flexpart
courtesy:
A.Stohl /NILU

results from
the IPY

Aerosol transport and chemistry (and ice darkening)

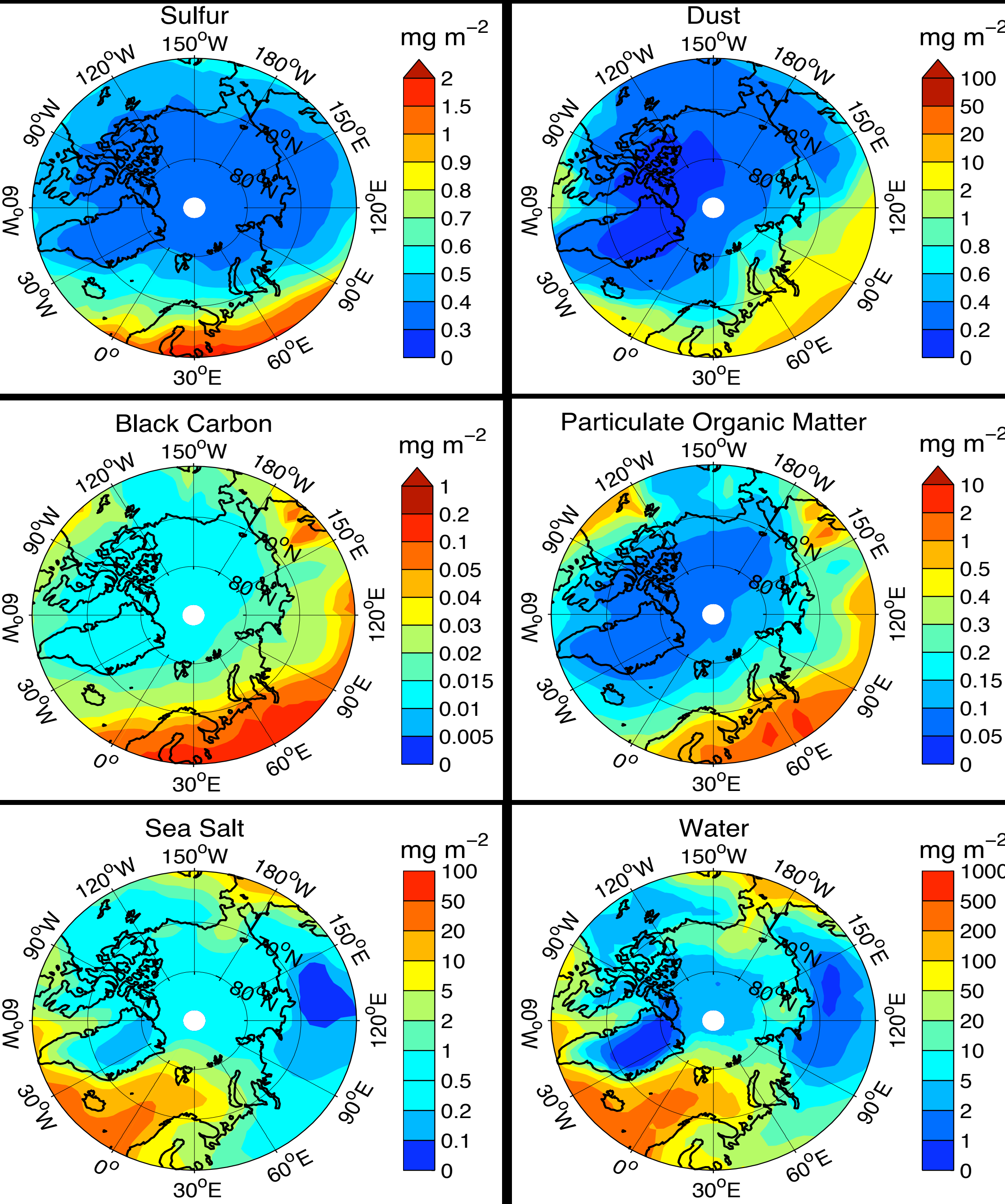

ECHAM 5.3 + HAM, T42 L19
Aerocom forcing, fluxes for 2000
Simulation: J. von Hardenberg, ISAC-CNR

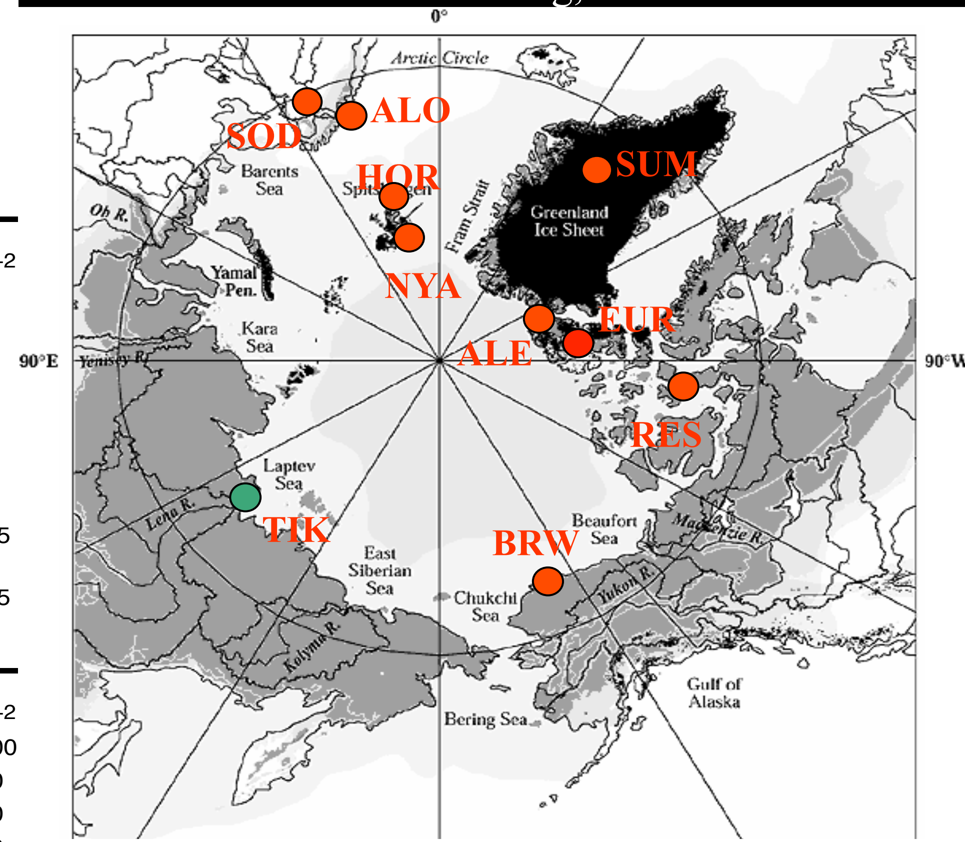

aerosol ground-based data
(in-situ and/or columnar)
POLAR-AOD network
Chair: Claudio Tomasi, ISAC-CNR

Impacts on environment and ecosystems: survival and population dynamics

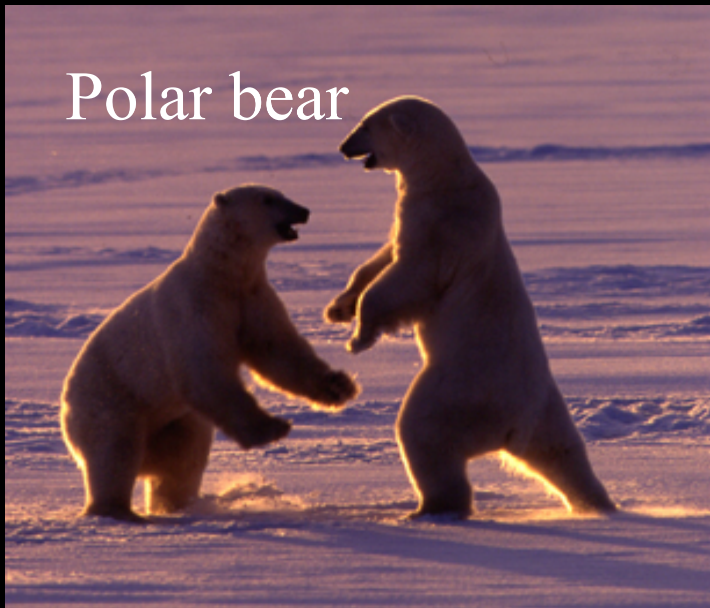

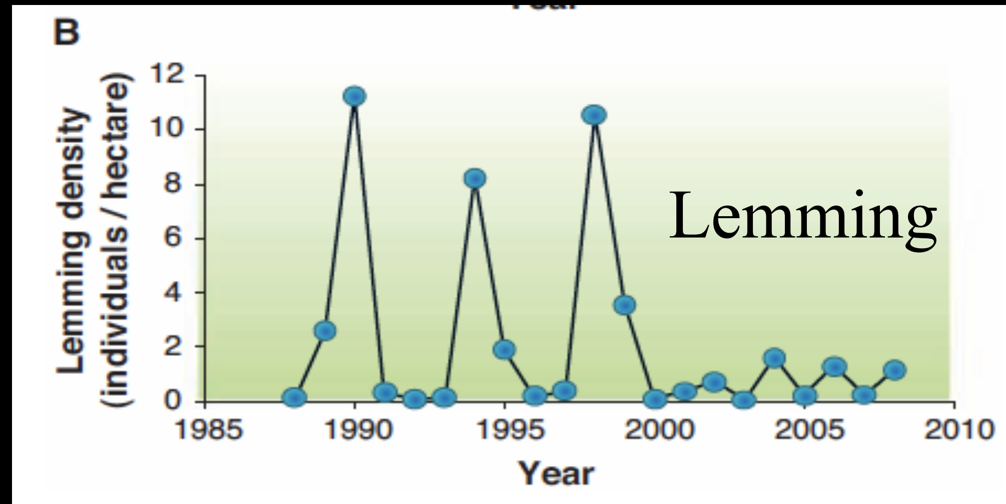

O. Gilg, B. Sittler, I. Hanski, *Glob. Change Biol.* 10.1111/j.1365-2486.2009.01927.x (2009).

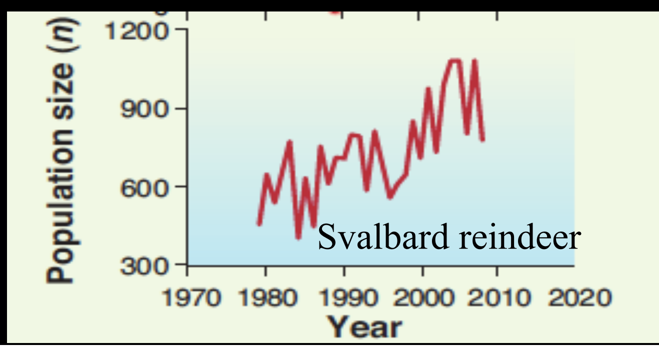

N. J. C. Tyler, M. C. Forchhammer, N. A. Øritsland, *Ecology* **89**, 1675 (2008).

Post et al, 2009. Ecological Dynamics Across the Arctic Associated with Recent Climate Change. *Science, 325, 1355*.
Hunter et al, 2010. Climate change threatens polar bear populations: a stochastic demographic analysis. *Ecology.*

Impacts on environment and ecosystems: phenology

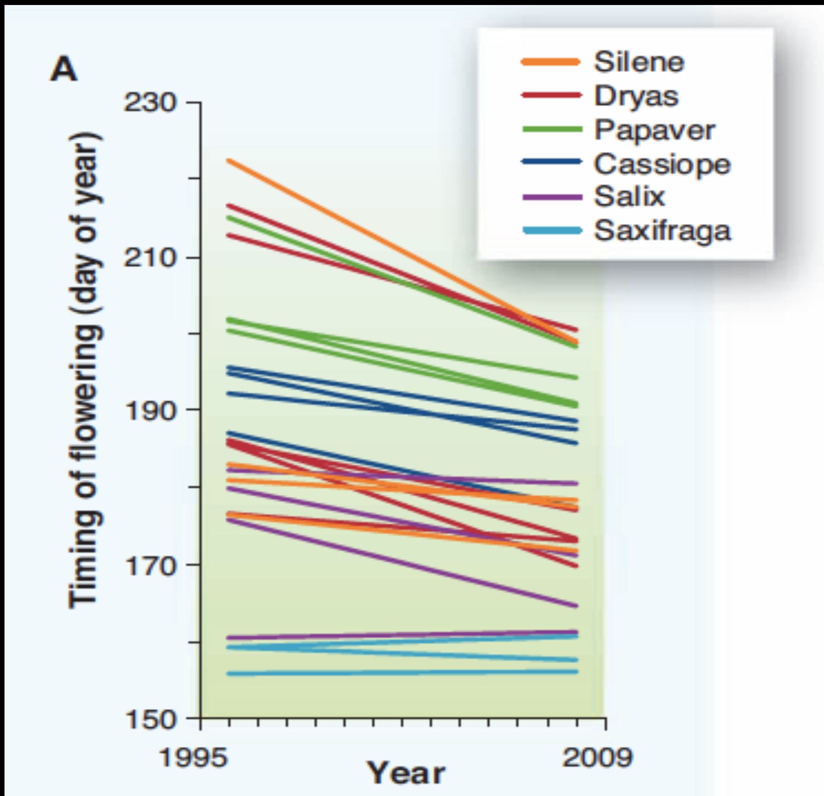

T. T. Høye, E. Post, H. Meltofte, N. M. Schmidt, M. C. Forchhammer, *Curr. Biol.* **17**, R449 (2007).

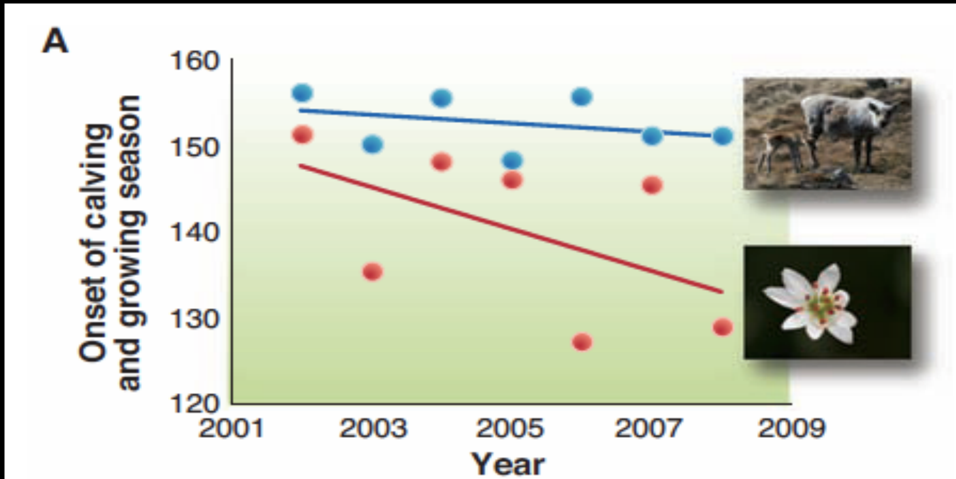

E. Post, M. C. Forchhammer, *Philos. Trans. R. Soc. B* **363**, 2369 (2008).

N. Saino, R. Ambrosini, D. Rubolini, J. von Hardenberg, A.Provenzale, K. Hüppop, O. Hüppop, A. Lehikoinen, E. Lehikoinen, K. Rainio, M. Romano, L. Sokolov, 2010. Demographic consequences of increasing ecological mismatch at arrival in migratory birds. *Sub judice.*

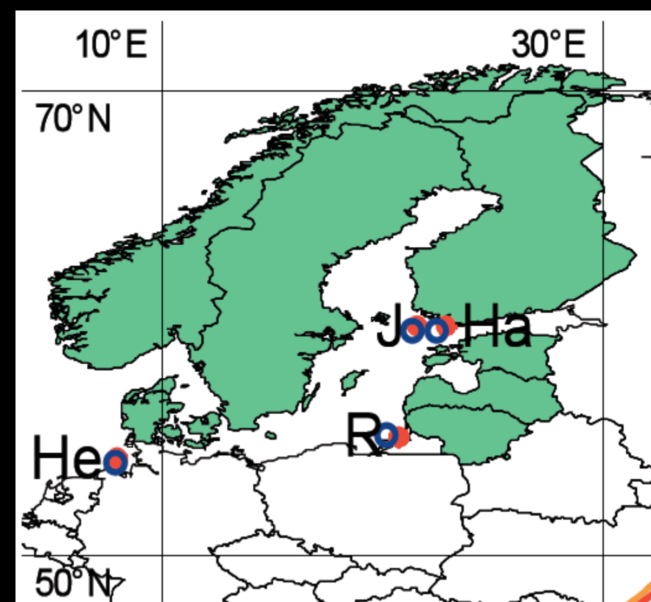

Impacts on environment and ecosystems: phenology

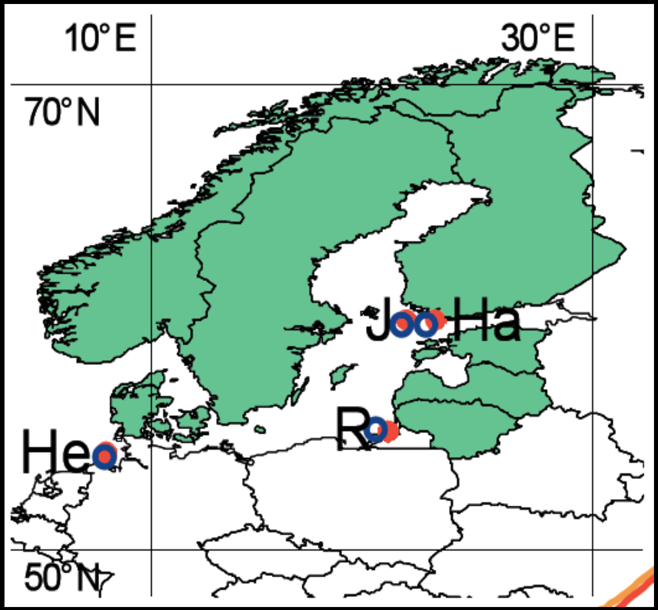

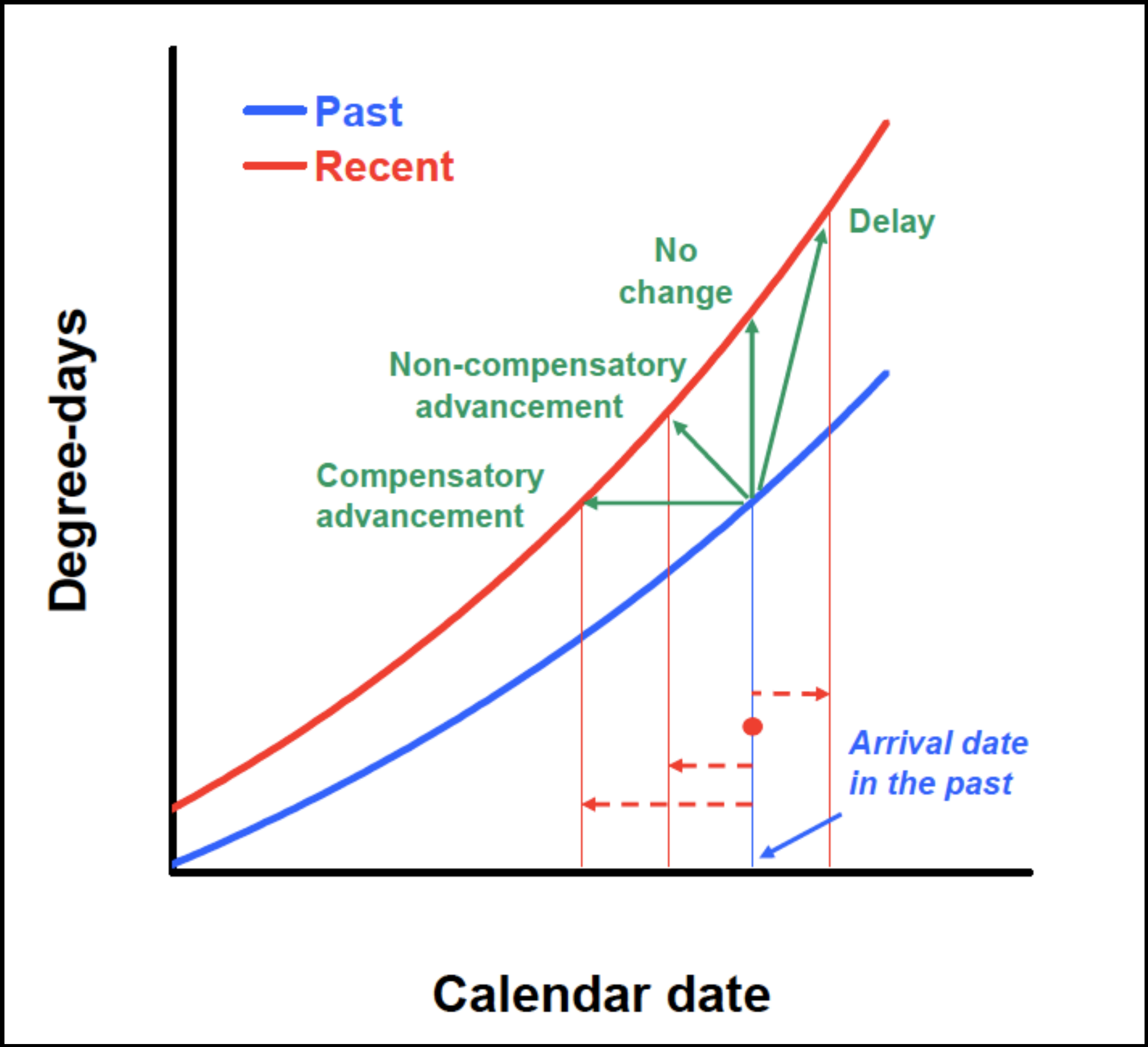

N. Saino, R. Ambrosini, D. Rubolini, J. von Hardenberg, A. Provenzale, K. Hüppop, O. Hüppop, A. Lehikoinen, E. Lehikoinen, K. Rainio, M. Romano, L. Sokolov, 2010. Demographic consequences of increasing ecological mismatch at arrival in migratory birds. *Sub judice.*

Impacts on environment and ecosystems: northward range expansion

insect pests and birch forests

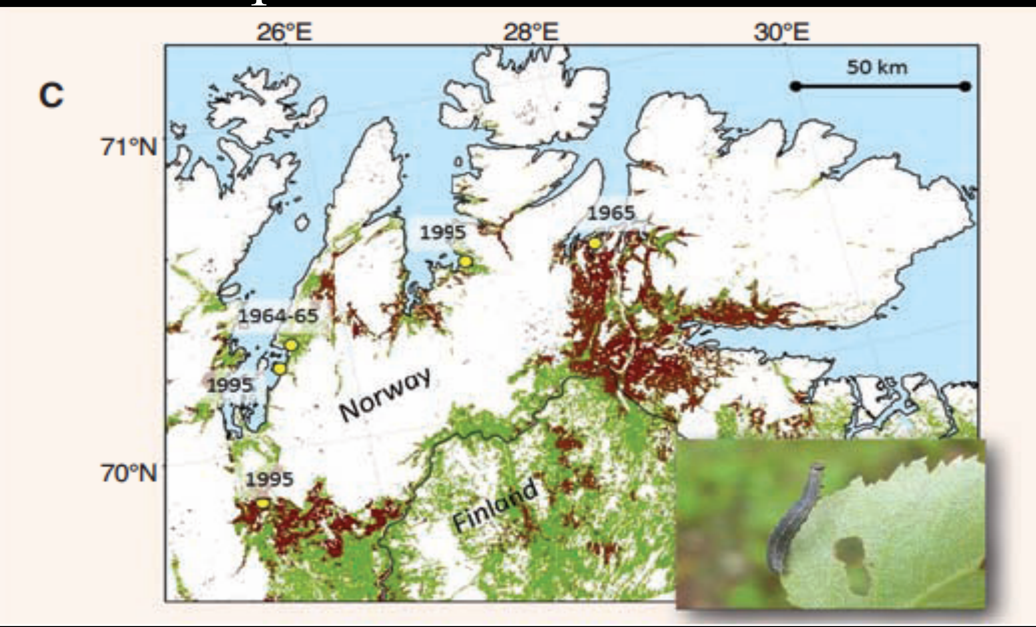

J. U. Jepsen, S. B. Hagen, R. A. Ims, N. G. Yoccoz, *J. Anim. Ecol.* **77**, 257 (2008).

from Sturm et al. 2001

shrub expansion,
with feedback on climate
(albedo, evapotranspiration)

E. Post et al, 2009. Ecological Dynamics Across the Arctic Associated with Recent Climate Change. *Science, 325, 1355.*

Permafrost temperature increase

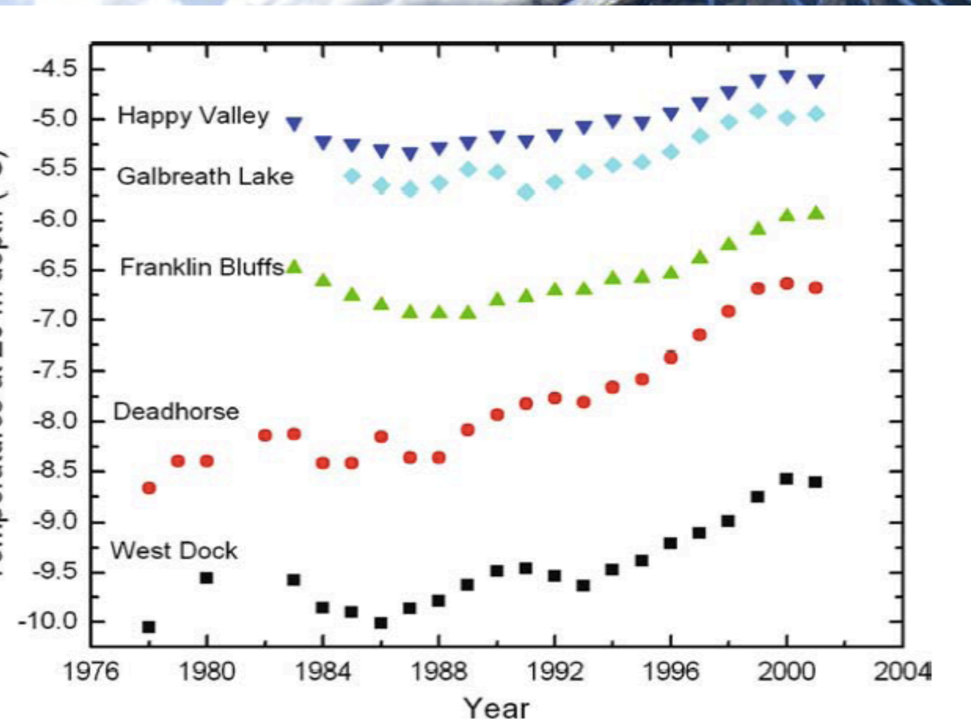

from Osterkamp 2003

Permafrost thawing has profound impact on human activities: transport, infrastructures, traditional and industrial activities

and: methane emission from thaw lakes

Walter et al. *Nature* 2006

Photo credit: www.swisseduc.ch

Larger variability and unpredictability of Arctic meteoclimatic conditions: impact on traditional and industrial activities

Hinzman et al., *Climate Change* 2006

Predictability of Arctic climate variability: the Arctic Oscillation and midlatitude climate

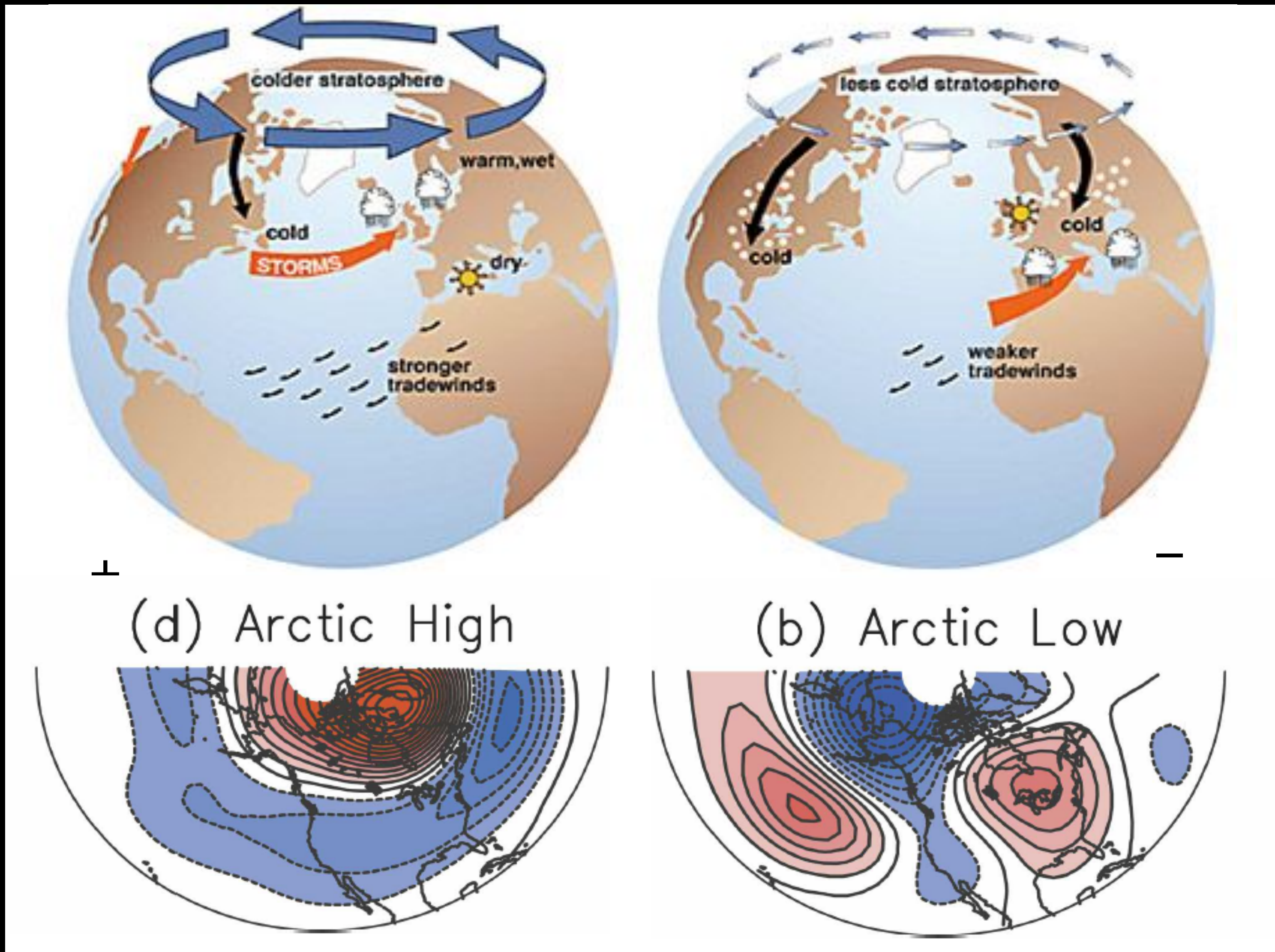

Straus, Corti, Molteni, *J. Climate* 2007

Mountain regions are the world "water towers"

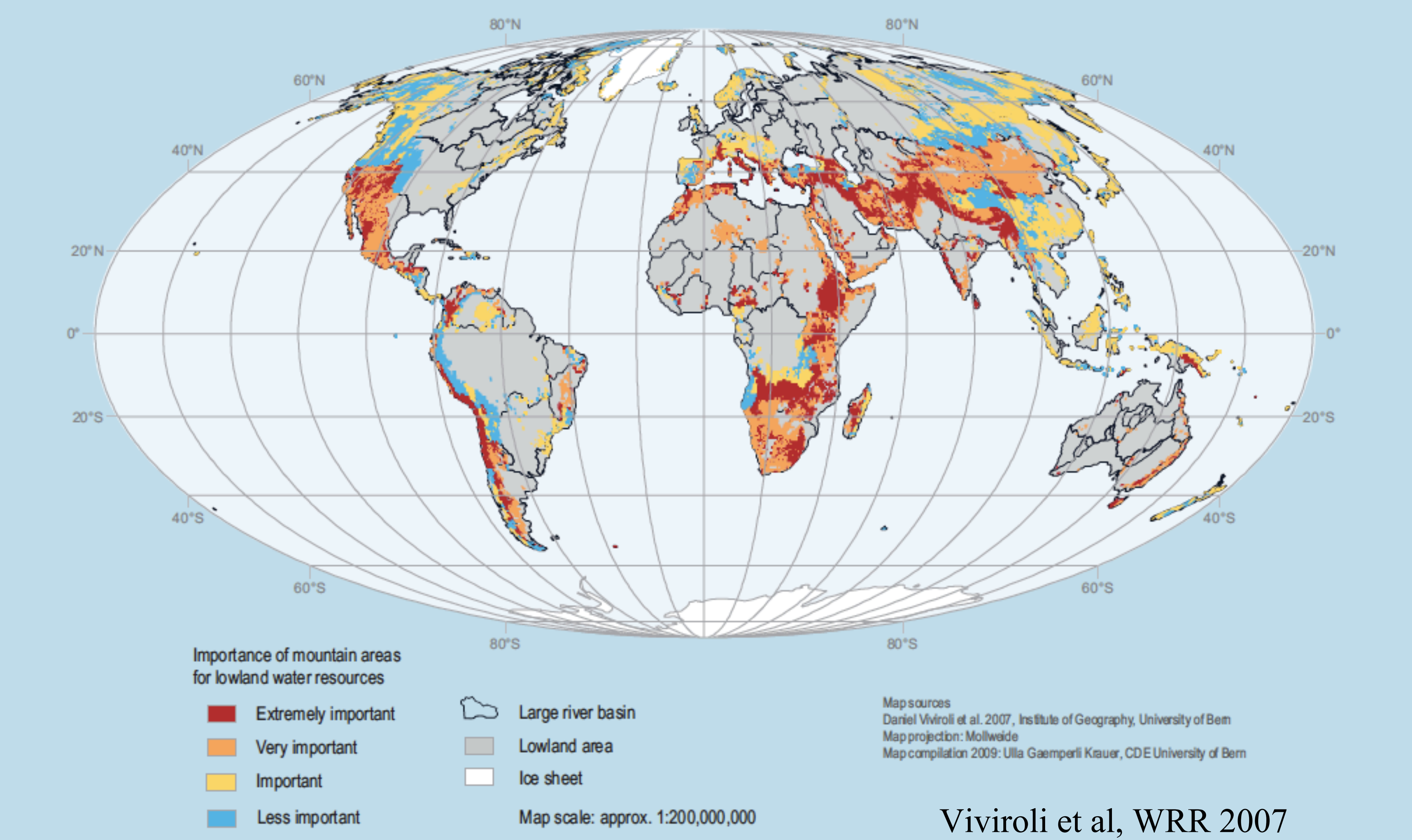

Viviroli et al, WRR 2007

Water availability in Hindu-Kush, Karakorum and Himalaya

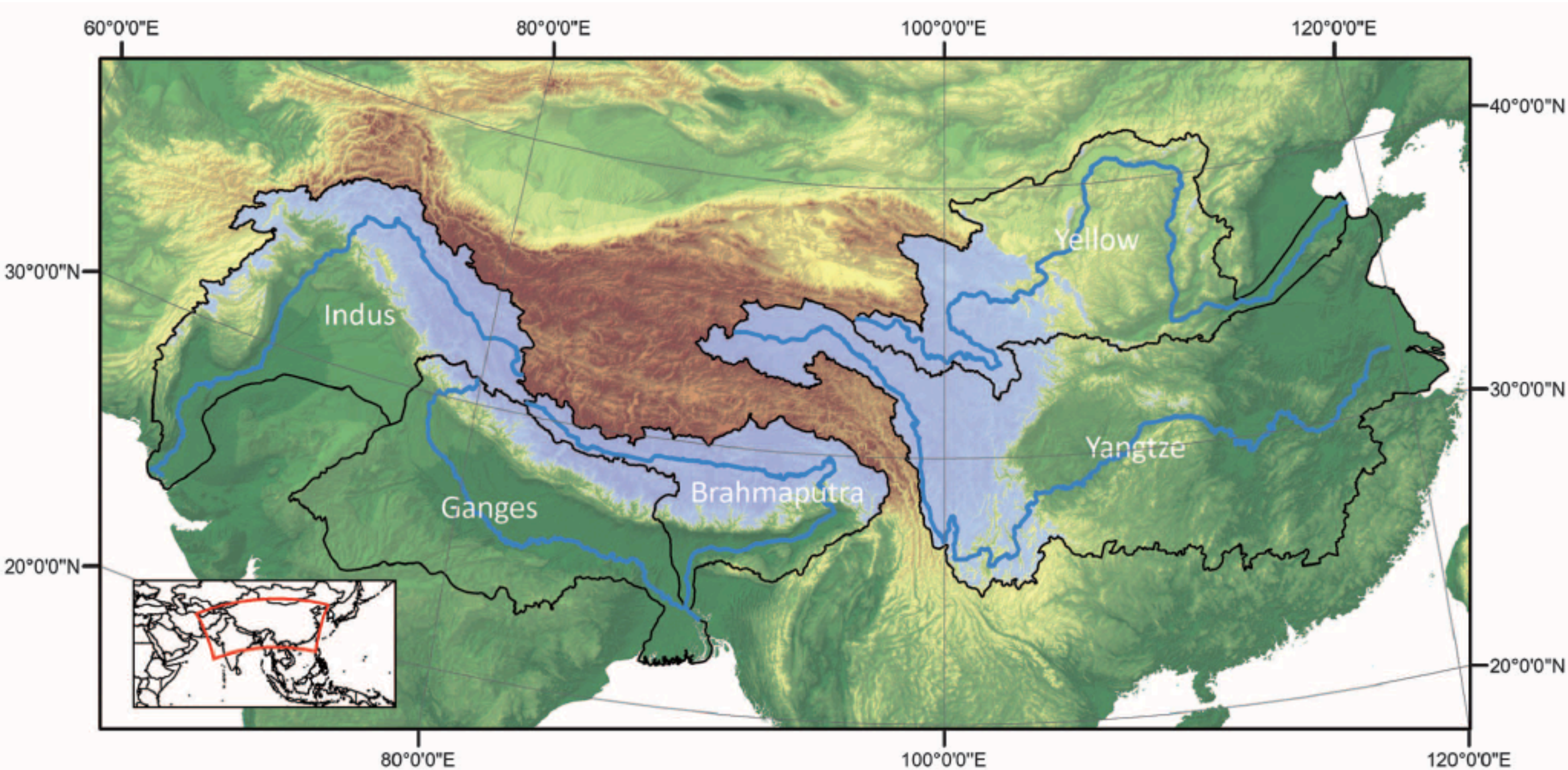

Immerzeel,van Beek, Bierkens, Science 2010

2. Water in the HKKH: Role of snow and glacier melt

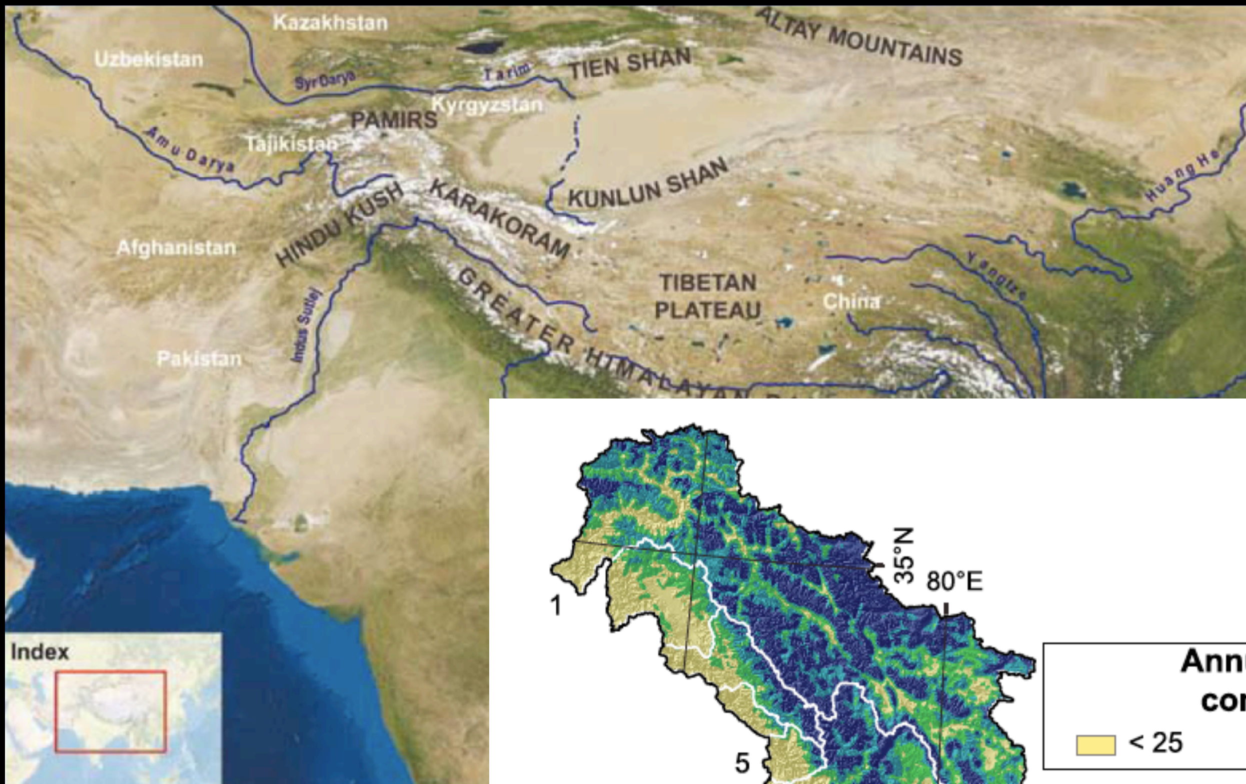

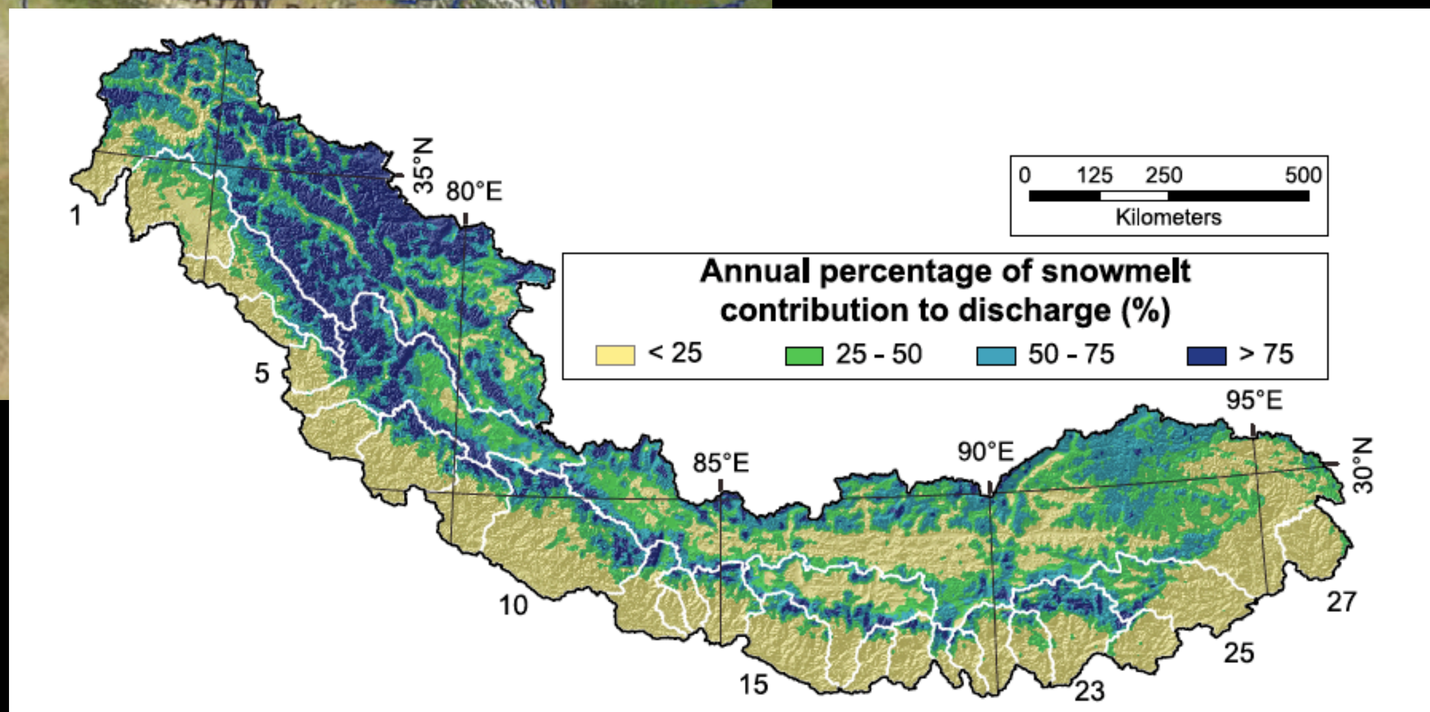

Bookhagen and Burbank, JGR 2010

Atmospheric Brown Cloud in Asia and aerosol load

Project SHARE – Ev K2 CNR

Nepal Climate Observatory – Pyramid (5079 m s.l.m.)

ISAC

EvK2CNR

Atmospheric Brown Cloud in Asia and aerosol load

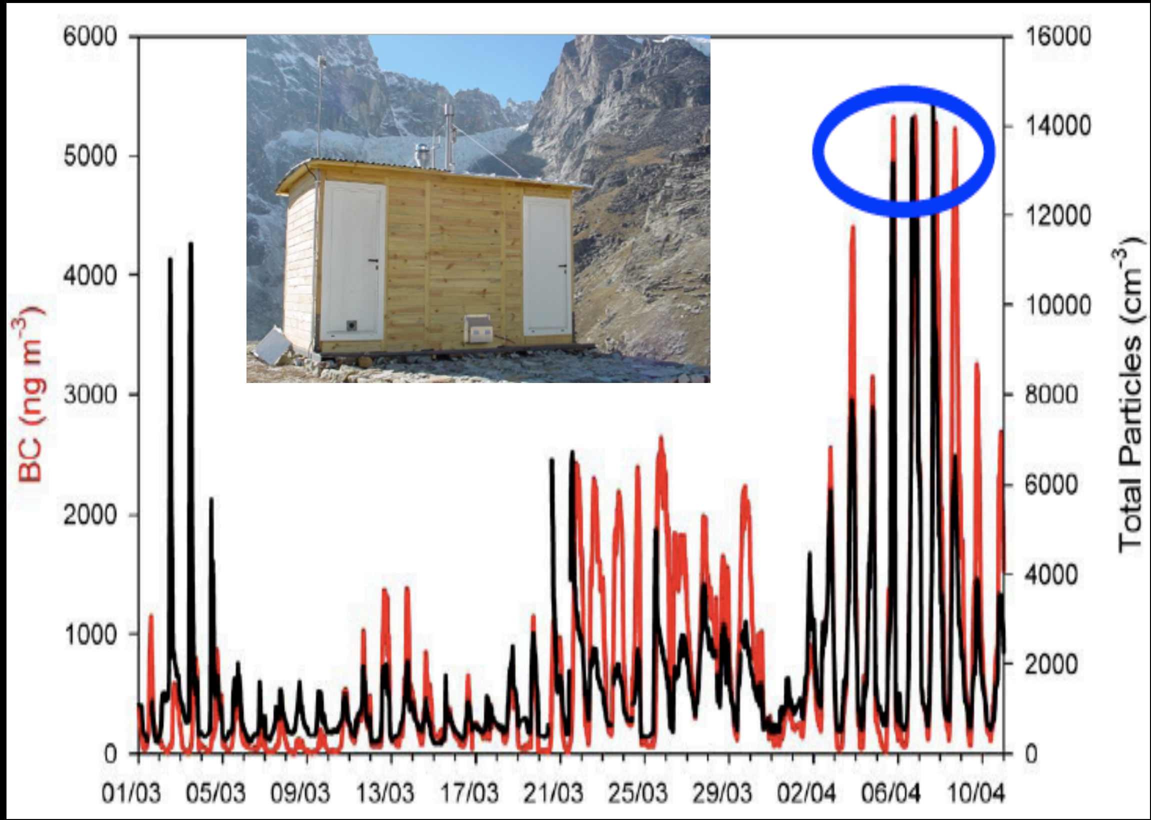

High Concentration of Black Carbon Observed in the High Himalaya

Bonasoni, Cristofanelli, Marinoni et al. BC Bullettin 2010

SHARE

Project SHARE – Ev K2 CNR
Nepal Climate Observatory – Pyramid

Comparison between data at the Pyramid (Nepal) And the Po plain (measured at Monte Cimone)

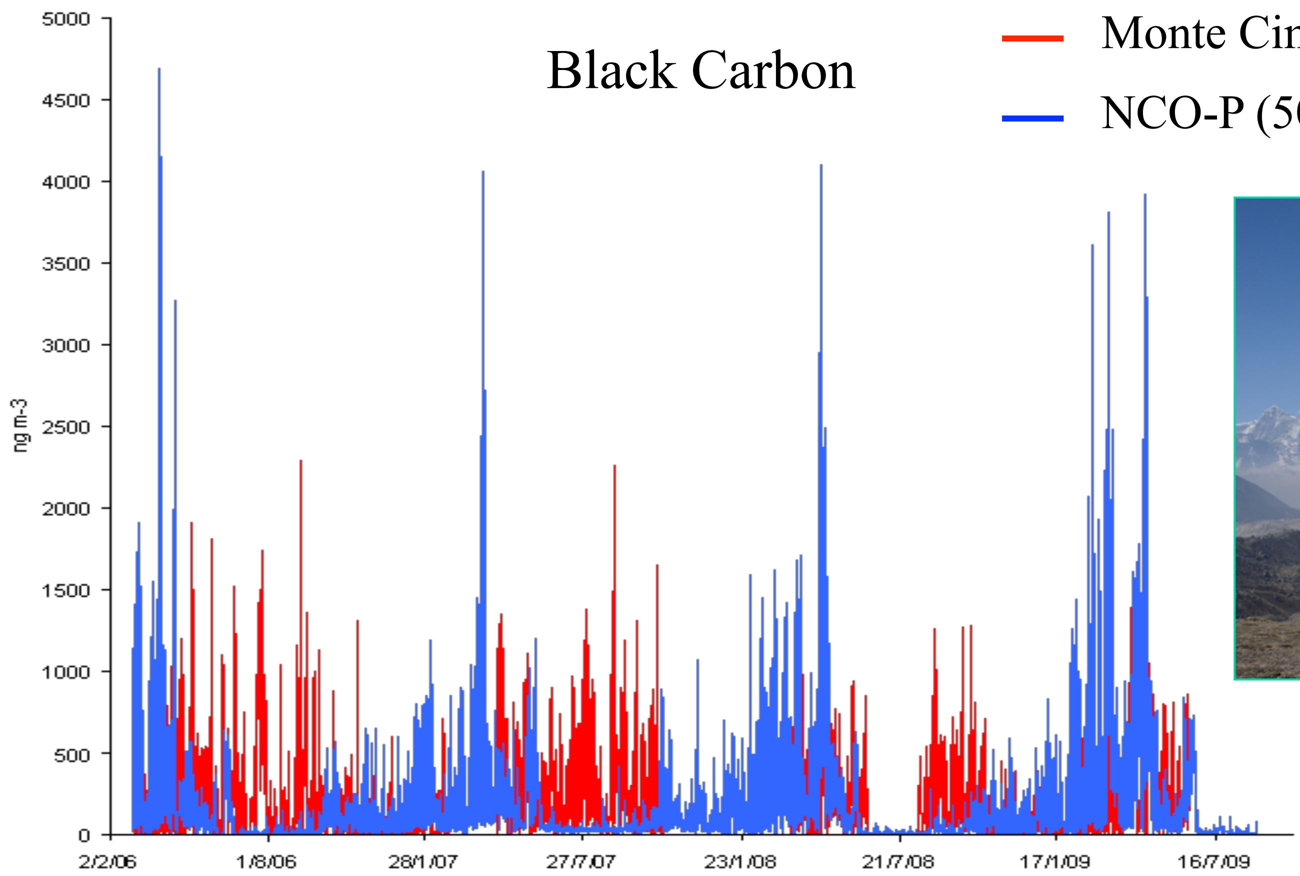

Effects of black carbon aerosols: direct (radiative), indirect (clouds) and deposition

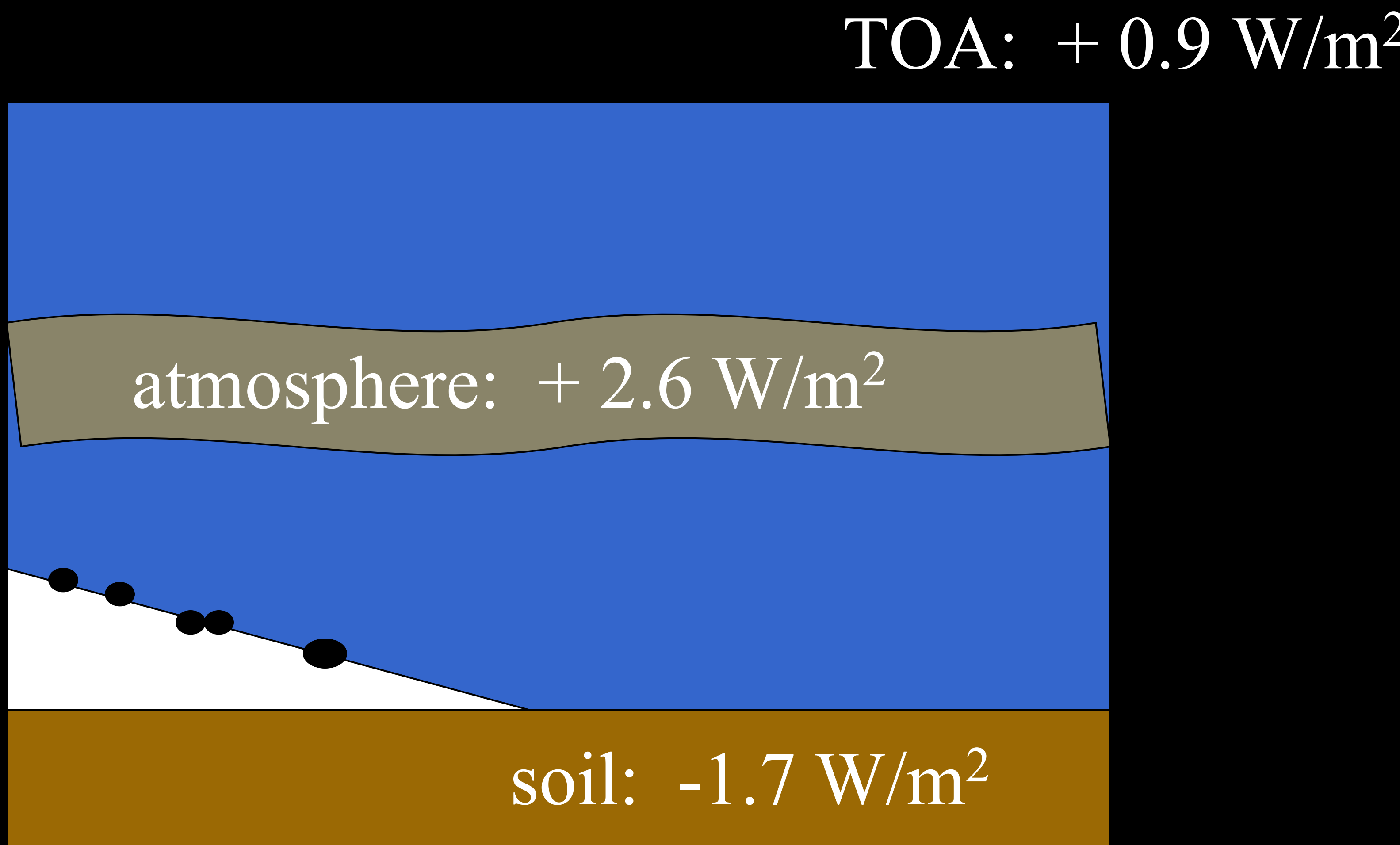

Aerosols and the Indian Monsoon:

Elevated Heat Pump mechanism
(Lau and Kim 2006)

versus

Solar dimming
(Ramanathan et al. 2005)

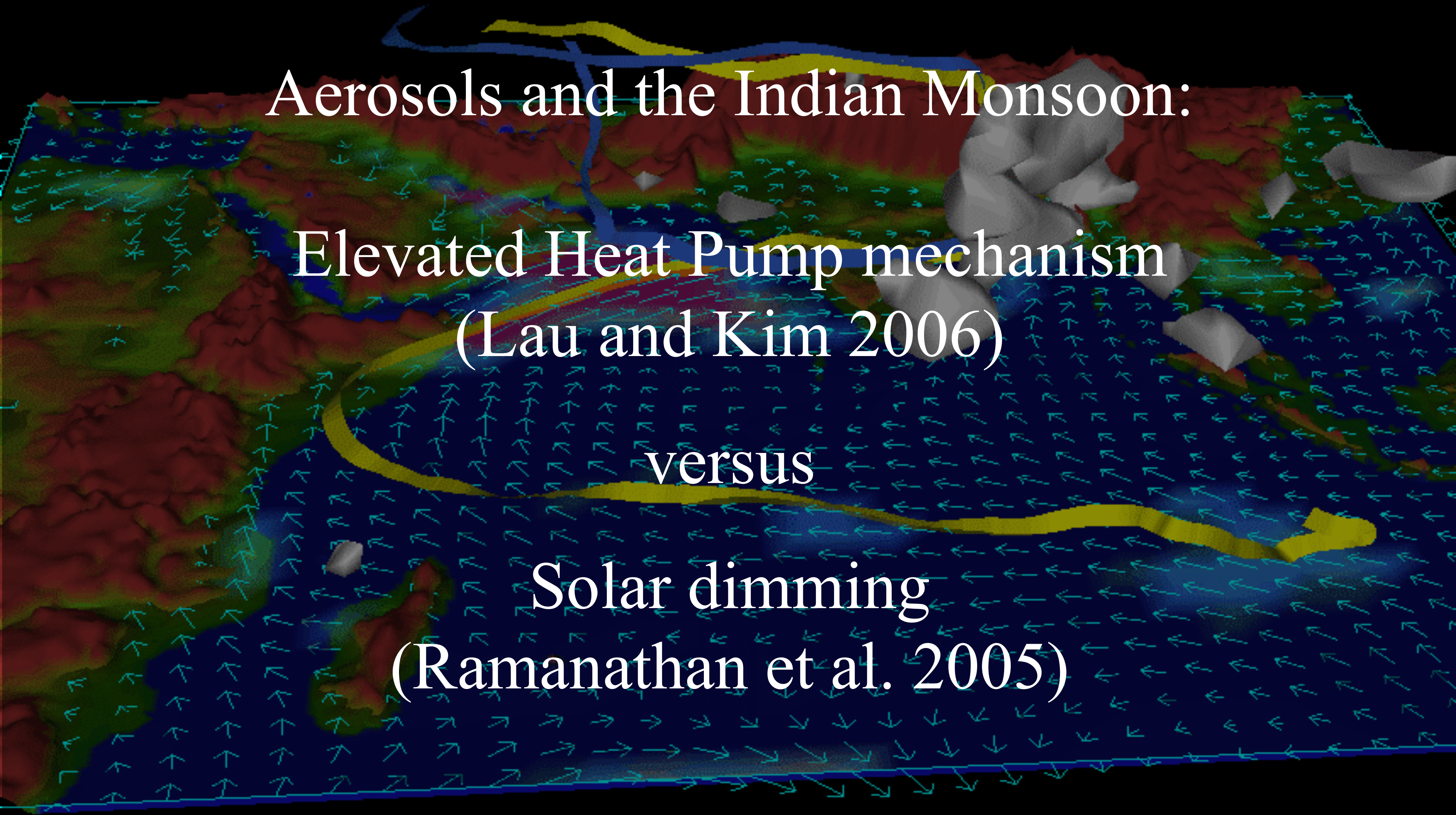

A hot topic: water availability in HKKH

Circulation patterns in the Hindu-Kush Karakoram Himalaya (HKKH) and the Indian Subcontinent

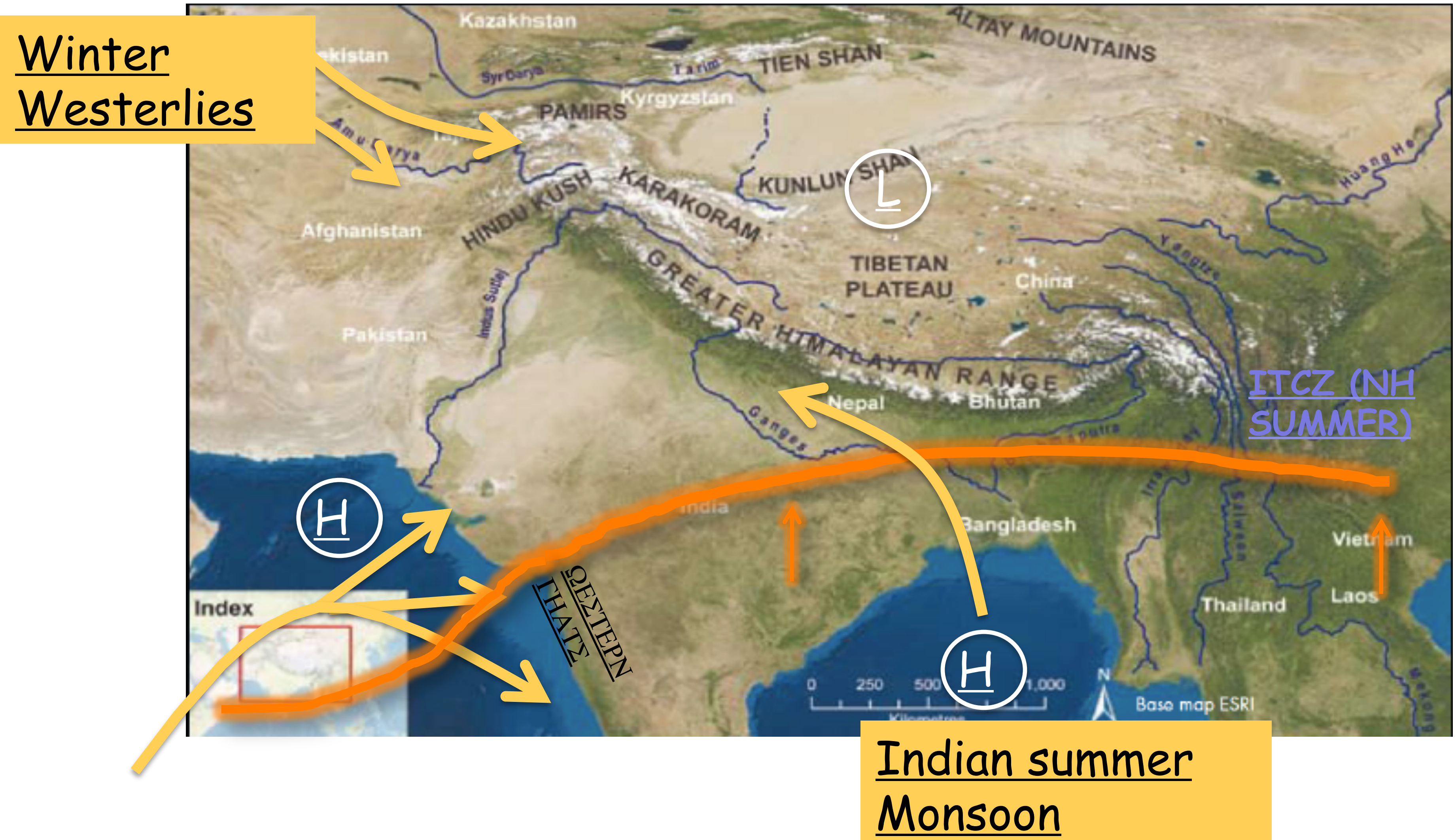

Circulation in the Indian Monsoon area

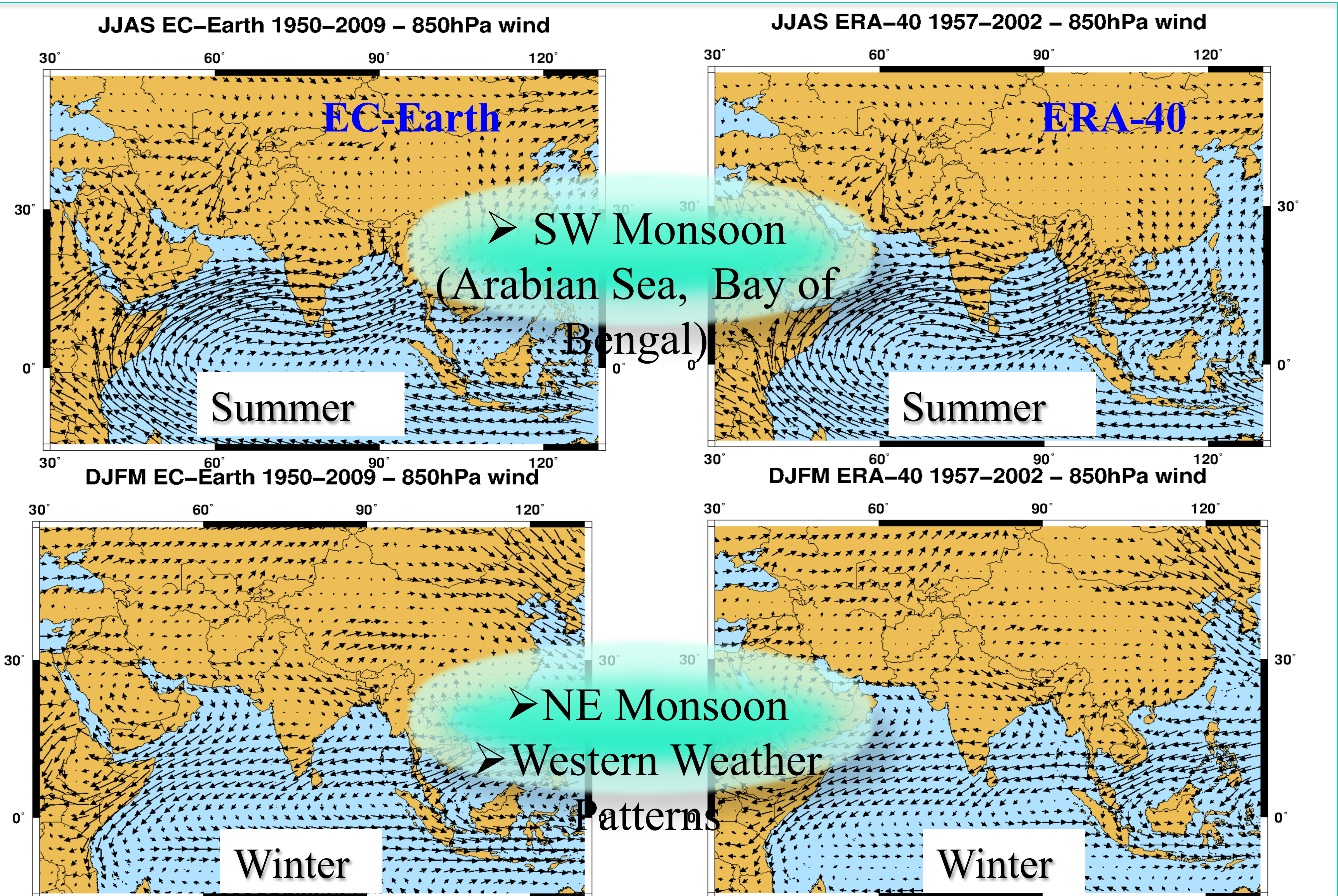

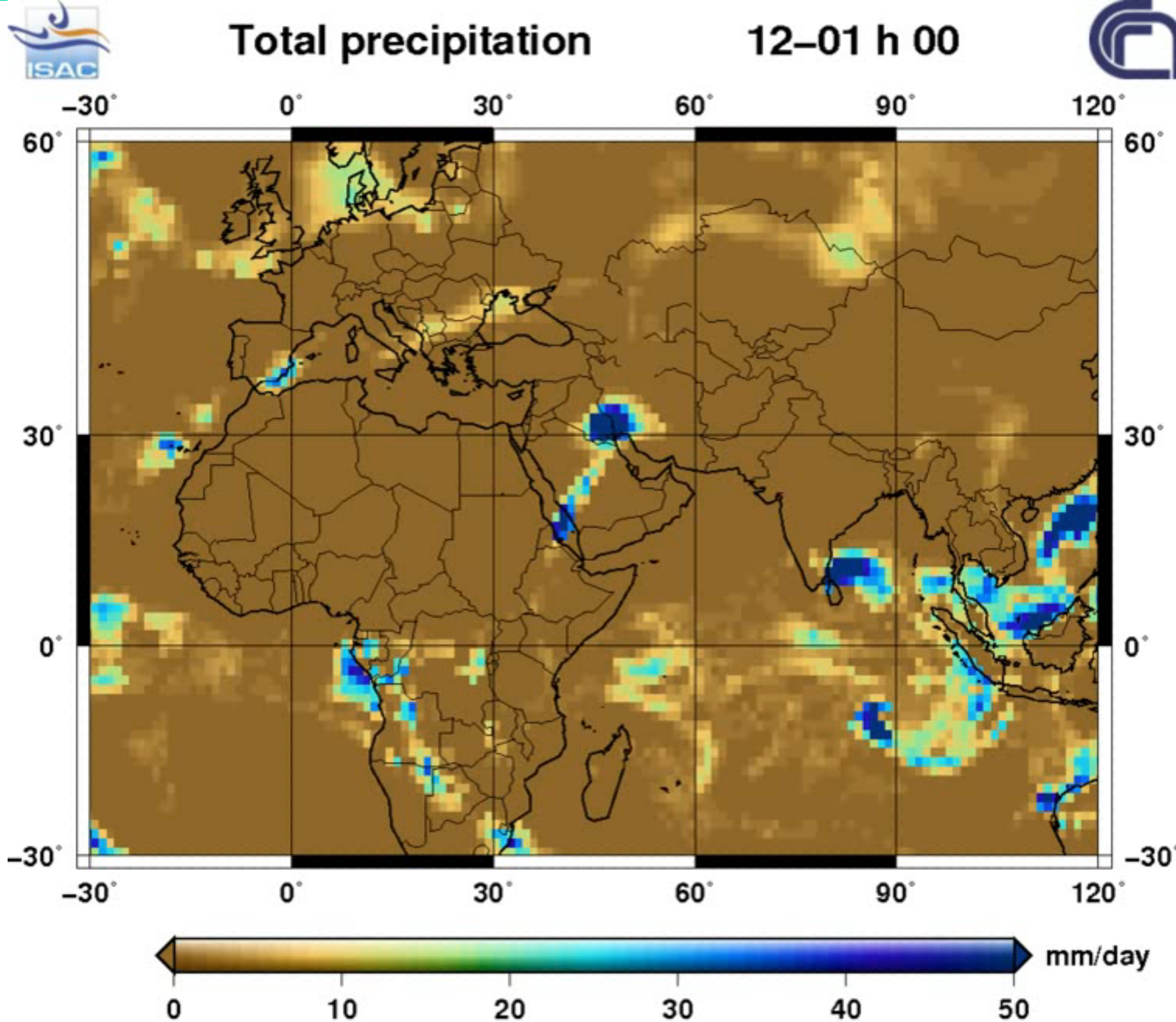

Total precipitation
12–01 h 00
ISAC
–30°
0°
30°
60°
90°
120°
60°
30°
0°
–30°
mm/day
0
10
20
30
40
50

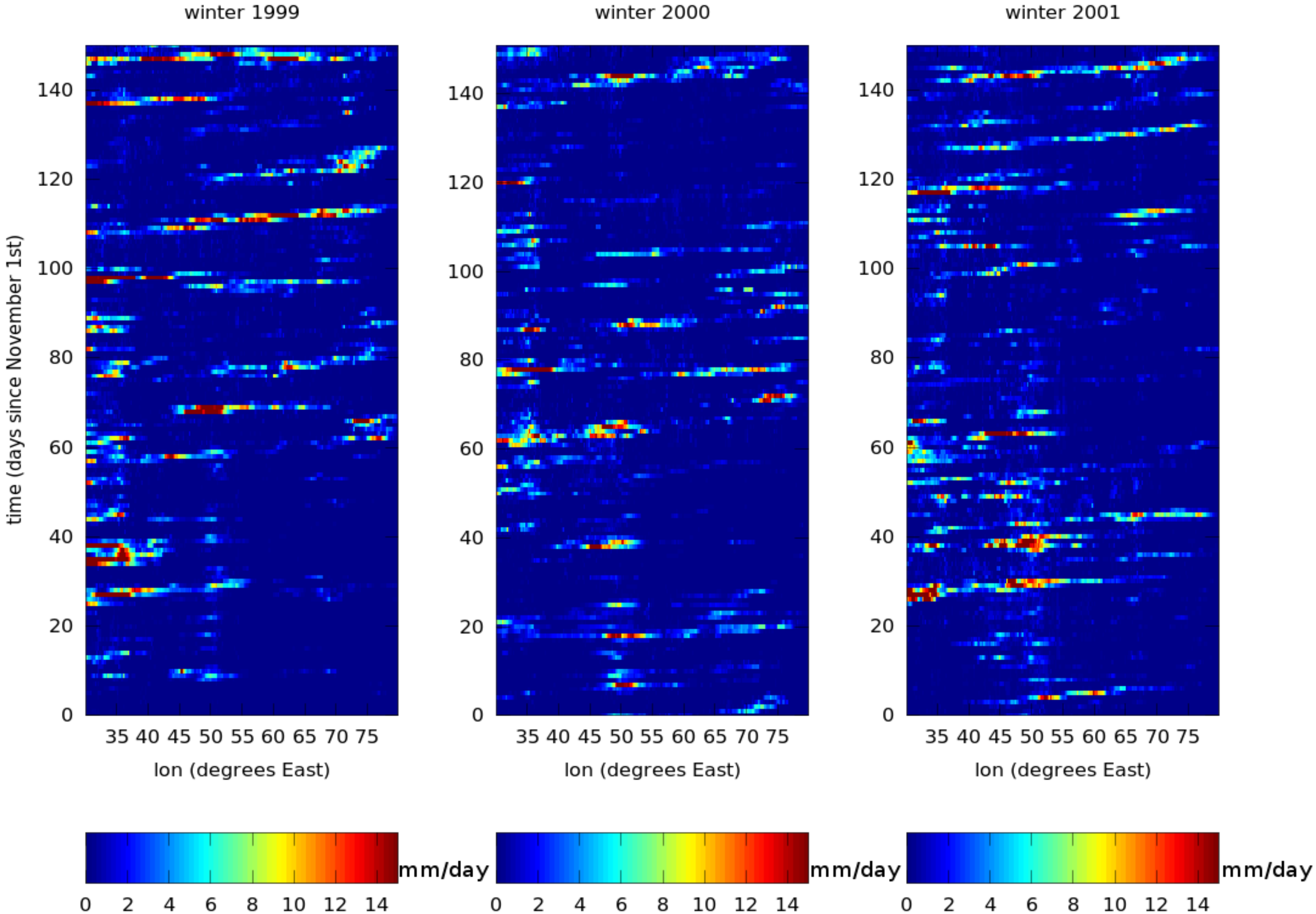

Figure 1.3.2 TRMM daily precipitation averaged over latitudes from 30°N to 40°N, plotted as a function of longitude (from 30°E to 80°E) and time for winters (NDJFM) 1999, 2000 and 2001 (left to right).

L. Filippi, Master Thesis

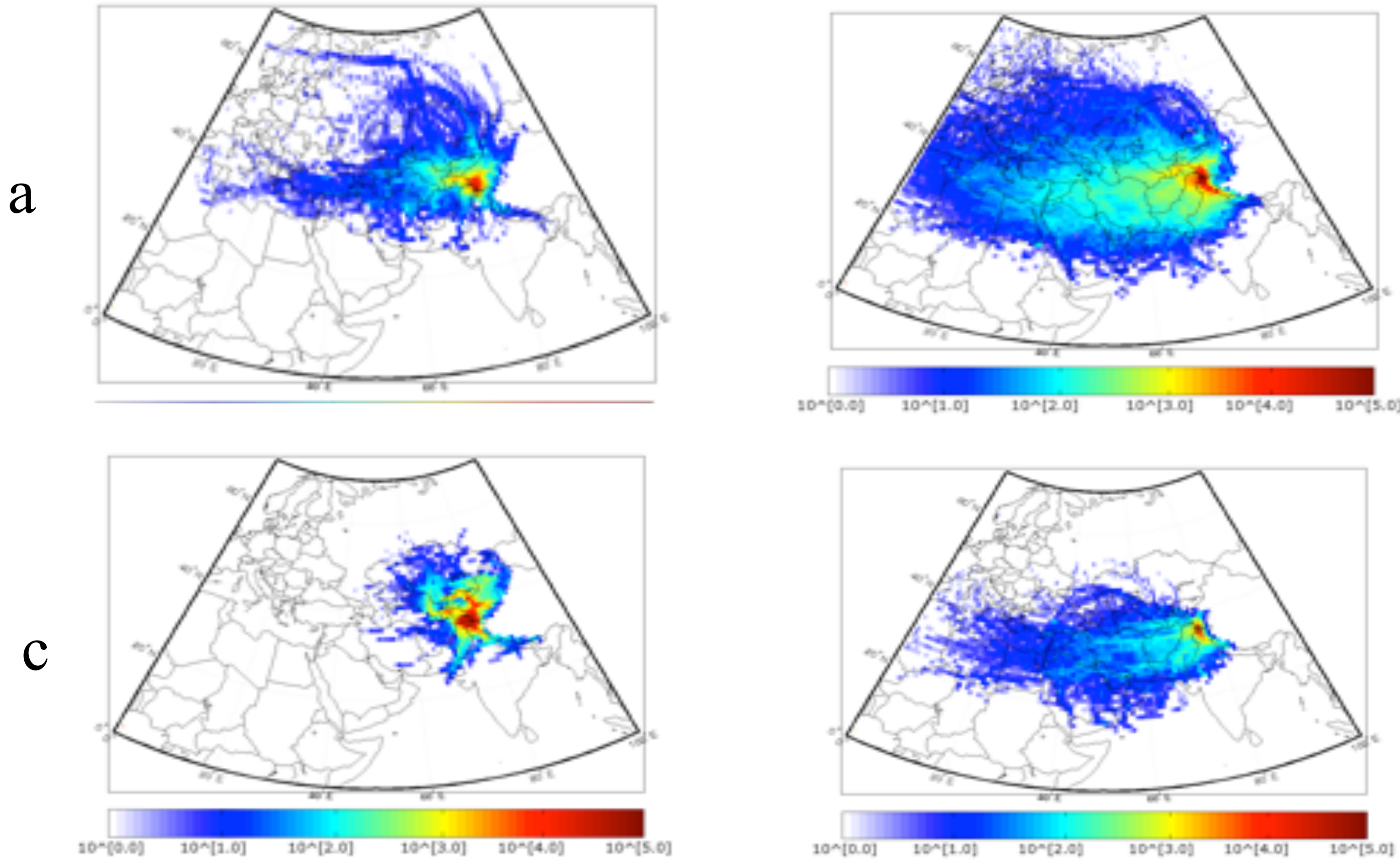

Air-mass back-trajectories describing the synoptic-scale atmospheric circulation in northern Pakistan. The coloured logarithmic scale indicates the number of back-trajectory points for summer (left column plots) and for winter (right column plots). a,b) back-trajectory ensembles for all events; c,d) back-trajectory ensembles associated to precipitation events over the target area.

Palazzi et al, sub judice 2013

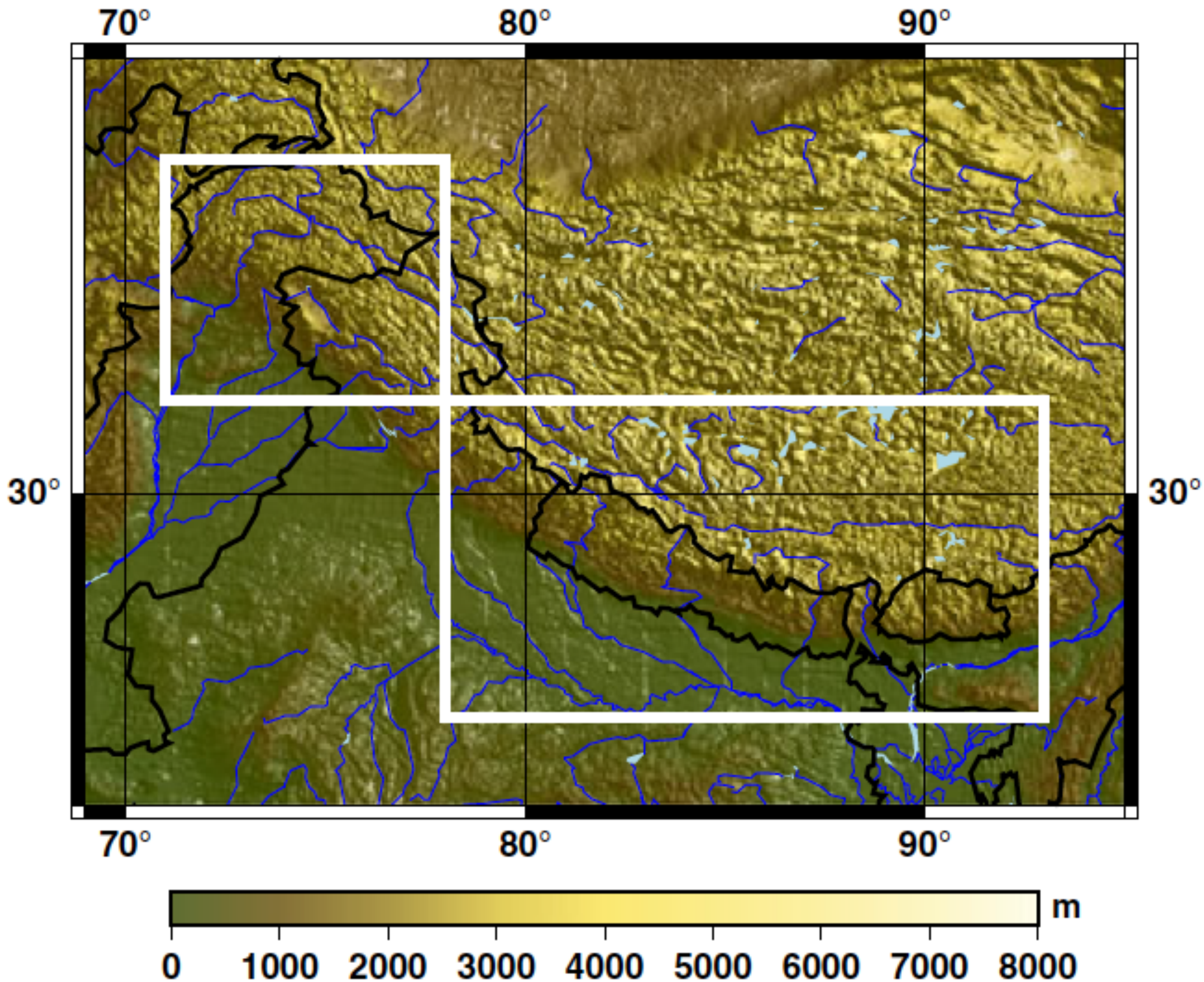

Figure 1. Map of the study area and the HKK (West) and Himalaya (East) domains.

Palazzi et al, JGR Atmosphere 2013

Precipitation datasets

Satellite

TRMM (Tropical Rainfall Measuring Mission)
1998-2007
3B42 product
3-Hour
0.25 x 0.25 ° (30x30 km) from 50°S-50°N.

Merged Satellite + in-situ

Global Precipitation Climatology Project (GPCP) NOAA
1979-2010
Version V2.2
Monthly means of precipitation derived from satellite and gauge measurements.
2.5°x2.5° from 88.75°S-88.75°N and 1.25°E-358.75°E

In-situ gridded

APHRODITE (Asian Precipitation - Highly-Resolved Observational Data Integration Towards Evaluation of Water Resources)
1951-2007
APHRO_MA (Monsoon Asia) _V1003R1 product
Daily precipitation datasets derived from rain gauges 0.25 x 0.25 ° in the domain 60°E-150°E, 15°S-55°N

Global Precipitation Climatology Centre (GPCC)
1901-2009
Gauge-based gridded monthly precipitation data sets 0.5° x 0.5°

Climate Research Unit (CRU)
1901-2009
TS 3.10 product precipitation
Monthly
0.5° x 0.5°

Reanalyses

ERA-Interim 1979-present, Daily, 0.75°x0.75°

Summer precipitation (JJAS), Multiannual average 1998-2007

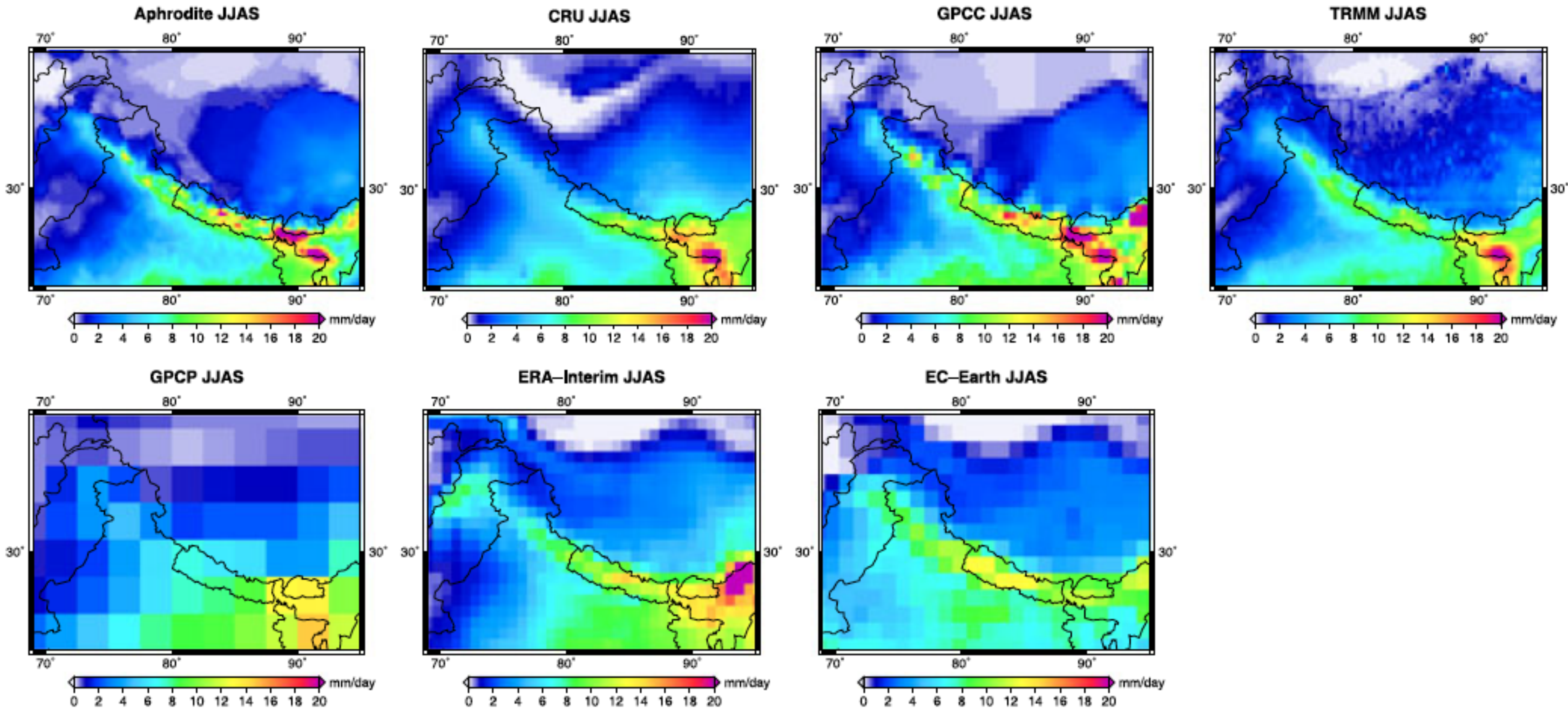

Figure 2. Multiannual mean (1998–2007) of summer (JJAS) precipitation over the region between 69°E–95°E and 23°N–39°N from the APHRODITE, CRU, GPCC, TRMM, GPCP, ERA-Interim, and EC-Earth model data sets.

Winter precipitation (DJFMA), Multiannual average 1998-2007

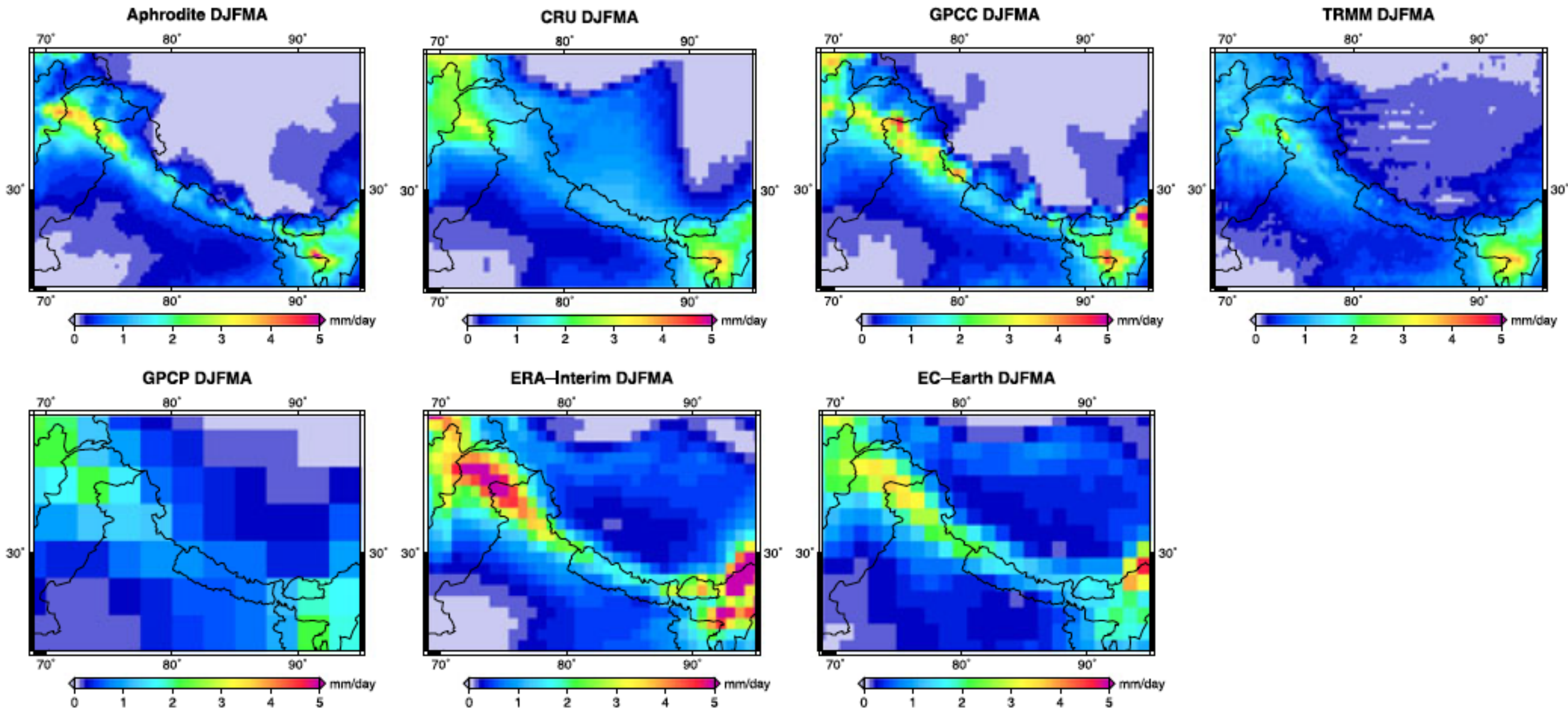

Figure 3. Same as Figure 2 for winter (DJFMA).

Precipitation seasonality in the HKK and Himalaya

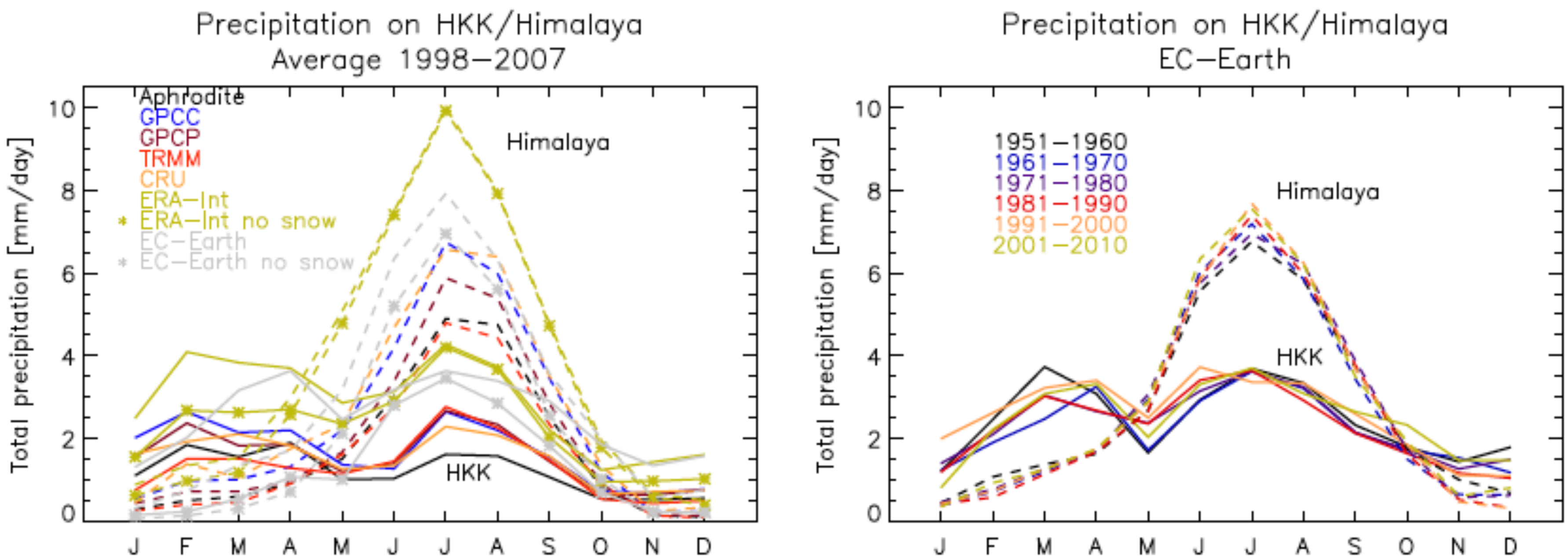

Figure 6. (left) Monthly climatology of precipitation (averaged over the period 1998–2007) for the HKK domain (solid lines) and the Himalaya domain (dashed lines), for the APHRODITE, GPCC, GPCP, TRMM, CRU, ERA-Interim, and EC-Earth data sets. The lines marked with stars indicate liquid precipitation only (obtained subtracting the snowfall flux from total precipitation for ERA-Interim and EC-Earth). (right) Mean annual cycle of precipitation in the HKK domain (solid lines) and Himalaya domain (dashed lines) from the EC-Earth model, averaged over different model decades as indicated in the figure legend.

Long-term trends

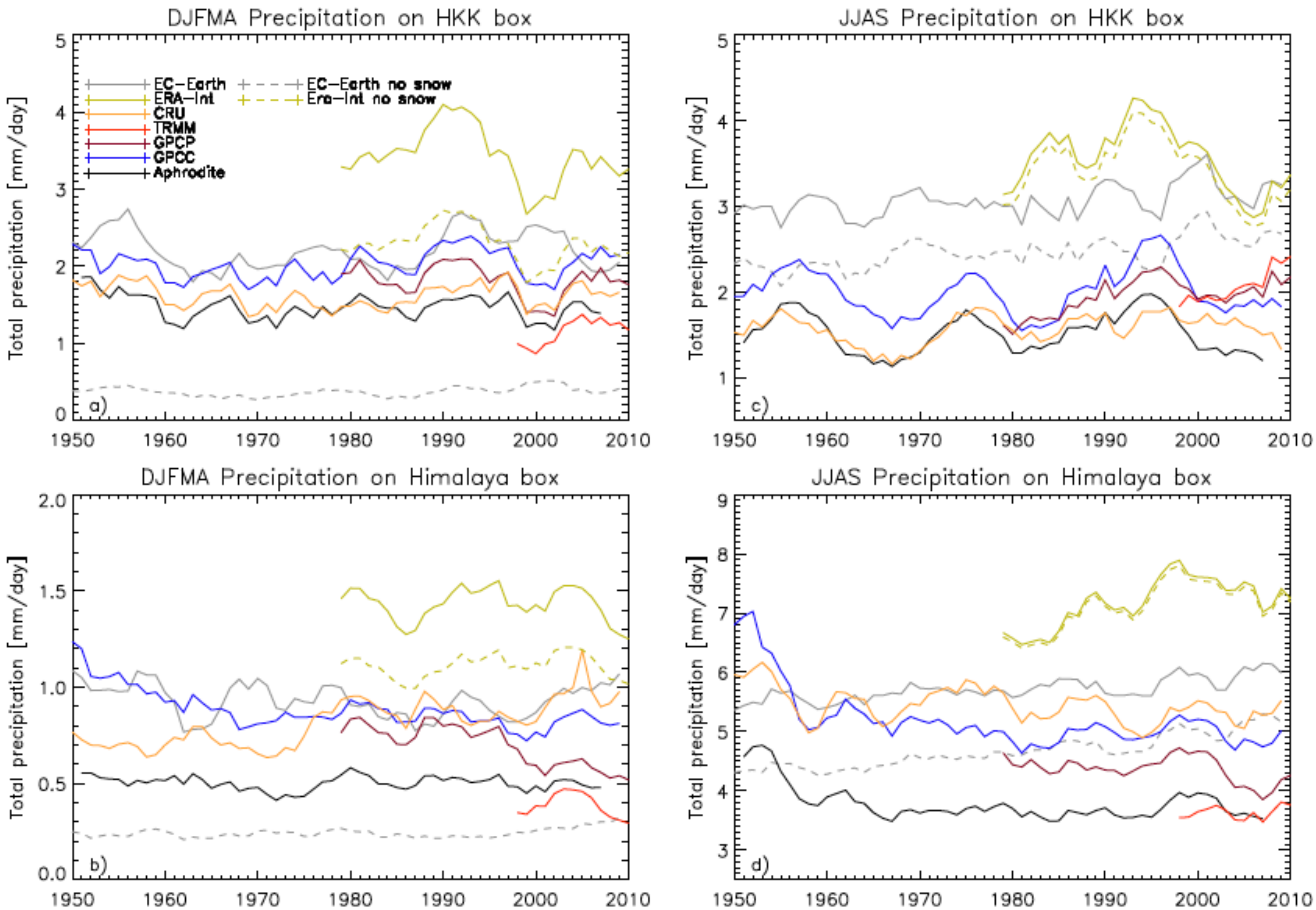

EC-Earth ensemble (8 members) over the Himalaya

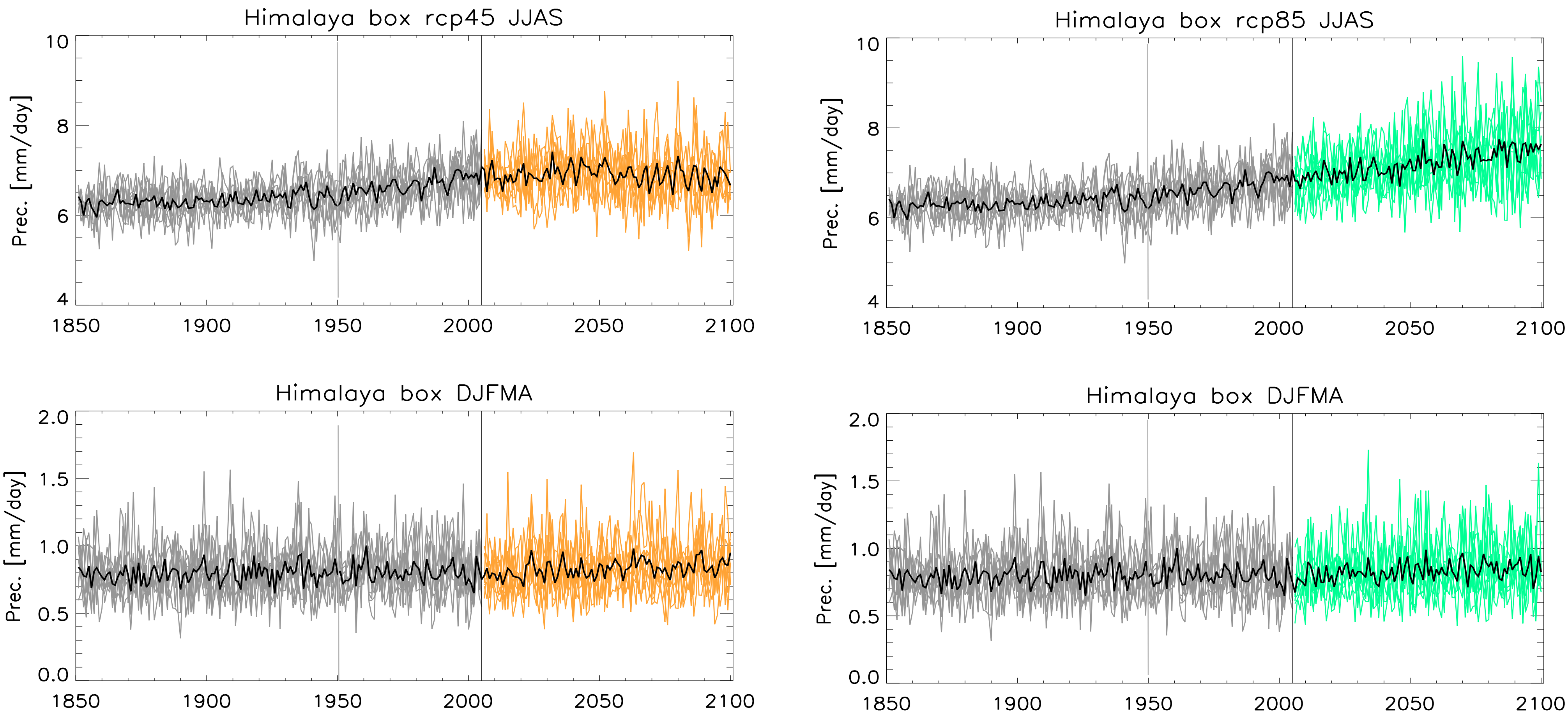

Significant trend during summer in the Himalaya: historical and RCP 8.5 scenario

EC-Earth ensemble (8 members) over HKK

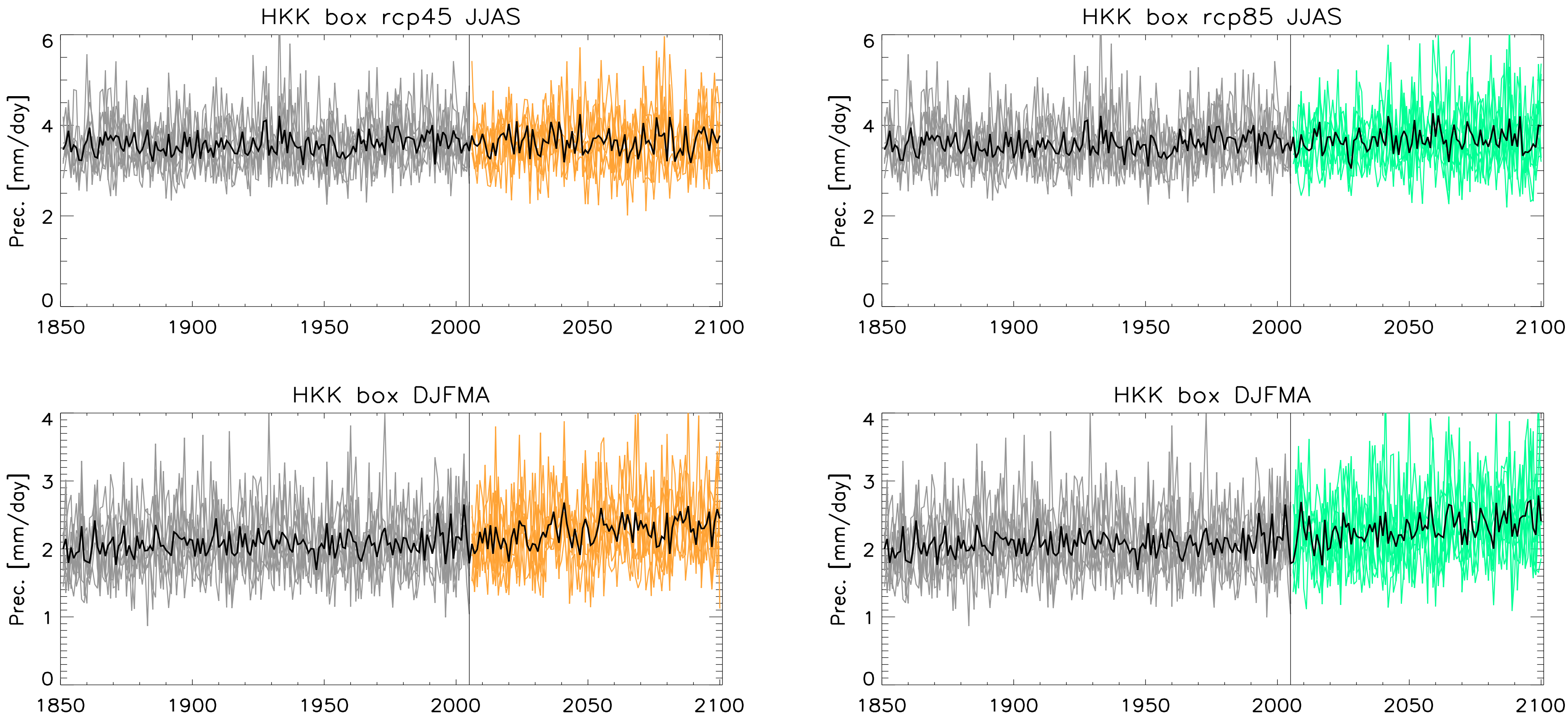

Remarks

o The HKK and Himalaya differ in circulation patterns, sources and types of precipitation. The HKKH cannot be treated as a single region

o Improvement in the monitoring of this area would require additional gauges going into the analysis and the capability to detect precipitation in solid form

To simulate regional climate
and the impacts of climate variability
one needs a zoom on the region of interest

Example: water resources in the Upper Indus Basin

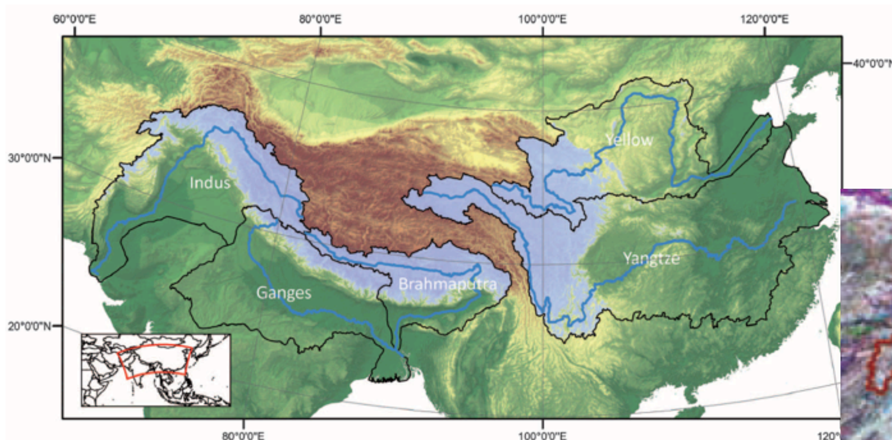

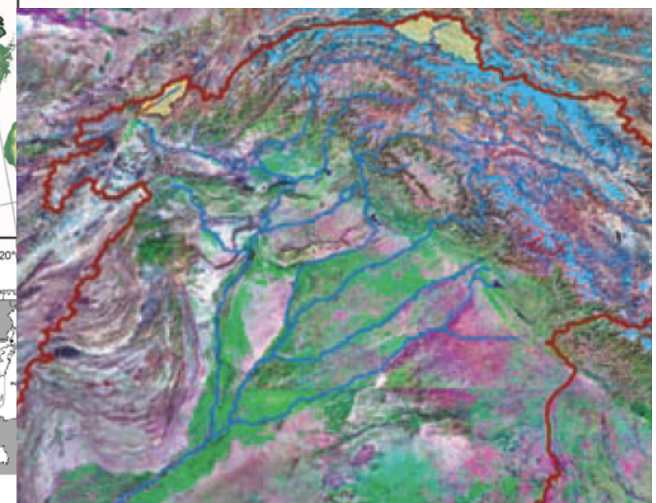

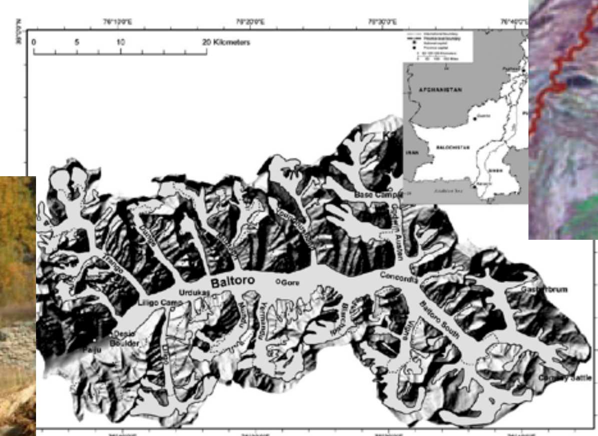

. Overview of the Baltoro drainage basin and the location of Baltoro glacier in Pakistan. The glacier as classified in this paper is shown ey on the background of the shaded digital elevation model. The main locations and glaciers are shown on the map. The 5000 m ur line is displayed as a dashed line.

Different options:

Dynamical downscaling:
nesting regional models into global models

High-resolution global models
(often, atmosphere-only)

Statistical/stochastic downscaling

PROTHEUS Model

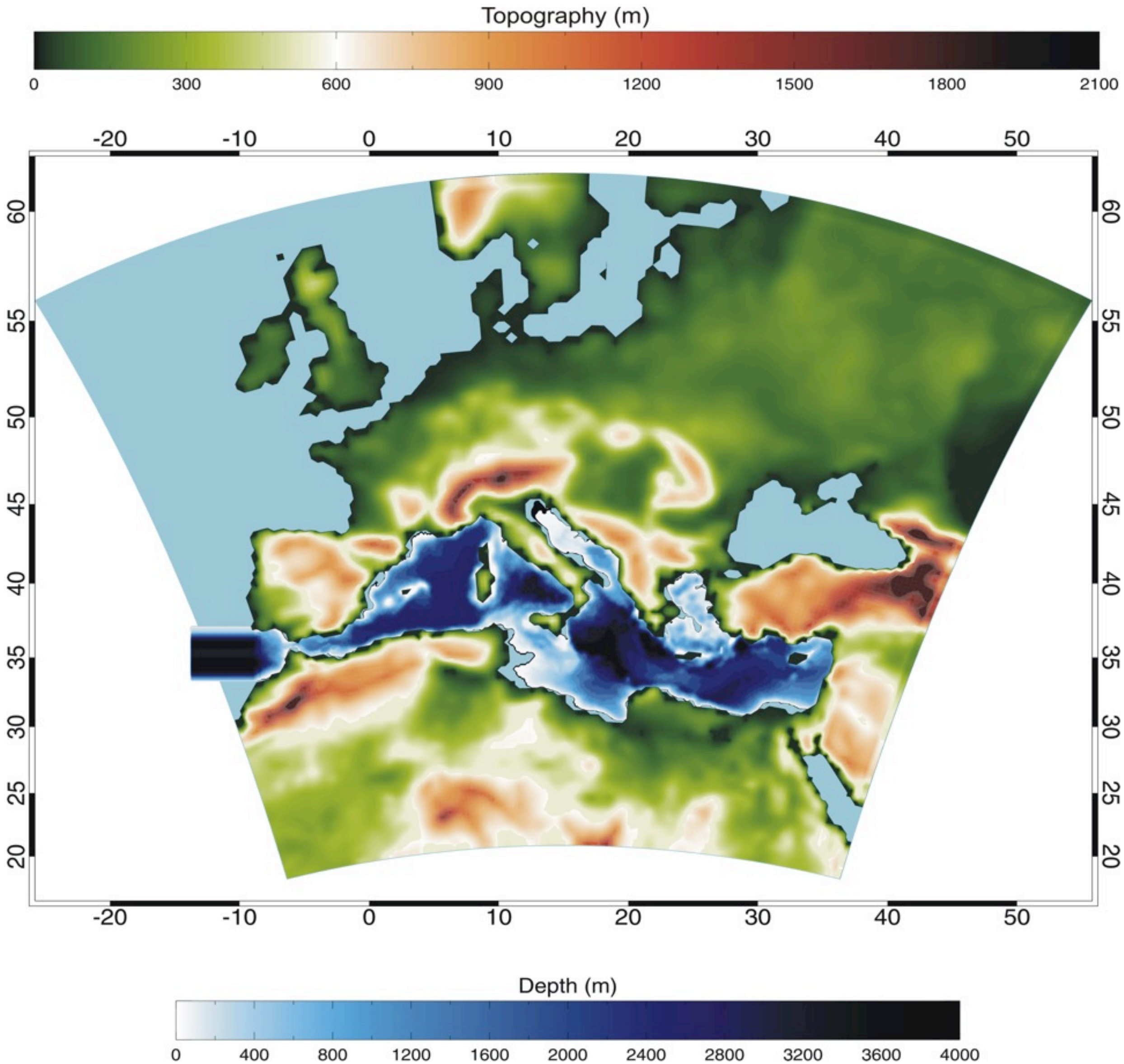

Model domain

Model components

RegCM3

18 sigma vertical levels

30 Km horizontal resolution

BATS + IRIS

BATS: **Biosph.-Atmosph. Transfer Scheme**

IRIS: interactive RIvers Scheme

SST

OASIS 3
Freq. 6h

HF-WF-Wind

MedMIT

42 zeta vertical levels (partial cell)

1/8° x 1/8° horizontal resolution

Run global atmosphere-only simulations
at resolution about 20 km

driven by an ocean
from a previous simulation
with coarser resolution

Scenarios on water availability

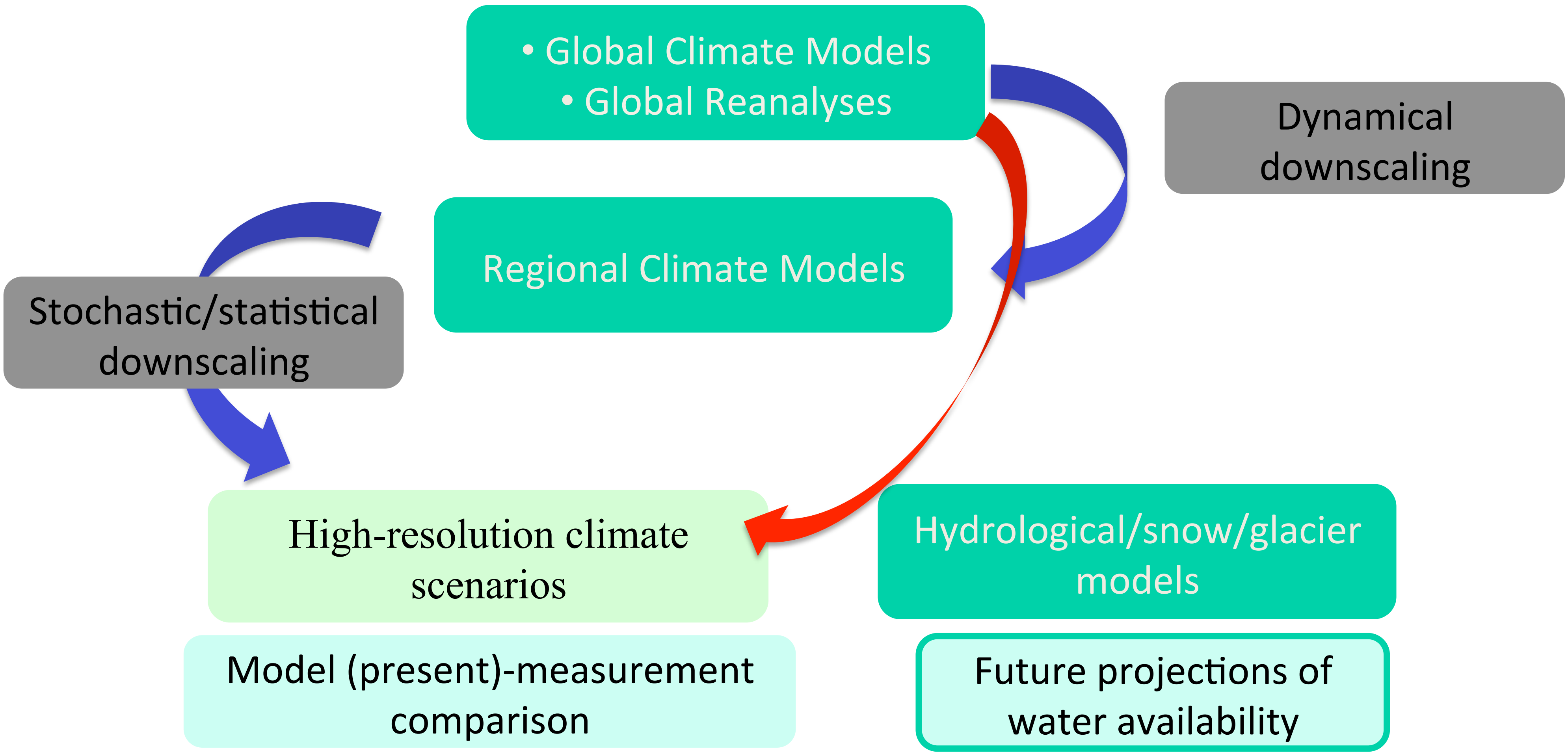

CIMA *Research Foundation*

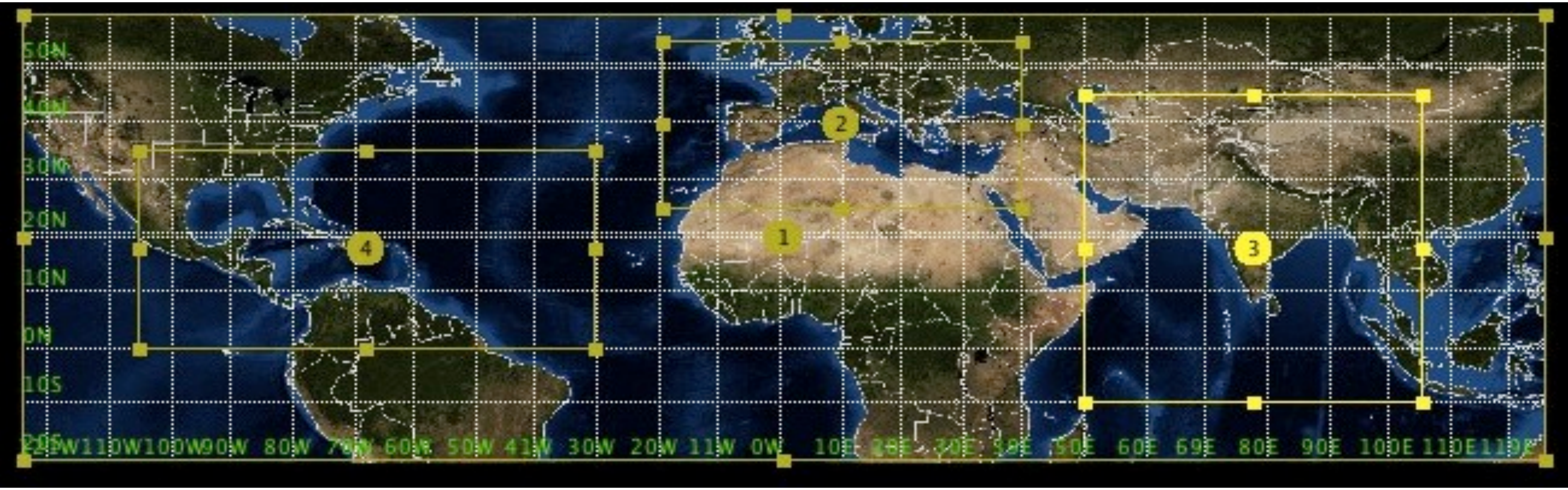

The GAUSS-EXPRESS Project (PI: A. Parodi):

The non-hydrostatic model WRF

nested into ERA-Interim and EC-Earth

42 Million hours of CPU time

Spatial resolution: 3.5 km

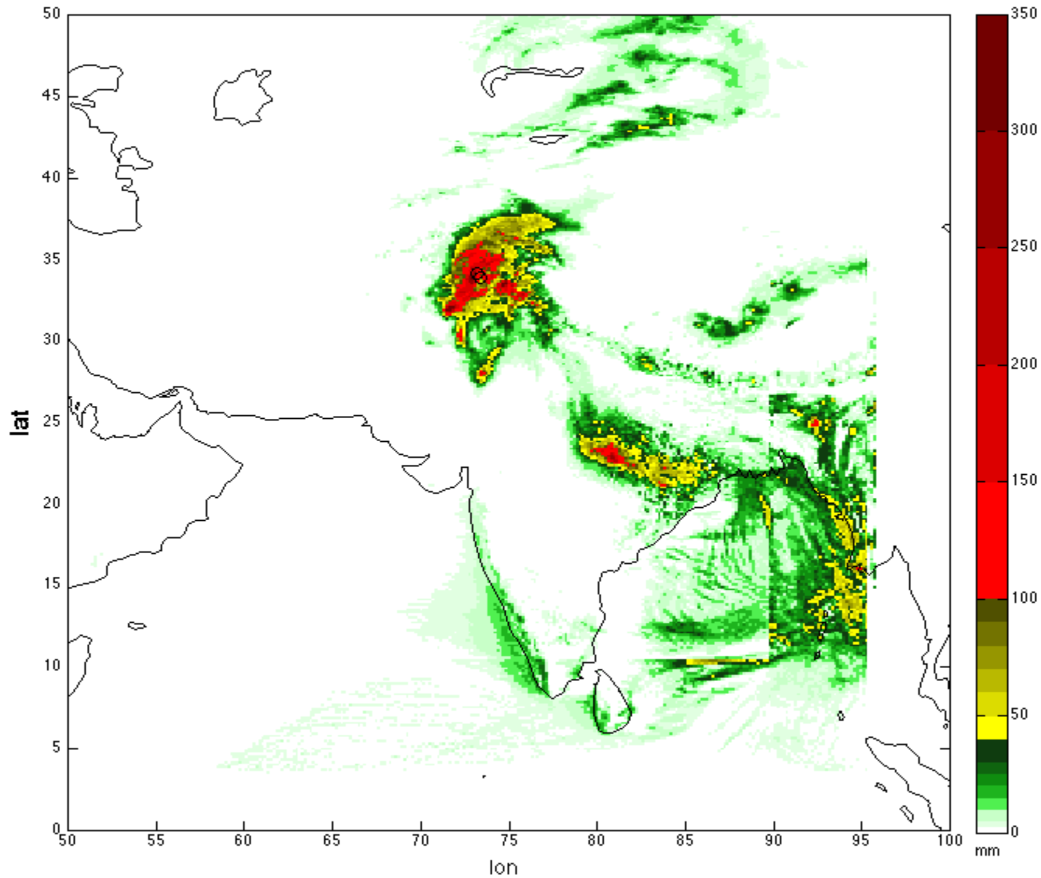

Rain event on 9-10 Sept 1992
Simulation with WRF model,
©Antonio Parodi, CIMA Foundation

Stochastic downscaling as a method to generate the statistic of extreme events

D. D'Onofrio et al, in preparation 2012

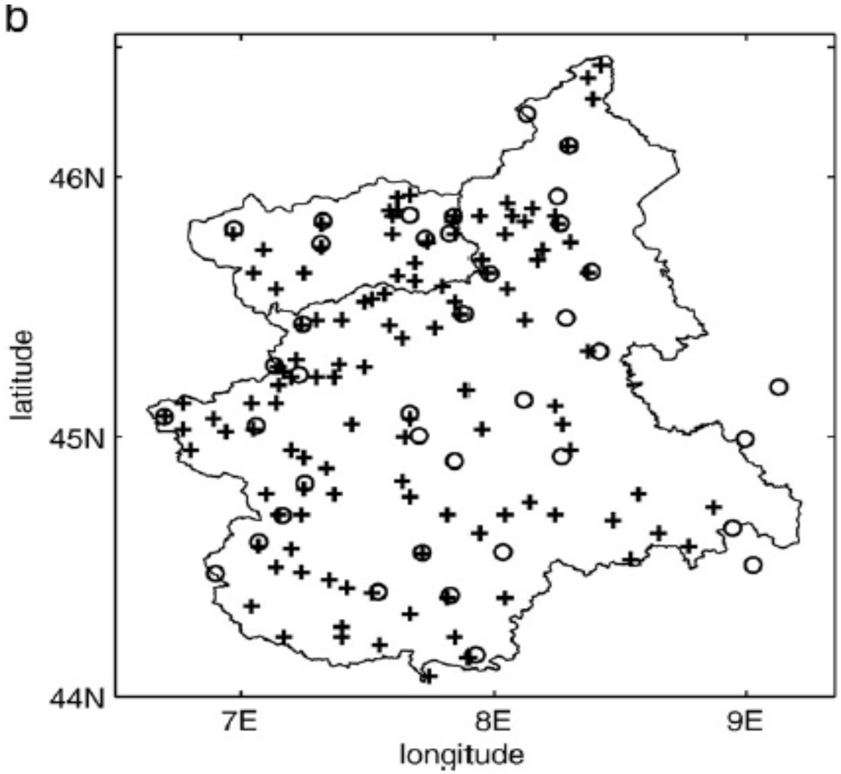

Ciccarelli et al,
Global Plan. Change 2008

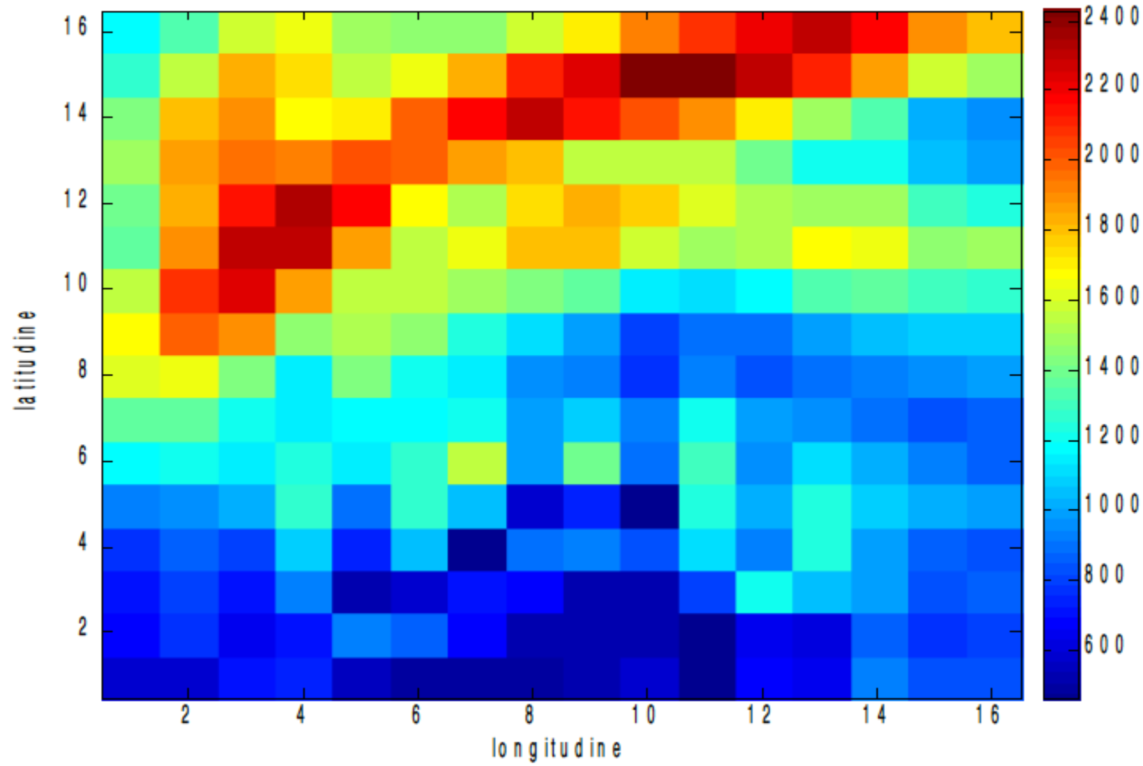

"*An Atmosphere-Ocean Regional Climate Model for the Mediterranean area: Assessment of a Present Climate Simulation*". The Protheus Group, Clim. Dynamics. 2009

Stochastic downscaling as a method to generate the statistic of extreme events

D. D’Onofrio et al, in preparation 2012

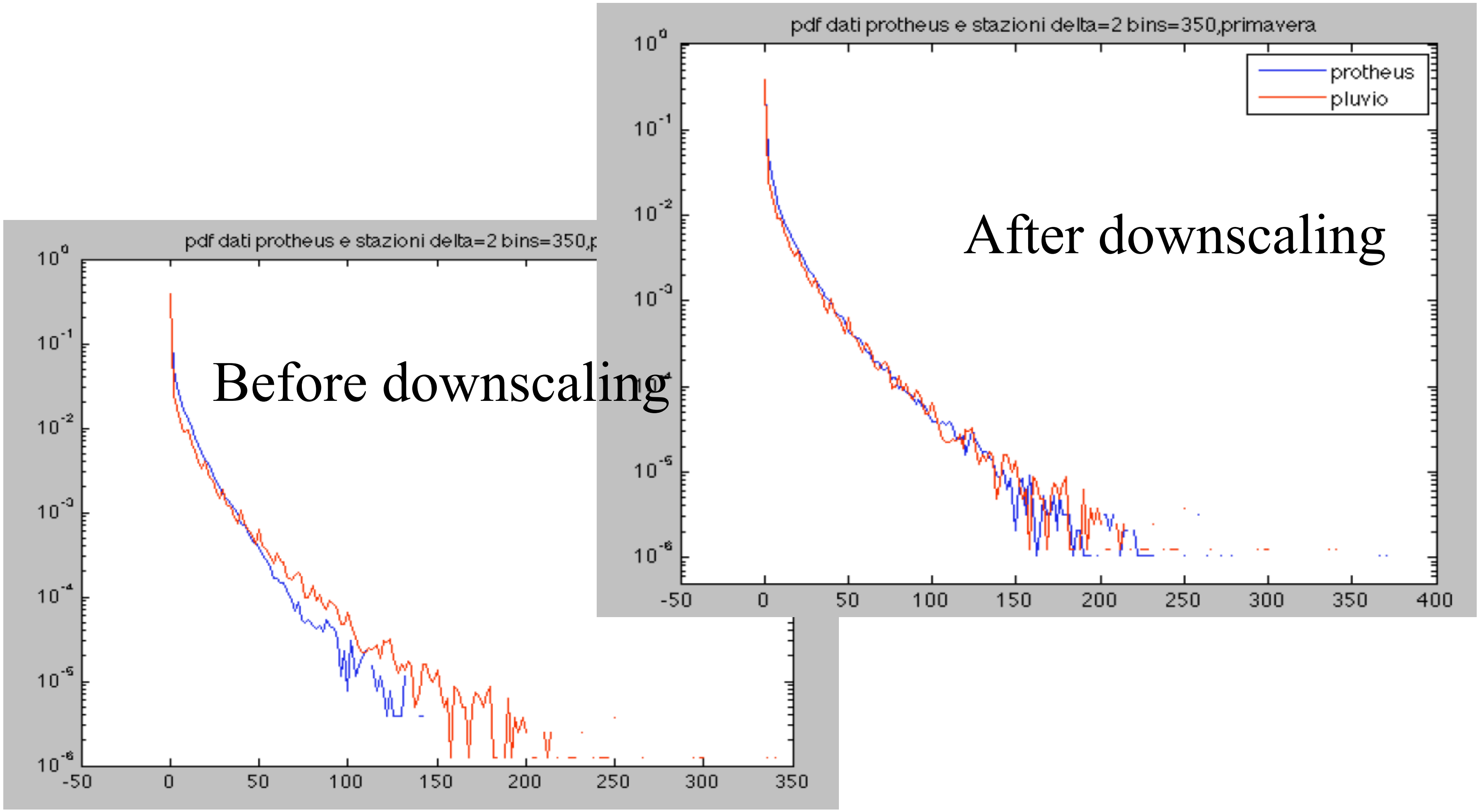

Then, empirical or dynamical models driven by the downscaled climate simulations

Rainfall-runoff
Glacier dynamics
Snow and permafrost
Ecosystem
Agriculture
Energy production
Economic models

Appendix: Stochastic rainfall downscaling for climate impact studies

The problem of scale: Mismatch between the resolution of climate models and the scales needed for impact studies

Downscaling approaches:

Dynamical downscaling

Regional Climate Models

(eg RegCM, Protheus)

Non-hydrostatic models

(eg COSMO-CLM, WRF)

Statistical Downscaling

Stochastic (rainfall) Downscaling

Statistical downscaling:

Find relationships between
large-scale properties (eg indices)
and small-scale behavior:

1. Find a large-scale predictor
2. Determine its correlation with a predictand
3. Use the projected value of the predictor
to estimate the future value of the predictand

(Also for seasonal predictions)

Stochastic downscaling:

Highly intermittent fields such as rainfall
can be difficult
for dynamical or statistical downscaling.

An alternate approach is
stochastic downscaling
which leads to ensemble projections

The problem with intermittent fields

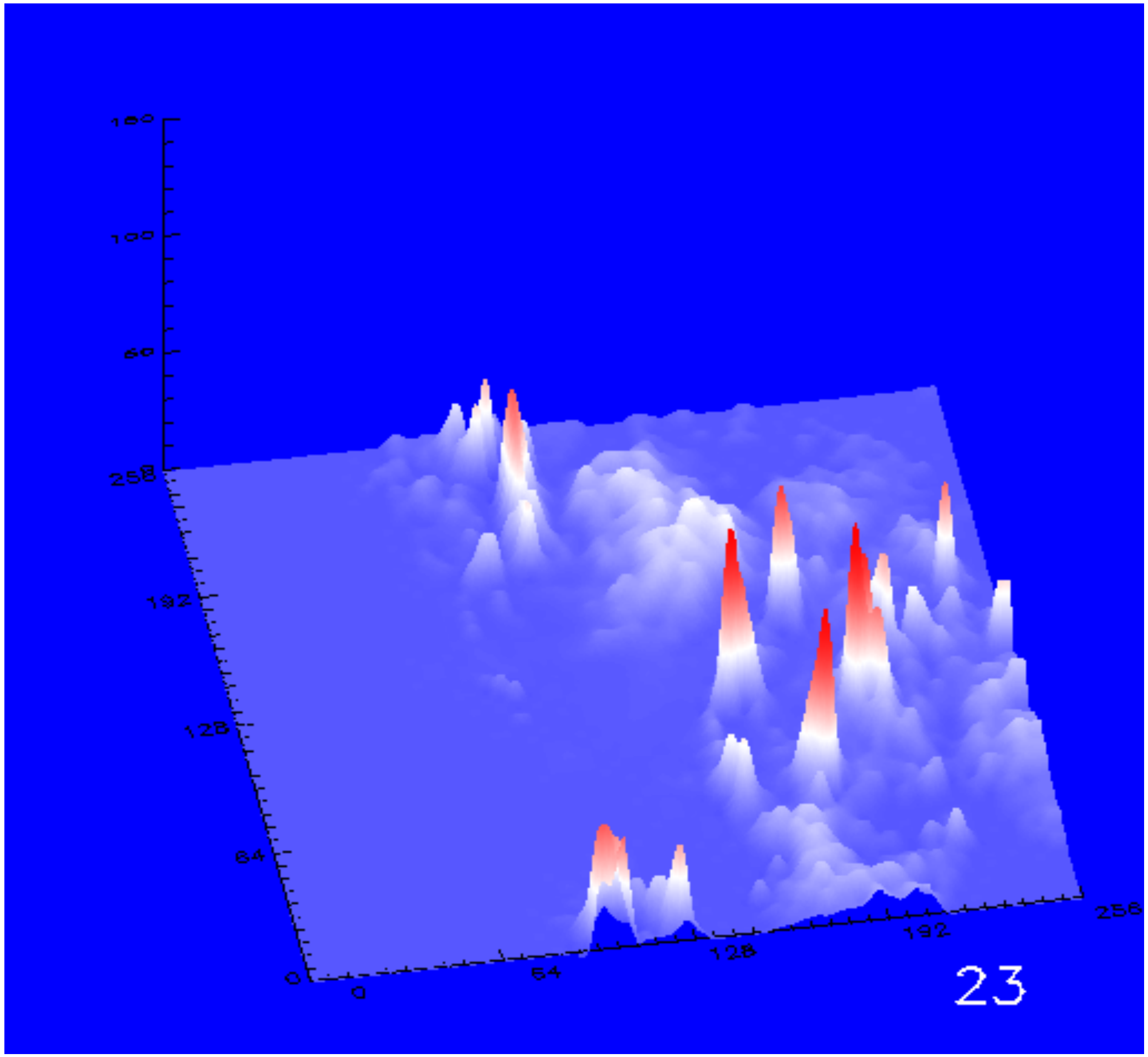

Another approach: stochastic downscaling

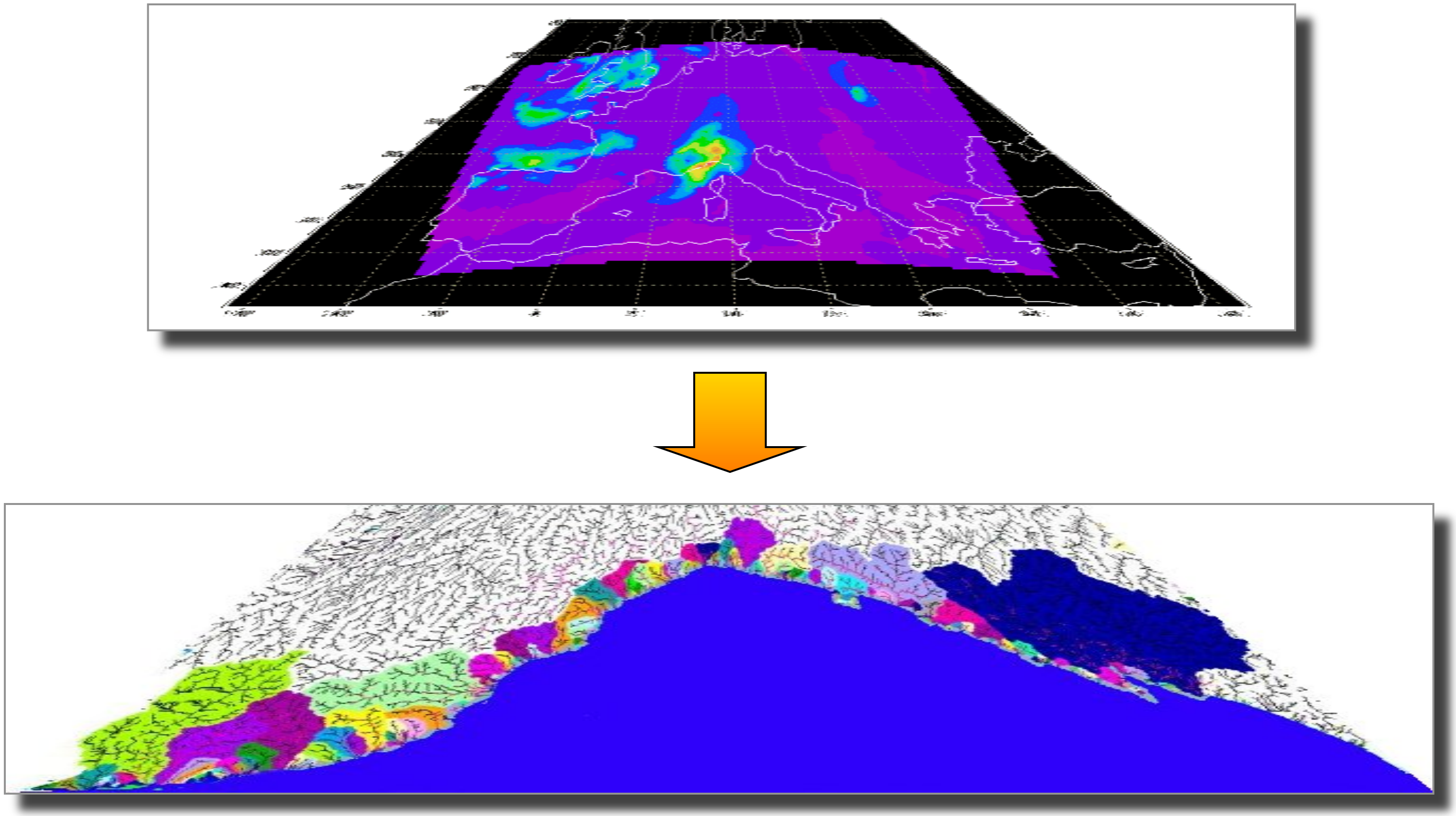

Downscaled fields must reproduce the original fields on large scale and have reliable statistical properties on small scale

Stochastic downscaling is best suited for ensemble predictions

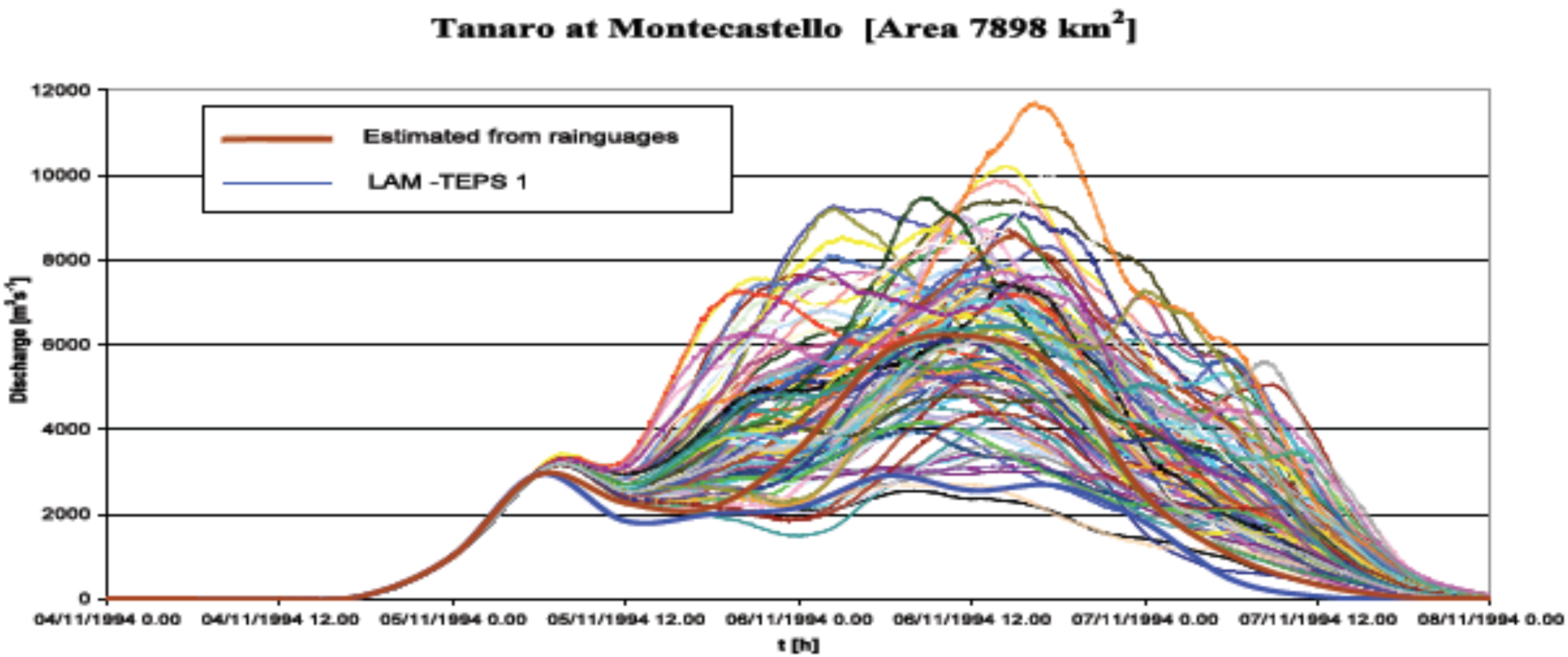

What are the small-scale statistical properties of precipitation?

Information from
Rain gauges
Radar data
High-res simulations

Probability distribution

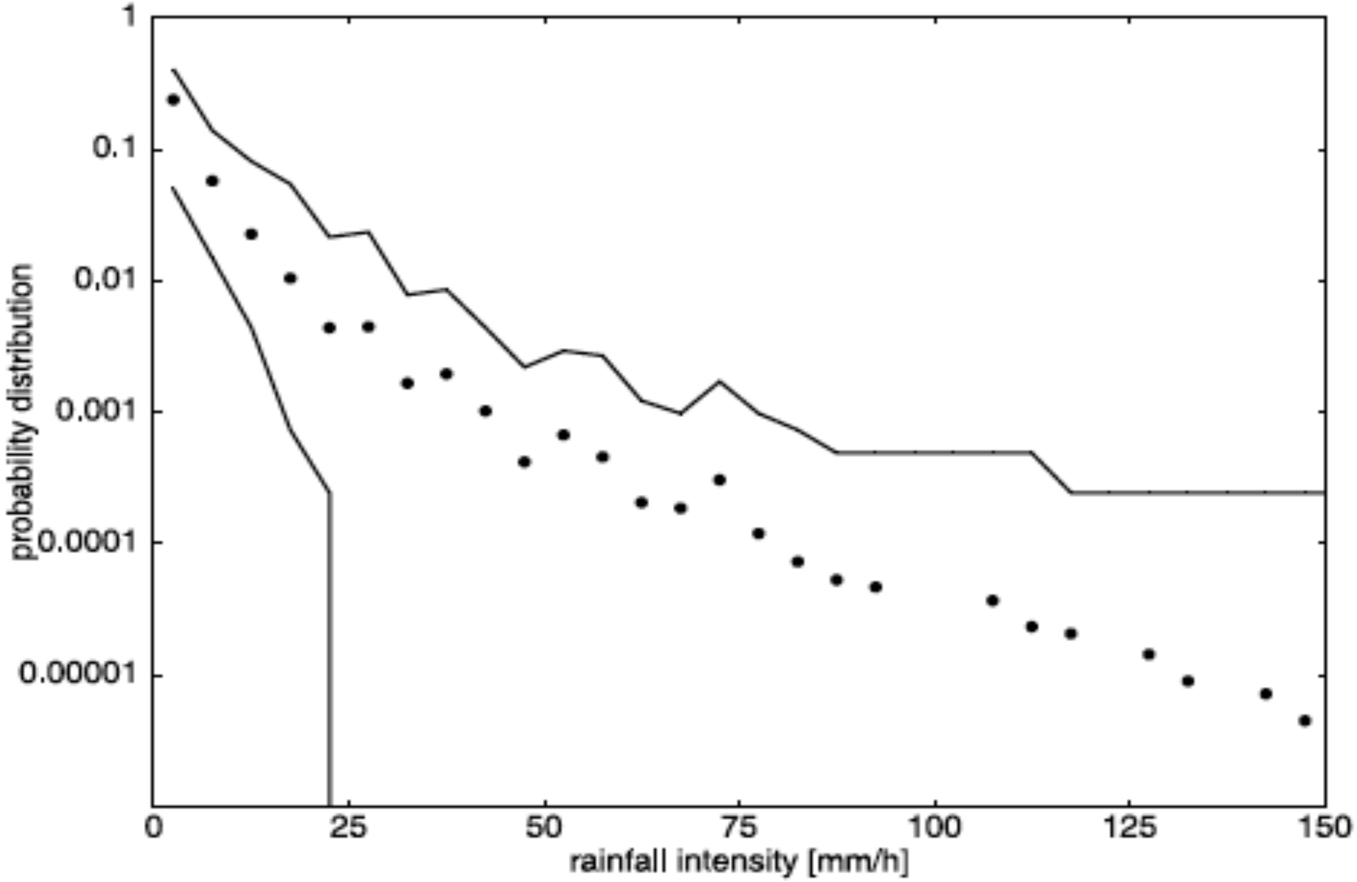

GATE radar data

Power spectra

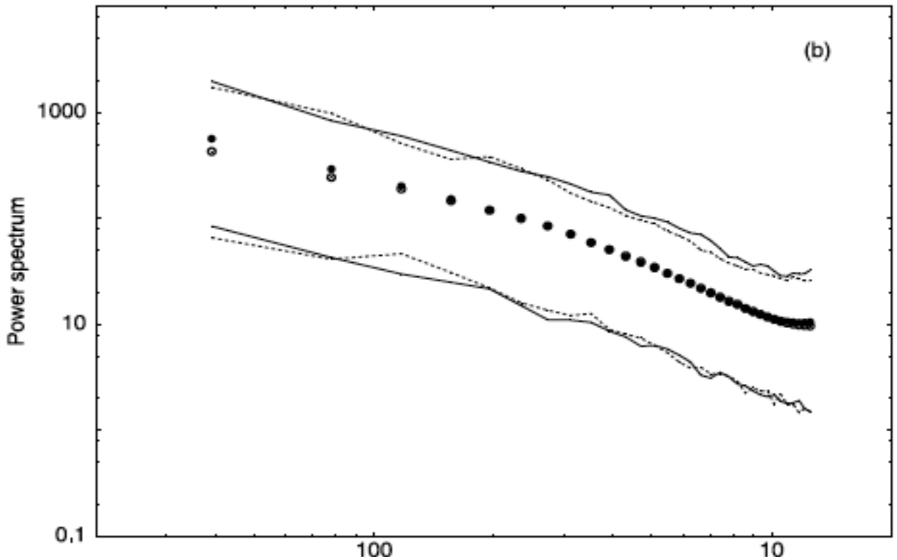

GATE radar data

Midlatitude radar data

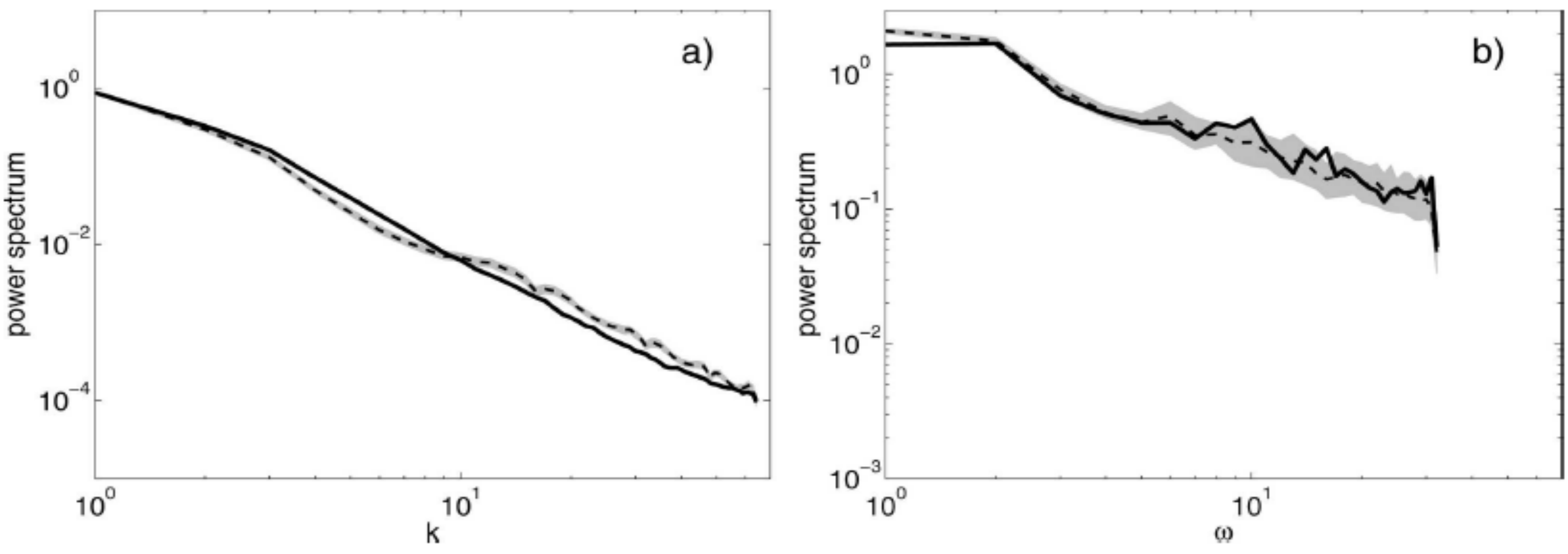

Spatial autocorrelation

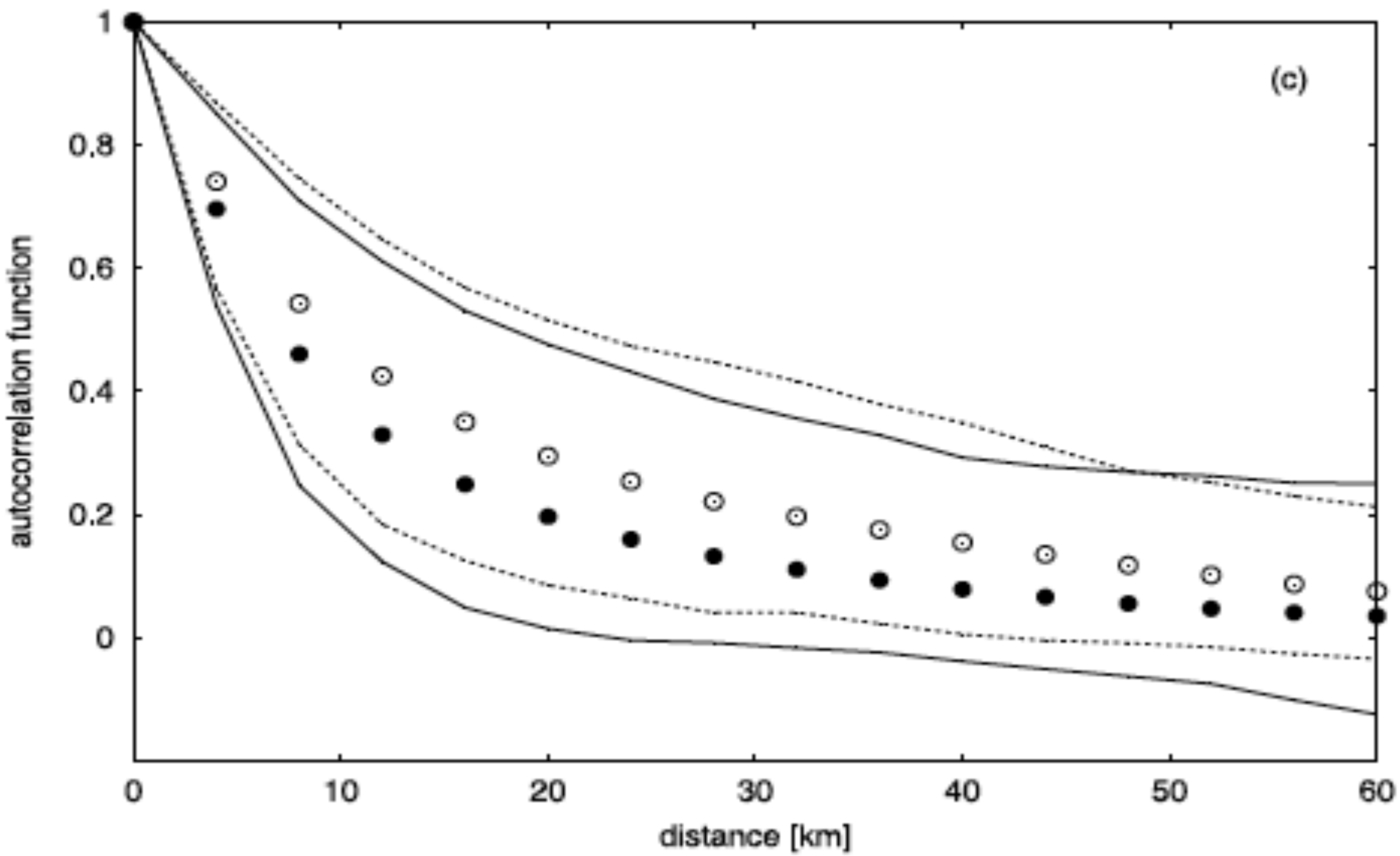

GATE radar data

Partition functions

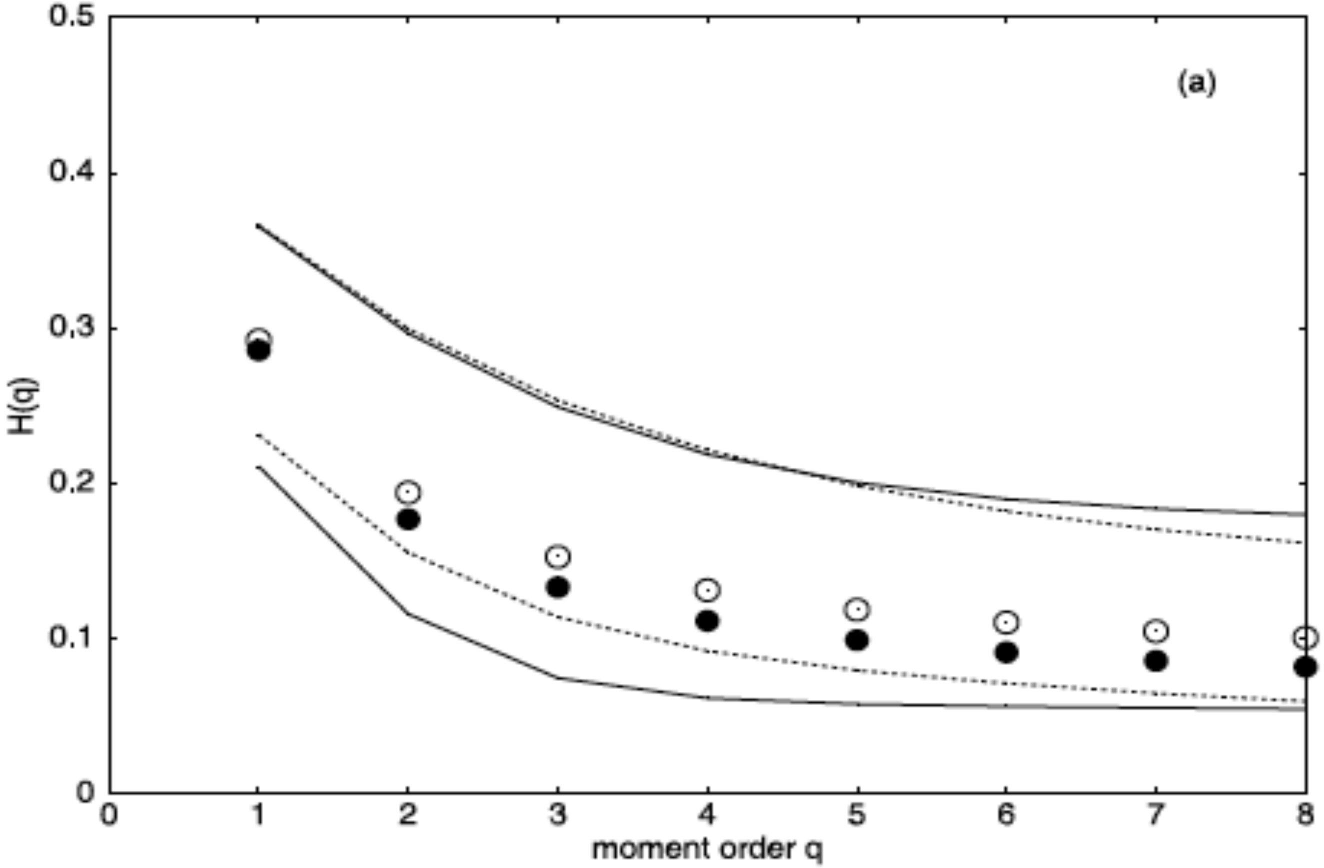

GATE radar data

$$\mathcal{S}_1(\lambda,q) = \langle |p(x_1+\lambda,x_2) - p(x_1,x_2)|^q \rangle \qquad \mathcal{S}_1(\lambda,q) \sim \lambda^{qH_1(q)}$$

$$\mathcal{S}_2(\lambda,q) = \langle |p(x_1,x_2+\lambda) - p(x_1,x_2)|^q \rangle \qquad \mathcal{S}_2(\lambda,q) \sim \lambda^{qH_2(q)}$$

Box-counting dimension

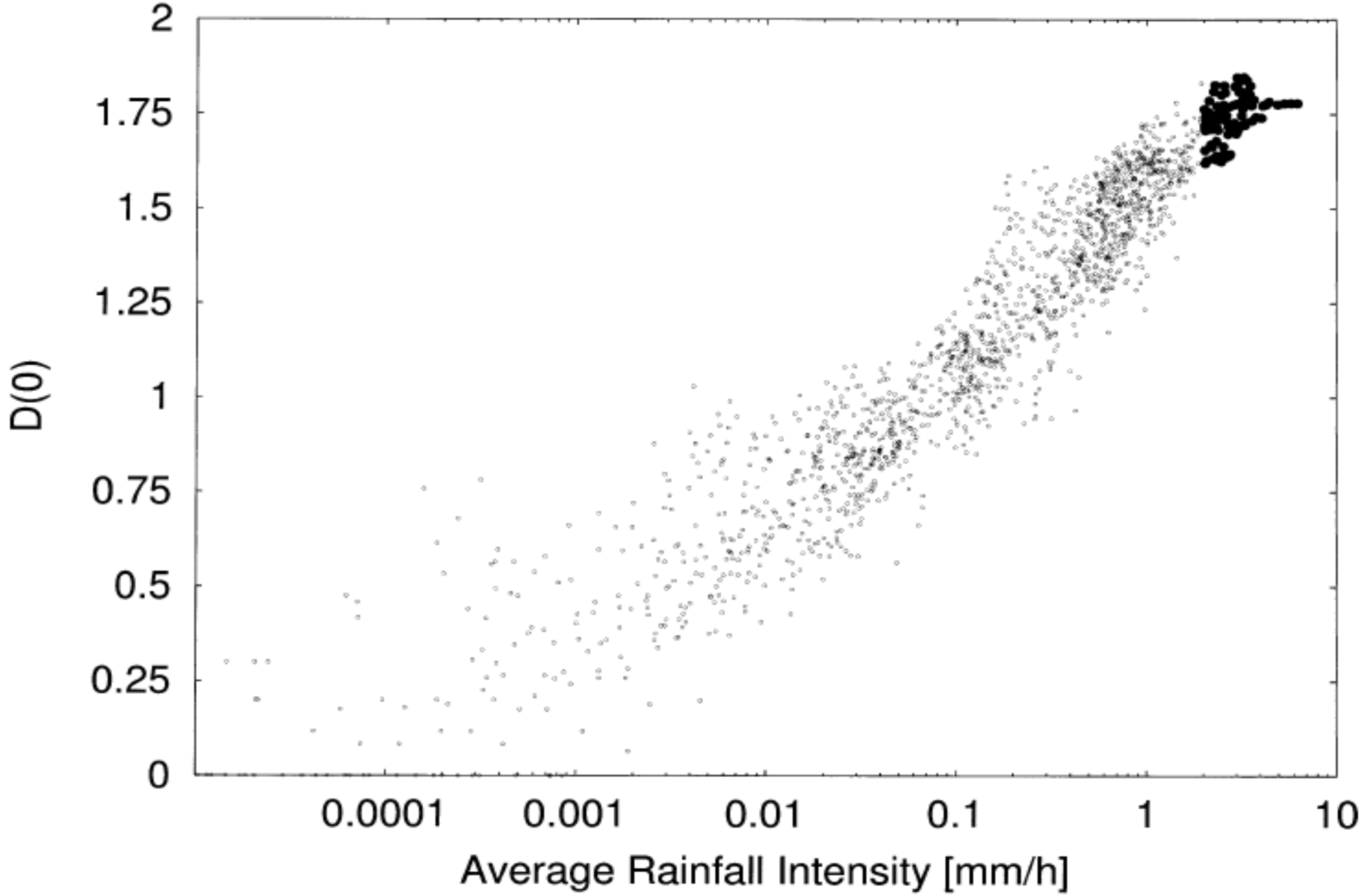

GATE radar data

Shape of rainfall cells

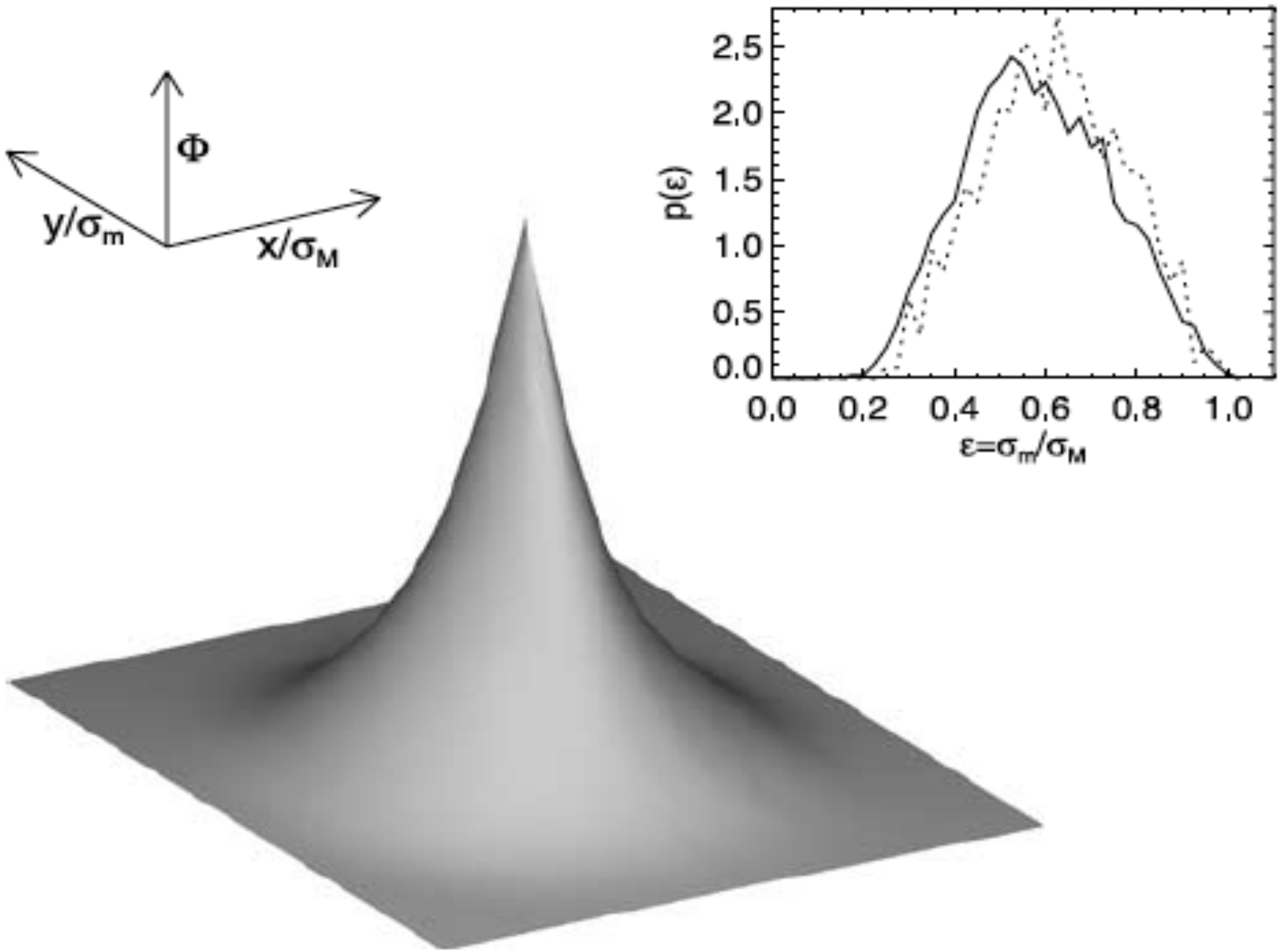

GATE and TOGA COARE radar data

Shape of rainfall cells

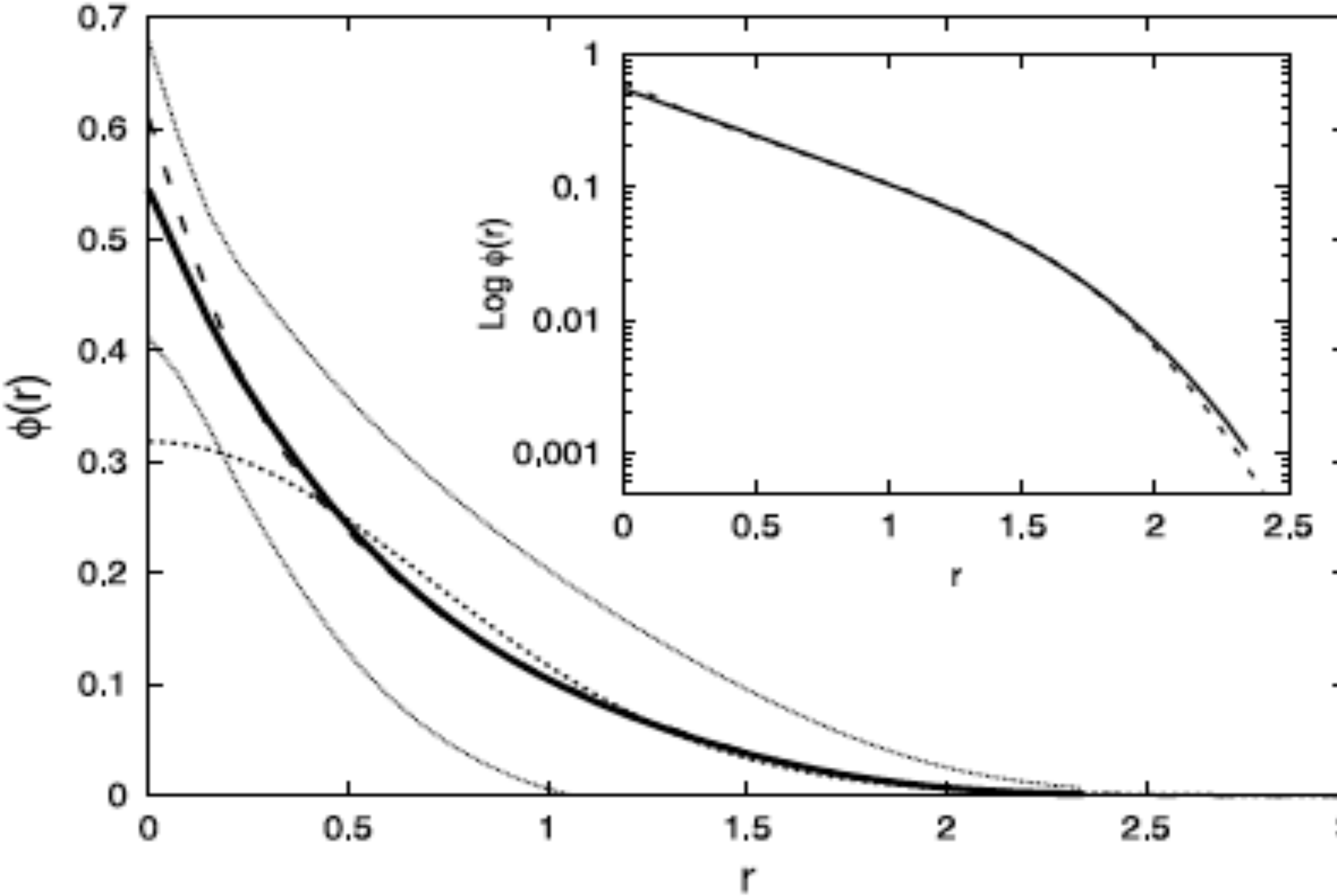

GATE and TOGA COARE radar data

Stochastic rainfall downscaling models

Random distributions of rain cells

Multifractal cascades

Nonlinearly transformed spectral models

Spectral-based rainfall downscaling

Ferraris, Gabellani, Parodi, Rebora, von Hardenberg, Provenzale, JHM 2003

Ferraris, Gabellani, Rebora, von Hardenberg, Provenzale, WRR 2003

von Hardenberg, Ferraris, Provenzale, GRL 2003

Rebora, Ferraris, von Hardenberg, Provenzale, JHM 2006

Rebora, Ferraris, von Hardenberg, Provenzale, NHESS 2006

von Hardenberg, Ferraris, Rebora, Provenzale, NPG 2007

Gabellani, Boni, Ferraris, von Hardenberg, Provenzale, AWR 2007

Brussolo, von Hardenberg, Ferraris, Rebora, Provenzale, JHM 2008

Brussolo, von Hardenberg, Rebora, JHM 2009

Metta, von Hardenberg, Ferraris, Rebora, Provenzale, JHM 2009

Biabanaki, von Hardenberg, Rebora, Provenzale, *in preparation* 2011

A space-time stochastic downscaling method nested into meteo-climatic models:

We model
the precipitation field in terms of
a nonlinear (static) transformation
of a linear autoregressive process

$$r(x,y,t) = \Phi[g(x,y,t)]$$

$$\left|\hat{g}\right|^2 = P(k_x, k_y, \omega)$$

The RainFARM:
Rainfall downscaling by a Filtered AutoRegressive Model
(Rebora, Ferraris, von Hardenberg, Provenzale, JHM 2006)

• model output, $P(X,Y,T)$

• Assume a power-law form of the spectrum and estimate or fix the spectral slopes of P: a , b

• Generate a random gaussan field, g, by inverting the power-law spectrum with random phases

• Take $r = A \exp (g)$

• Substitute the low-pass filtered part of the random field, $R=\langle r \rangle$, with P

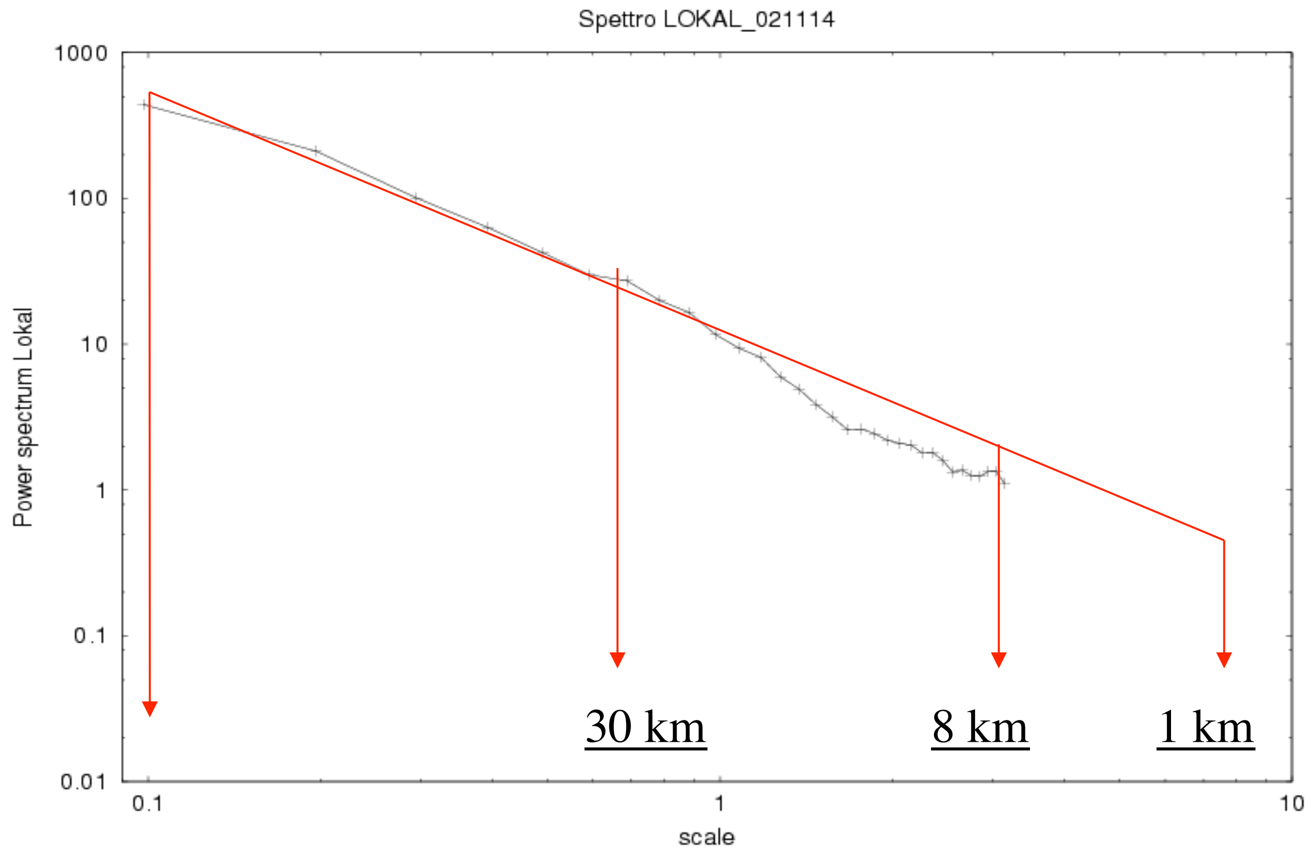

Extension of the spectrum at small scales
(we assume a power-law spectral shape)

The parameters are determined from the large scales

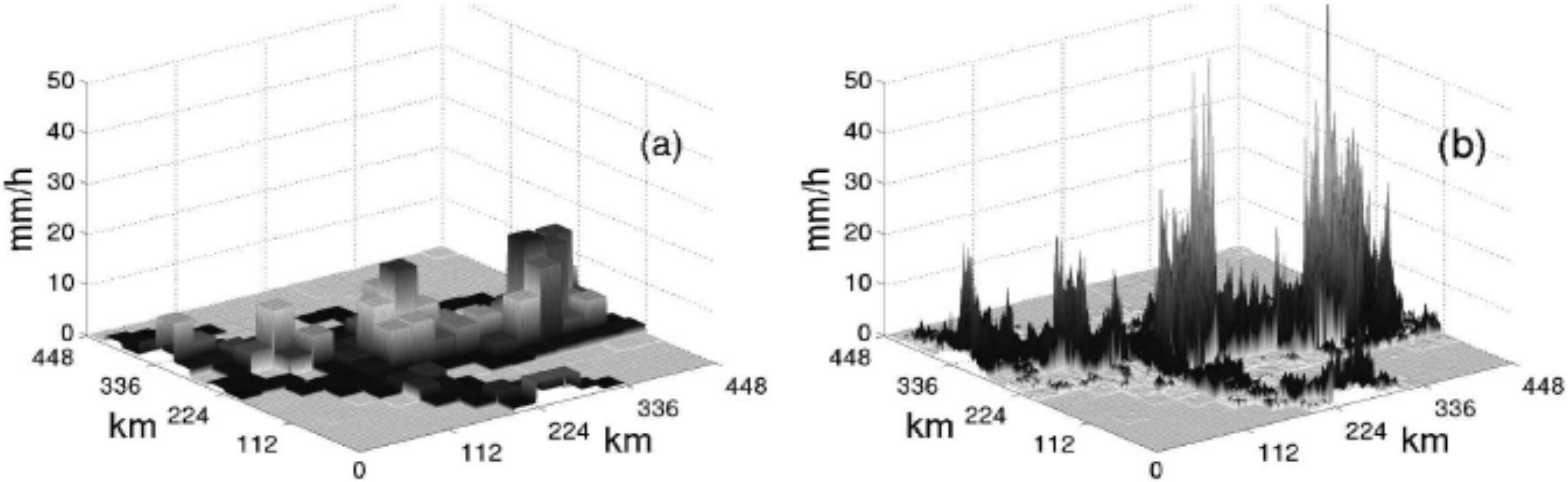

FIG. 10. (a) A snapshot of the forecasted rain field obtained from the LAM forecast and (b) one example of a downscaled field obtained by application of the RainFARM. The vertical scale indicates precipitation intensity (mm h^{-1}) and it is the same for the two fields.

Test of the RainFARM on radar precipitation data

We use radar data from the meteorological radar at
San Pietro Capofiume, ARPA SMR, Bologna
(courtesy of P. Alberoni)

Event of intense precipitation starting on 00:00 UTC, 25 Dec 2001
Data resolution : 1 km , 15 min ; Maximum scales: 128 km, 16 hr

We aggregate (cumulate, coarse grain) the data
to a field of 8x8x8 pixels with resolution 16 km, 2 hr

We apply the RainFARM and verify whether we produce fields with the correct large-scale pattern and small-scale statistical properties

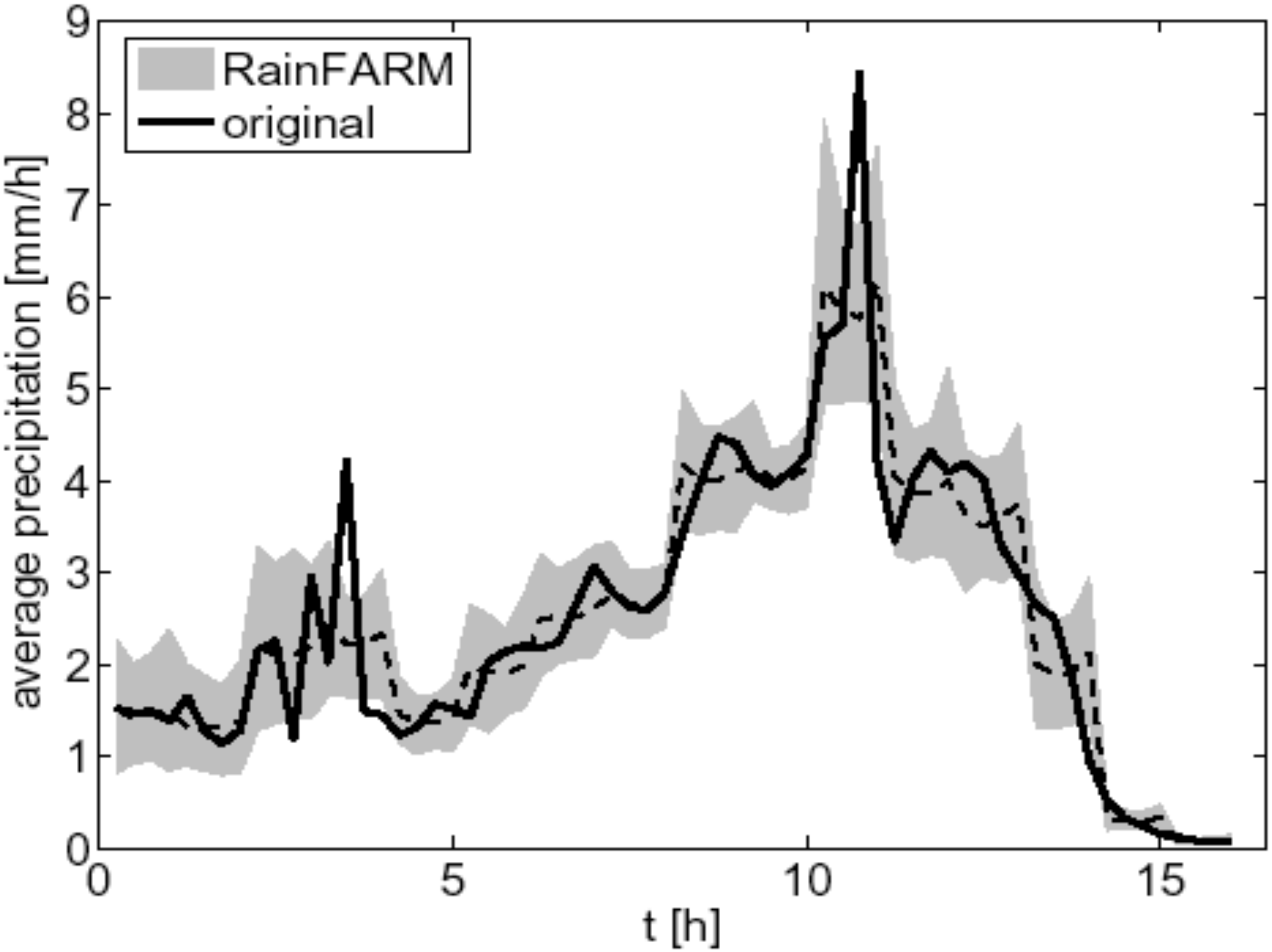

Instantaneous spatial averages

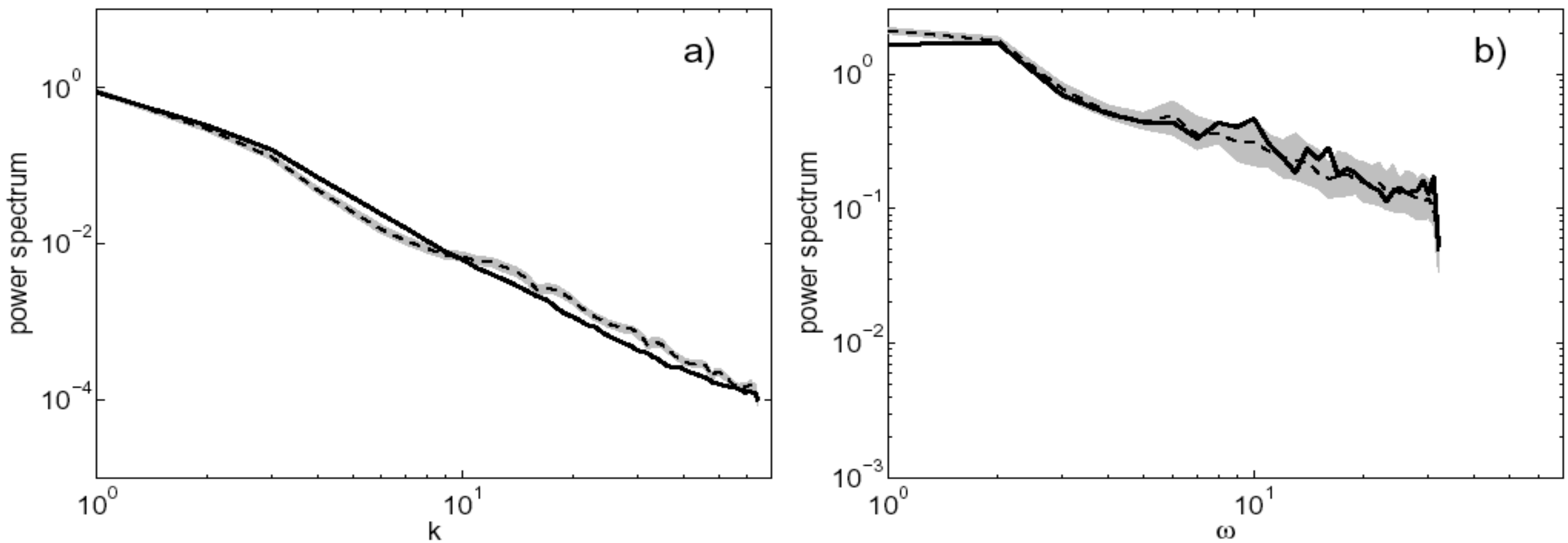

Space and time spectra

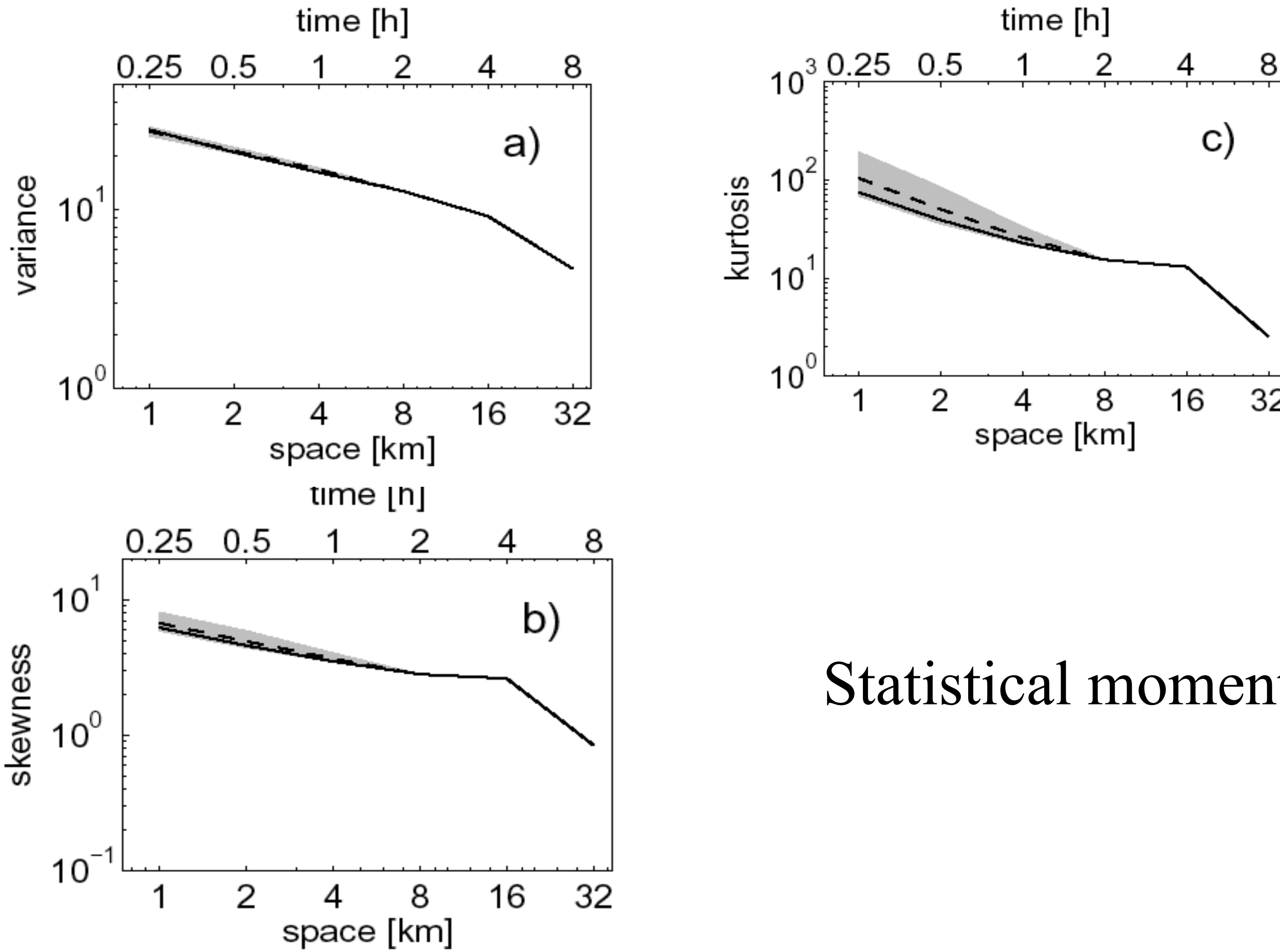

Statistical moments

Applications:

Risk assessments and statistics of extreme rain events and floods

Soil-atmosphere fluxes

Snow and permafrost

Validation of weather and climate models

Stochastic downscaling as a method
to compare model output and data (Brussolo et al 2008)

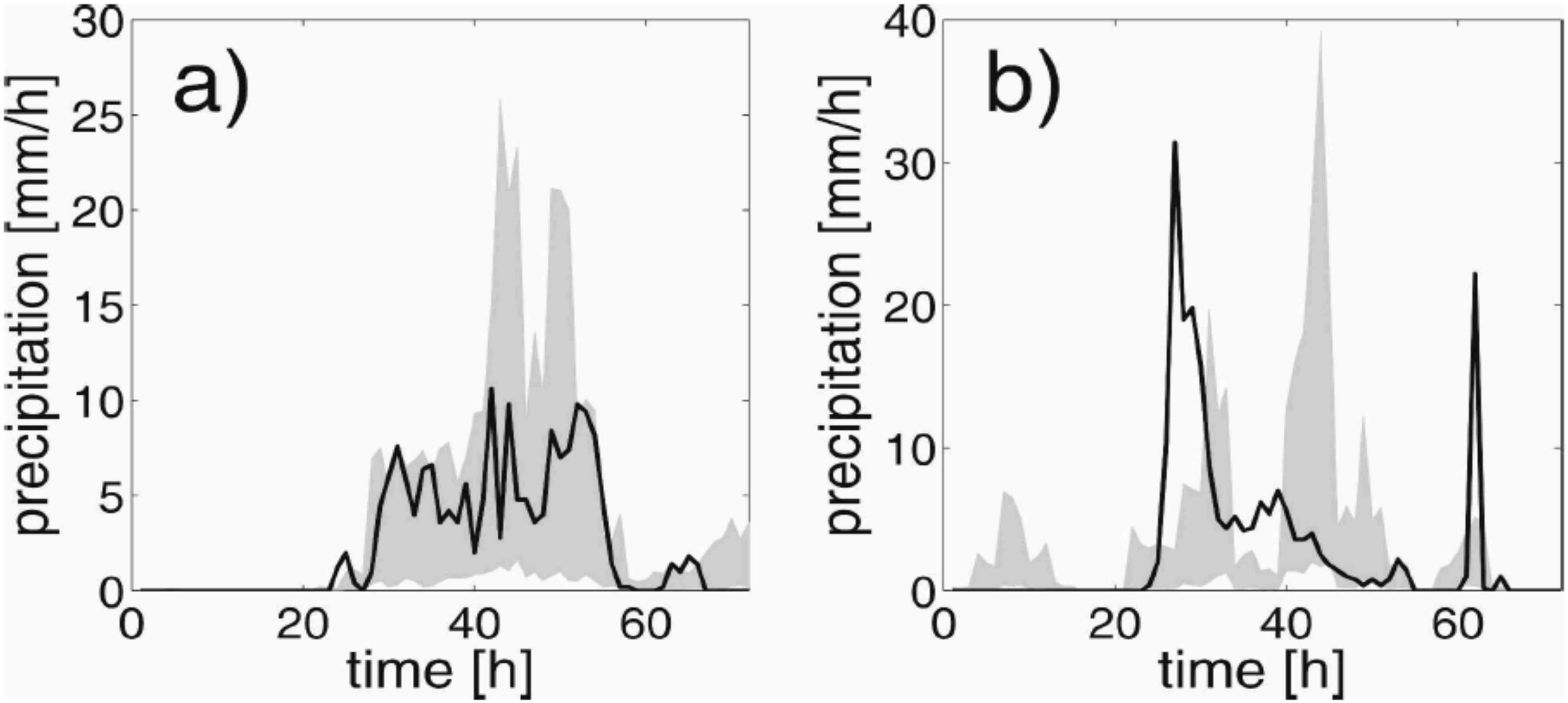

FIG. 3. Examples of single-site rain gauge time series. The gray bands include 95% of the individual members of the ensemble obtained by stochastically downscaling the numerical forecast. (a) Rain gauge at Front Malone, Turin, Italy. (b) Rain gauge at Colle San Bernardo, Cuneo, Italy. Both cases refer to the event of 13–15 Sep 2006. In the downscaling procedure, the forecast was considered reliable down to scales of L_0 = 28 km and T_0 = 3 h.